Cellular and Molecular Atlas of the Macaque Dorsal Horn

by

Cynthia Mary Arokiaraj

B.Tech., Anna University, 2015

Submitted to the Graduate Faculty of the

School of Medicine in partial fulfillment

of the requirements for the degree of

Doctor of Philosophy

University of Pittsburgh

2021

UNIVERSITY OF PITTSBURGH

SCHOOL OF MEDICINE

This dissertation was presented

by

Cynthia Mary Arokiaraj

It was defended on

October 15, 2021

and approved by

Dr. Bradley K. Taylor, Professor, Anesthesiology and Perioperative Medicine

Dr. Kathryn M Albers, Professor, Neurobiology

Dr. William Stauffer, Assistant Professor, Neurobiology

Dr. Andreas R Pfenning, Assistant Professor, Computational Biology

Dr. Victoria Abraira, Assistant Professor, Cell Biology and Neuroscience

Dissertation Director: Dr. Rebecca P. Seal, Associate Professor, Neurobiology

Copyright © by Cynthia Mary Arokiaraj

2021

Cellular and Molecular Architecture of the Macaque Dorsal Horn

Cynthia Mary Arokiaraj, PhD

University of Pittsburgh, 2021

The spinal cord dorsal horn occupies a key position in the central nervous system, as it is the first site of integration of somatosensory input from the periphery. Local interneurons of the dorsal horn process the incoming peripheral information while projection neurons relay it to supraspinal regions via ascending pathways. However, the exact mechanisms through which this occurs in normal or maladaptive states, and the neuron populations involved, remains to be understood. Identification of the neuronal cell types present in the dorsal horn will enable us to determine their functional organization. Thus, a goal of this thesis is to achieve a consensus in the cell types and their classification.

To do this, we performed single-nucleus RNA-sequencing (snRNA-seq) of the Rhesus macaque dorsal horn. Mapping out the cellular and molecular organization of the non-human primate allows us to develop a reliable species-independent classification scheme for the cell types that can then facilitate translation of rodent dorsal horn studies to primate. From the snRNA-seq, we identified 11 excitatory neuronal clusters (GLUTs) and 5 inhibitory clusters (GABAs). Based on the cytoarchitecture of the spinal cord, layers or laminae have been described along the dorso-ventral axis, and these appear to correspond well with the functional organization of neuron populations. *In situ* hybridization revealed that a majority of the clusters reside within specific lamina(e). A comparative analysis between clusters of the macaque and mouse meta-analysis showed a strong correspondence between both species as well as several interesting species-specific differences at the gene level.

An additional goal of this thesis is to describe a strategy for the identification of regulatory elements in transcriptionally active regions of individual dorsal horn cell types using single nucleus Assay for Transposase-Accessible Chromatin coupled with sequencing

(snATAC-seq). We found that the snATAC-seq derived clusters correspond well with our snRNA-seq clusters i.e., all 16 cell-types identified from the snRNA-seq have good representation in the scATAC-seq data. These data further validate our proposed classification scheme of dorsal horn cell types while also providing candidate regulatory regions that drive expression in specific cell types.

Table of Contents

List of Tables

List of Figures

Preface

The work done in Chapters 2 and 3 of this thesis is under review at Neuron with the title "A Comparison of the Cellular and Molecular Atlases of the Macaque and Mouse Dorsal Horns."

Appendix B contains data reprinted from "Mechanical Allodynia Circuitry in the Dorsal Horn Is Defined by the Nature of the Injury" published in Neuron by Cedric et al. I performed intraspinal injections in the mouse and in situ hybridization experiments to molecularly characterize three different dorsal horn populations in the mentioned study. This work complements the over-arching goal of this thesis which is to determine whether conserved molecular cell types have conserved functional roles across species.

Appendix C contains a book chapter that I co-authored titled "Multiplex in situ Hybridization of the Primate and Rodent DRG and Spinal Cord" for the book titled, "Contemporary Approaches to the Study of Pain: From Molecules to Neural Networks." This work is currently in press. This book chapter provides a comprehensive overview of the *in situ* technique employed in Chapters 2-3, with a special focus on primate tissue.

Appendix D contains a book chapter that I co-authored titled "The use of intraspinally injected chemogenetic receptor, PSAM-GlyR, to probe the functional role of spinal dorsal horn neurons." This chapter is part of the same book described above and complements the rationale highlighted in Chapter 4 for the investigation of dorsal horn neurons using a combination of viral tools and chemogenetics.

Acknowledgements

There are several people who guided, motivated and sculpted me during my PhD journey. At the forefront, is my PhD advisor, Dr. Rebecca P. Seal. I would like to thank her for the time she took to mentor and help me grow as a researcher. There were many teachable moments, be it for grant writing or scientific presentations, during which she imparted tips and fun aphorisms that I will always fondly remember. She also left no stone unturned to make sure I had the resources and help that I needed to carry out my experiments. I am also grateful for her support in allowing me to pursue a translational thesis project as this kept me continually motivated.

I would like to extend my warmest gratitude to the members of my dissertation committee – Professors Bradley Taylor (Chair of the committee), Andreas Pfenning, Kathy Albers, William Stauffer and Victoria Abraira. Dr. Pfenning, who collaborated with us, played a tremendous role in providing me with unique input and expertise pertaining to bioinformatics. All of the committee members were generous with their time and provided me with intellectual insight to ensure that the science being conducted was meaningful. I have been fortunate to have had the opportunity to be a part of the Pittsburgh Center for Pain Research and to interact with its members. I thoroughly enjoyed the Pain-focused classes and seminars as it shaped my understanding of the multifaceted challenges surrounding pain.

I would like to thank all of the members of the Seal Lab – past and present, for their unwavering support and friendship. I learned valuable skills from each of the postdoctoral scholars- Dr. David Ferreira, Dr. Joe Brague, Dr. Myung-chul (Sam) Noh, and Dr. Priyabrata

Halder. Their persistence and diligence inspired me to keep challenging myself. The Seal Lab members have created an environment that fosters team-work and has allowed positivity to triumph over the uncertainties of science research.

I would like to express my deepest gratitude to my family: Appa, Amma, Ben, my grandparents, and in-laws for their love and prayers, without which I would not be where I am today. My parents have always supported my endeavors and their confidence is what led me to pursue a PhD in Neuroscience. I am grateful to have been able to share the joy of crossing every little milestone with them.

During countless occasions, my friends have offered me sound advice and words of encouragement. I was comforted knowing that they were always just a phone call away. I am truly lucky to have had their support.

Lastly, my love and gratitude extend to my husband, Louis Prateek Rajan. I am thankful that he entered into my life at the perfect time. He has kept me grounded and understood me like no other.

1.0 Introduction to the Spinal Cord Dorsal Horn

1.1 Structure and Cytoarchitectonic Scheme

The spinal cord, like other parts of the central nervous system, is composed of white and gray matter. The spinal gray matter is butterfly-shaped and is divided into two horns: dorsal and ventral, based on its location in relation to the central canal. In certain segments i.e., from the first thoracic to the second lumbar segment and sacral segments 2-4 in humans, there is an additional lateral horn, which lies adjacent to the central canal.

In 1952, Rexed divided the cat dorsal horn into six layers or laminae based on the cytoarchitecture i.e., the size, shape, density and distribution of the neuronal cell bodies (**Figure 1**) (Rexed, 1952, 1954). This lamination scheme has since been widely adopted in many species as a standard reference system for investigations of the dorsal horn as well as the spinal cord as a whole (Molander et al., 1984; Schoenen & Faul, 1990; Sidman et al., 1971). Lamina I, also called as the marginal layer, was described by Rexed as "a thin veil of grey substance, forming the dorsal most part of the spinal gray matter" (Rexed, 1952). Lamina II which lies below lamina I, was previously named as the substantia gelatinosa, due to its characteristic translucent appearance in unstained sections. Lamina II follows the shape of lamina I as it curves around the lateral border of the dorsal horn and ends about half way down the lateral edge. This lamina is thicker than lamina I, and in most species, is divided into an inner (II_i) and outer (II_o) zone. In the human dorsal horn however, the neurons in lamina II

appear more homogenous and so there is no clear distinction between the inner and outer zones (Schoenen & Faul, 2004). Together with lamina I, this forms the superficial part of the dorsal horn. Interestingly, lamina II is thickest laterally in humans while in rodents, it is thickest medially (Molander et al., 1984; Molander et al., 1989; Schoenen & Faul, 2004). Lamina III lies ventral and parallel to lamina II and can easily be distinguished from the latter owing to the presence of myelinated fibers in lamina III (Molander et al., 1984). Cells of lamina III are less densely packed and larger in size compared to lamina II (Beal & Cooper, 1978; Schoenen & Faul, 2004; Sengul et al., 2012; Szentagothai, 1964). Lamina III and IV correspond to the dorsal and ventral parts respectively of the nucleus proprius of classical literature. Lamina IV is thicker than the more dorsal laminae (I-III), and extends from the base on the medial side of the dorsal horn to the lateral edge. It is comparatively more difficult to distinguish the dorsal and ventral borders of lamina IV. However, a distinguishing feature of this lamina is the presence of some very large cells (Heise & Kayalioglu, 2009; Molander et al., 1984; Schoenen & Faul, 2004). Laminae V and VI run straight across from the medial to lateral edge of the dorsal horn and correspond to the 'neck' and 'base' of the dorsal horn from classical literature (Brown, 1982). In human, cells of laminae V and VI are reportedly homogenous and hence the two laminae are indistinguishable from one another (Schoenen & Faul, 2004). Lamina VI, the most ventral layer of the dorsal horn, is present only in the cervical and lumbosacral enlargements (Molander et al., 1984; Molander et al., 1989; Rexed, 1954; Sengul et al., 2012). Laminae V and VI can each be divided further into a compact medial zone, where there are small to medium-sized cells that are tightly packed, and a lateral zone consisting of large cells and thick fiber bundles giving it a reticulated appearance (Rexed, 1954; Schoenen & Faul, 2004; Sengul et al., 2012).

Rexed's laminar scheme continues to be the most commonly used classification system for the spinal cord as subsequent studies have shown that neurons within each lamina possess

distinct dendritic architecture and chemoarchitecture. Importantly, the termination pattern of primary afferents to the spinal cord, as well as the descending tracts from the brain to the spinal cord, often respect the laminar boundaries, thereby suggestive of a functional organization for the dorsal horn that largely depends on its laminar organization.

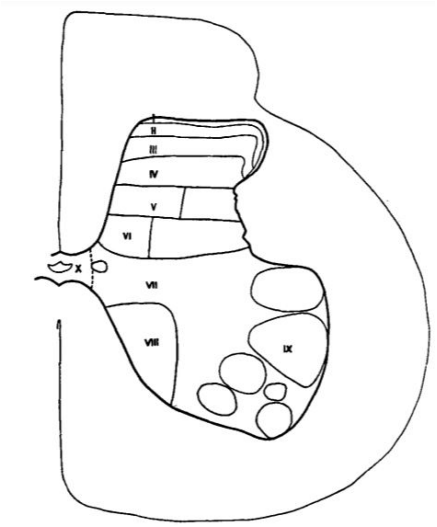

Figure 1. Rexed's schematic drawing of the 7th lumbar spinal cord segment in adult cat.

1.2 Primary Afferents

Primary sensory neurons play a fundamental role in transducing information about the mechanical, thermal and chemical states of the body, and transmitting it to the central nervous system (CNS). Afferent neurons are pseudounipolar with an axon that bifurcates into a peripheral process that innervates the skin, viscera, muscle or joints, and a central process that extends to the spinal cord or brainstem. The cell bodies of primary afferents lie in the dorsal root ganglia (DRG) or trigeminal ganglia (TG).

1.2.1 Classification of Primary Afferents

Cutaneous afferent fibers can be classified on the basis of diameter, myelination and conduction velocity into three groups: i. Large, heavily myelinated Aβ-fibers (16-100 m/s) ii. Medium, thinly myelinated Aδ-fibers (5 – 30 m/s) and iii. Small, unmyelinated C-fibers (0.2 – 2 m/s) (Light, 1993; Perl, 1992). Aβ-fibers predominantly respond to innocuous mechanical stimuli such as touch, vibration, pressure and texture (Mackenzie et al., 1975). However, some Aβ-fibers also function as nociceptors (Djouhri & Lawson, 2004). In contrast to the Aβ afferents, a majority of the Aδ- and C- fibers are nociceptors or thermoreceptors. In general, A-fiber nociceptor activation results in fast, sharp pain while nociceptive C-fibers signal a dull, aching or burning pain (Beissner et al., 2010; Nagi et al., 2019). There are however certain Aδ-fibers (Those that innervate hair follicles) and C-fibers that respond to innocuous low-threshold mechanosensation (Brown & Iggo, 1967; Burgess et al., 1968; Dhandapani et al., 2018; Li et al., 2011; Olausson et al., 2002; Seal et al., 2009). Low-threshold mechanoreceptors (LTMRs) respond to innocuous skin indentation, stroking, vibration and hair follicle deflection. Aδ-LTMRs along with C-LTMRs account for more than 50% of all cutaneous LTMRs that innervate hairy skin (Abraira & Ginty, 2013).

Organization of the primary afferents based strictly on the aforementioned characteristics does not provide sufficient specificity as there are several exceptions to this broad classification scheme. Therefore, the field has taken advantage of histological and transcriptomic approaches to identify molecular markers for primary afferent subsets (Chiu et al., 2014; Li et al., 2016; Ma & Ribeiro-da-Silva, 1995; Perry & Lawson, 1998; Ribeiro-da-Silva, 1995; Usoskin et al., 2015). This has provided an additional layer of specificity for

investigations into how specific classes of primary afferent neurons transduce somatosensory stimuli.

Classically in mouse, nociceptors have been classified as peptidergic based on their expression of calcitonin gene-related peptide (CGRP) or substance-P, or as non-peptidergic based on their expression of the P2X3 purinergic receptor or surface α-D-galactose residues which bind isolectin B4 (IB4) (Ju et al., 1987; Silverman & Kruger, 1990). While these two populations are mostly distinct in the mouse, the same does not hold true for primates including in human, where there is a large overlap in the expression of *CALCA* (Encodes CGRP) and *P2RX3* in the DRG (Kupari et al., 2021; Shiers et al., 2020; Shiers et al., 2021). A sub-population of nociceptors which express transient receptor potential cation channel subfamily V member 1 (TRPV1) responds to noxious heat and are activated by capsaicin (Caterina et al., 1997; Nagy & Rang, 1999). Interestingly, a larger proportion of neurons express TRPV1 in human DRG than in mouse, suggestive of a broader physiological role for these neurons in the primate DRG (Shiers et al., 2021). Another sub-population of thermoreceptors/nociceptors are those that express TRPM8 (Part of the Trp family), and mediate cold and cold pain (Knowlton et al., 2013; Peier et al., 2002). Transcriptomic analyses of macaque sensory neurons identified neurons that correspond to the Aδ-LTMRs of mouse by their conserved gene expression profiles (Kupari et al., 2021; Usoskin et al., 2015). In both species, these neurons show high expression of Neurotrophic Receptor Tyrosine Kinase 2 (*NTRK2*) which encodes the TrkB receptor. TrkB primary sensory neurons respond to rapid cooling of the skin as well as dynamic stimuli (Dhandapani et al., 2018; Rutlin et al., 2014). Of note, these neurons are tuned to hair deflection in the caudal-to-rostral direction and have also been found to be necessary to drive touch-evoked pain (mechanical allodynia) in neuropathic pain states (Dhandapani et al., 2018; Rutlin et al., 2014). C-LTMRs highly express vesicular glutamate transporter 3 (VGLUT3) and tyrosine hydroxylase (TH) in mouse. This fiber type contributes to mechanical hypersensitivity

after injury and has also been found to code for pleasant touch sensation in humans (Loken et al., 2009; Seal et al., 2009). Though C-LTMRs are present in primate sensory neurons, they are not marked by TH or VGLUT3 expression but are instead characterized by high expression of other genes such as visinin like 1 (*VSNL1*) or thyrotropin-releasing hormone receptor (*TRHR*) (Kupari et al., 2021).

All of these above examples illustrate the neurochemical and functional diversity of the primary sensory neurons. However, the coding properties of primary afferents are still poorly understood. Despite the polymodal nature of primary sensory neurons, there is evidence of certain 'labeled-lines' that convey information related to a single somatosensory modality to the dorsal horn. This labeled-line theory on its own is perhaps insufficient to account for the complexity of somatosensory perception. Another theory called population coding argues that there is significant crosstalk between the labeled lines, in which synergistic or antagonistic relationships between them modulate somatic sensation (Craig, 2003; Ma, 2010).

1.2.2 Primary Afferent Input to the Dorsal Horn

Neuroanatomical techniques and intra-axonal injections of horseradish peroxidase into single axons provided the basis for classical studies on the central termination patterns of primary afferents (Brown, 1982; Brown et al., 1977; Light & Perl, 1979b; Maxwell et al., 1984). These studies illuminated certain organizational principles for somatosensory processing. First, a somatotopic organization exists for the spinal cord that spans along both the rostrocaudal as well as mediolateral axis. To exemplify, information from rostral body parts such as the neck and forearm is processed by more rostral spinal cord segments than

information from caudal body parts such as the legs and feet. Along the mediolateral axis, input from more distal sites such as the glabrous skin of toe pads enters into the medial half of the dorsal horn while input from hairy skin of toes or from the proximally located thigh, enters more laterally into the dorsal horn (Wilson et al., 1986). Second, primary afferent input to the dorsal horn follows a modality-specific organization along the dorsoventral axis that largely coincides with the laminar organization. Importantly, this organization of sensory neuron input to the dorsal horn appears to be largely conserved across species (Light & Perl, 1979a).

In the spinal cord, A-fiber nociceptors synapse on to second-order neurons in laminae I, II and V while C-fiber nociceptors are found to synapse in laminae I-II. A remarkable column-shaped somatotopic organization has been observed with the central terminations of Aβ-, Aδ- and C-LTMRs whose peripheral endings are associated with the same or adjacent hair follicle (Li et al., 2011). The central endings of C-LTMRs form flame-shaped terminals in lamina II_i. Aδ-LTMRs innervate lamina II_i as well as lamina III, and lastly Aβ-LTMRs arborize in lamina III-V and the dorsal part of lamina VI. Thus, the central projections of these LTMR classes occupy distinct but slightly overlapping positions across the dorsal laminae. Some Aβ-LTMRs also send branches that ascend the dorsal column and synapse on to dorsal column nuclei neurons, forming the "direct pathway".

Primary afferents form either axo-axonic or axo-dendritic synapses with the spinal cord neurons. Additionally, all primary afferents are presumed to use glutamate as a neurotransmitter, and thus can mediate fast, excitatory synaptic transmission to certain dorsal horn neurons (Broman et al., 1993; Schneider & Perl, 1988). Most of the myelinated primary afferents innervating the deeper laminae contain the vesicular glutamate transporter 1 (VGLUT1) but some contain both VGLUT1 and VGLUT2 (Todd et al., 2003). On the other hand, unmyelinated nociceptors appear to contain low levels of VGLUT2.

1.3 Descending Input

Activity at various points of the dorsal horn circuitry is modulated by axons from descending pathways. Briefly, there are two principal descending monoaminergic-containing pathways which includes a serotonergic system that originates from the nucleus raphe magnus and a noradrenergic pathway that originates from the locus coeruleus and other pontine regions. These pathways are potentially involved in stimulation-produced analgesia (Reynolds, 1969). Fibers from these descending pathways are found to terminate across all dorsal laminae. Corticospinal fibers originating from the sensory cortex largely decussate in the lower medulla and terminate in lamina III-VI (Brown, 1982). Descending control from the periaqueductal gray (PAG) – rostral ventromedial medulla (RVM) system has also been widely studied for its reportedly facilitatory as well as inhibitory influences on the dorsal horn. Thus, ongoing work is focused on understanding how the descending pathways interface with the spinal nociceptive pathway (Heinricher et al., 2009; Porreca et al., 2002).

1.4 Projection Neurons

Dorsal horn neurons are broadly classified into two groups, namely projection neurons and interneurons, based on where their axons terminate. Projection neurons send axons rostrally to terminate within different regions of the brain such as: thalamus, lateral

parabrachial nucleus (LPb), hypothalamus, PAG, lateral reticular nucleus, nucleus of the solitary tract, caudal ventrolateral medulla (CVLM) and medial brainstem reticular formation (Wercberger & Basbaum, 2019). In contrast, interneurons have axons that remain within the dorsal horn. Projection neurons being the sole output cells of the dorsal horn, are therefore important players in the spinal touch, pain and itch circuit.

Understanding the organizational principles of projection neurons and their role in somatosensory processing is complicated by their relatively low representation in the dorsal horn. These neurons make up only ~5% of lamina I neurons in rat and are sparsely scattered in laminae III-VI, the lateral spinal nucleus (LSN) and around the central canal (Al-Khater et al., 2008; Todd et al., 2000). A majority of the lamina I projection neurons project to contralateral brain targets, however some cells do project bilaterally (Spike et al., 2003). Retrograde labeling studies from LPb, PAG and CVLM showed that lamina I neurons could be labeled from more than one of these brain regions and in the rat, nearly 85-95% of the projections to the LPb come from lamina I in the lumbar dorsal horn through the dorsolateral funiculus. (Al-Khater et al., 2008; McMahon & Wall, 1983; Spike et al., 2003). Additionally, all projection neurons are thought to be excitatory (Broman, 1994; Littlewood et al., 1995).

The spinothalamic tract which is part of the anterolateral system plays an important role in transmitting information about pain, temperature, crude touch and pressure to the somatosensory area of the thalamus. Surprisingly in rodents, the proportion of lamina I neurons in L4 that project to the thalamus is very low (<2% in rat) (Al-Khater et al., 2008). A comparatively higher number of neurons project to the thalamus from lamina I in C7 than L4; however, there are some discrepancies in what has been reported for the actual proportion of neurons belonging to the spinothalamic pathway (Al-Khater et al., 2008; Yu et al., 2005). There are also species-specific differences in what has been reported for the percentage of spinothalamic neurons originating from the lumbar dorsal horn in rats, cats and primates (Al-

Khater et al., 2008; Carstens & Trevino, 1978; Craig, 2008). It is clear however, that there are a greater number of spinothalamic neurons that are distributed across the dorsal laminae in the primate lumbosacral enlargement compared to the rodent (Willis et al., 1979). Of note, several of these reside in the lateral regions of lamina I and V and project to the lateral thalamus (Willis et al., 1979).

Another ascending pathway that has been described in many species including in primates is the spinocervical tract (Baker & Giesler, 1984; Brown, 1982). This pathway originates primarily from lamina IV but spinocervical tract neurons have also been observed in laminae I, III and V in cat (Craig et al., 1992). The axons of these neurons ascend in the medial and superficial parts of the dorsolateral funiculus, ipsilateral to the side the neurons are present, and terminate in the lateral cervical nucleus in the upper cervical cord. Information relating to light touch or noxious mechanical and thermal stimuli may be conveyed by the spinocervical pathway (Brown, 1982).

1.4.1 Molecular Markers of Projection Neurons

To interrogate the functional roles of projection neurons, Neurokinin 1-receptor (NK1R) has been the marker gene of choice since it is expressed by ~80% and ~90% of lamina I projection neurons in rat and mouse respectively (Cameron et al., 2015; Todd et al., 2000). These neurons have been categorized as fusiform, multipolar or pyramidal on the basis of their cell body shape and dendritic characteristics in the rat, cat as well as primate (Yu et al., 2005; Zhang & Craig, 1997; Zhang et al., 1996). NK1R is also expressed by 30-40% of the projection neurons in deeper laminae (III-V). The deeper NK1R neurons are large-sized cells with

dorsally directed dendrites which branch extensively in the superficial laminae (Mantyh et al., 1995; Naim et al., 1997). Interestingly, it has been observed that these dorsal dendrites receive numerous contacts from the nociceptive substance-P containing primary afferents (Naim et al., 1997). Activation of these afferents can thus result in the release of substance-P which binds to NK1R. Ablation of NK1R-expressing neurons by intrathecal administration of a cytotoxin-saporin conjugated with substance-P resulted in a significant decrease in mechanical allodynia and thermal hyperalgesia (increased sensitivity to noxious stimuli) in inflammatory and neuropathic pain models (Nichols et al., 1999). However, these phenotypes cannot be attributed specifically to projection neurons because there are dorsal horn interneurons that also express NK1R. Other studies have speculated that the intensity of the peripheral stimulus could dictate the release of glutamate exclusively, versus glutamate together with substance-P from the aforementioned afferents, and this subsequently could alter the excitability of the projection neurons (Cao et al., 1998; De Biasi & Rustioni, 1988; Rusin et al., 1992).

More recently, studies have questioned the acceptance of NK1R-expressing projection neurons as a homogenous population. Particularly because, spinothalamic lamina I neurons have been shown to have diverse response properties due to convergent primary afferent input. They can be broadly classified as nociceptive-specific (NS) if they respond to noxious heat, pinch or both; thermoreceptive-specific (COOL) if they respond to cooling; polymodal nociceptive (HPC) if they respond to noxious heat, pinch and noxious cold; and wide dynamic range (WDR) if they respond in a gradient fashion to innocuous as well as noxious stimulation (Allard, 2019; Craig et al., 2001; Davidson et al., 2012). Moreover, the failure of NK1R antagonists to produce analgesia in clinical trials emphasizes the need to understand how the seemingly functionally heterogenous population of projection neurons are recruited in chronic pain or itch states (Hill, 2000).

In one study, the projections of *Tacr1* (Encodes NK1R)-expressing neurons were compared to the projections of superficial dorsal horn neurons expressing G-protein coupled receptor 83 (*Gpr83*) using transgenic mouse lines (*Tacr1*^{CreERT2} and *Gpr83*^{CreERT2}) (Choi et al., 2020). These two populations are largely non-overlapping and they both project to the LPb, medial and posterior thalamic nuclei, lateral region of the PAG and the midbrain reticular nucleus. They show distinct differences in their physiological properties; *Tacr1* spinoparabrachial neurons preferentially respond to innocuous thermal stimuli and capsaicin while *Gpr83* spinoparabrachial neurons respond to mechanical stimuli (Choi et al., 2020). Both however respond to noxious heat and cold stimuli. This can be explained in part by differences in the primary afferent input to these neurons. *Tacr1* spinoparabrachial neurons as discussed above for NK1R, receive peptidergic nociceptive input while *Gpr83* spinoparabrachial neurons receive input from Aδ-LTMRs and both reportedly receive input from polymodal non-peptidergic primary afferents labeled by mas-related G-protein-coupled receptor D (*Mrgprd*) expression (Choi et al., 2020).

Another more recent mouse study performed a large-scale sequencing analysis along with retro-TRAP (translating ribosome affinity purification) to examine and compare the molecular profiles and functional characteristics of spino- and trigeminoparabrachial neurons that are NK1R^{+} with those that are NK1R^{-} (Wercberger et al., 2021). This study confirmed previous findings that showed overlap of NK1R-expressing projection neurons with neurons that express tachykinin 1 (*Tac1*-encodes substance-P), *Lypd1*, or paired like homeobox 2A (*Phox2a*) (Haring et al., 2018; Huang et al., 2019; Roome et al., 2020). *Tac1*-lineage neurons in the spinal cord are found to be dispensable for reflexive-defensive behaviors but are involved in coping behaviors associated with sustained pain and chloroquine-induced itch (Huang et al., 2019). These results conflict with another study, in which a reportedly higher number of *Tac1* neurons were silenced using a viral strategy resulting in a reduction in withdrawal response to

cold and radiant heat but with no effect on withdrawal to chloroquine-evoked itch (Polgar et al., 2020). Additionally, Polgar et al found that ~40% of the lamina I spinoparabrachial neurons expressed Cre in the *Tac1*^{Cre} mice (Polgar et al., 2020). Nevertheless, neither study was able to specifically examine the functional contribution of the projection neurons since *Tac1* is also expressed by interneurons. There was also no distinction made between the functional properties of the superficial versus deeper *Tac1*-expressing neurons. The transcription factor PHOX2A, which is expressed throughout embryogenesis but is absent in the adult mouse dorsal horn, labels a population of spinoparabrachial neurons (Alsulaiman et al., 2021; Roome et al., 2020). These neurons also overlap with *Tac1* and *Lypd1*-expressing projection neurons. A subset of the *Phox2a* neurons have a small soma, weak NK1R expression, and may correspond to the cool cells identified by Hachisuka et al that respond exclusively to cold (Hachisuka et al., 2020). Genes that Wercberger et al found to be enriched in the NK1R^{-} projection neuron subset include cholecystokinin (*Cck*) in laminae III-IV, neuromedin B (*Nmb*), corticotropin-releasing hormone (*Crh*) and neuronal pentraxin (*Nptx2*) in superficial laminae (Wercberger et al., 2021).

1.4.2 Postsynaptic dorsal column neurons

Postsynaptic dorsal column (PSDC) neurons which reside in laminae III-IV and X, send axons through the dorsal column to terminate in the brainstem dorsal column nuclei i.e., the gracile and cuneate nucleus (Rustioni & Kaufman, 1977). Information related to innocuous touch and visceral pain is thought to be conveyed via the ascending PSDC pathway which is still poorly characterized (Hirshberg et al., 1996; Honda, 1985; Willis et al., 1999). We know

that in mouse, PSDC neurons receive excitatory synaptic input largely from local interneurons (60%) residing in laminae III-IV and Aβ primary afferents (34%), and to a lesser extent from descending cortical input (6%) (Abraira et al., 2017). A sub-population of spinal cord neurons that express the transcription factor Zinc finger protein 2- ZIC2 during development project to the dorsal column nuclei (Paixao et al., 2019). Chemogenetic activation of ZIC2 PSDC neurons resulted in an increased sensitivity to static stimuli (Using von Frey filaments) but did not affect dynamic brush or thermal response (Paixao et al., 2019).

There is also evidence of interneurons that form intersegmental connections across a short range (Bice & Beal, 1997; Liu et al., 2010). Though not well understood, they are proposed to play a role in the coordination of limb movement.

Advances in viral strategies and the high-resolution obtained from sequencing technologies have enabled us to make steady progress in identifying whether molecularly distinct subsets represent functionally distinct populations. However, we are still limited in our ability to manipulate and study projection neurons exclusively using the marker genes identified thus far, because all of them are also expressed by interneurons. Furthermore, projection neurons receive extensive synapses not only from primary afferents but also from interneurons in the dorsal horn. Thus, in order to study how the information is coded by projection neurons or alternatively, to determine whether modality-specific dorsal horn circuits exist, it is pertinent to examine the organization of the interneurons and their role in gating and modulating peripheral information.

1.5 Interneurons

Dorsal horn neurons, like primary sensory neurons, are remarkably heterogeneous in their morphology, electrophysiological properties, and neurochemical features as will be highlighted in the following sections. Based on primary afferent input to the dorsal horn, we observe a broad segregation in the functional organization where nociceptive input is processed and transmitted by superficial dorsal horn neurons while touch and proprioceptive input is processed by the deeper dorsal horn neurons. Apart from this, nociceptive information is also conveyed to the ventral horn where it contributes to spinally-mediated nocifensive (protective reflex produced in response to damaging stimuli) reflexes (Sivilotti & Woolf, 1994).

Within the dorsal horn, the balance between excitation and inhibition is critical for normal sensory processing (Sivilotti & Woolf, 1994; Todd, 2010). Under normal physiological conditions, there is a strong inhibitory control that prevents the recruitment of low-threshold fibers into the nociceptive network (Peirs & Seal, 2016). However, disruption to this circuitry can result in aberrant sensory experiences such as the development of neuropathic pain and its associated symptoms – allodynia, hyperalgesia or spontaneous pain. Indeed, impairment in inhibitory transmission at the spinal level has been shown to lead to allodynia (Sivilotti & Woolf, 1994; Yaksh, 1989). Central sensitization has been described for the dorsal horn where it manifests as an increase in membrane excitability and synaptic efficacy of neurons, coupled with reduced inhibition in response to inflammation or nerve injury (Latremoliere & Woolf, 2009). While the field has started to probe the functional role of various dorsal horn interneuron populations, our knowledge of the components and the circuitry underlying normal sensory processing and in maladaptive states is still limited. Here I provide an overview of several complementary approaches taken so far to determine dorsal horn cell types.

1.5.1 Morphological and Physiological Classification of Interneurons

As described above for lamina I projection neurons, lamina I interneurons show similar morphological classes i.e., pyramidal, fusiform and multipolar. Pyramidal neurons have a triangular cell body while fusiform neurons have a spindle-shaped cell body with longitudinal bipolar dendrites. Multipolar cells have a polyhedric or cuboidal cell body with four or more primary dendrites (Lima & Coimbra, 1986; Zhang & Craig, 1997; Zhang et al., 1996). There is a strong correspondence between the morphological features and physiological properties of the lamina I neurons (Prescott & De Koninck, 2002). The physiologically defined classes include: tonic cells which fire slowly and in a sustained manner; phasic cells which fire with a high frequency burst; delayed onset cells which show a delay to spike, and single spike cells which fire a single action potential. Fusiform cells are typically tonic, pyramidal cells could be weakly correlated to phasic firing patterns and multipolar cells show delayed or single spiking.

Lamina II neurons have vertical (previously called stalked neurons), radial, central or islet morphology which can all be visualized in the sagittal plane (Grudt & Perl, 2002). Grudt and Perl defined vertical cells as those with distinctive vertical orientation of dendrites. Most vertical cells show tonic or delayed firing patterns, with some firing in a sustained but irregular manner or with high-frequency bursts (Grudt & Perl, 2002). Radial cells have short, compact dendrites that radiate in all directions. All radial cells show a delayed firing pattern with irregular or high-frequency bursts of discharge (Grudt & Perl, 2002). Central cells are found primarily in the middle of the substantia gelatinosa and have dense dendritic arbors that extend in the rostro-caudal direction. Central cells have either tonic or phasic firing patterns. Islet cells

are similar to the central cells but with dendritic arbors that extend for a greater distance in the rostro-caudal direction. All islet cells display tonic firing patterns.

Laminae III-IV neurons have dendritic branches that extend dorsoventrally within these laminae or extend into lamina II and in some cases lamina I. Additionally, in lamina IV, the cells have dendritic trees that look like antennae and are characterized by dendritic spines present predominantly on the dorsal dendrites (Schoenen, 1982; Schoenen & Faul, 2004; Szentagothai, 1964). Laminae III-IV neurons also display tonic, phasic, delayed, irregular, single or reluctant firing patterns (Abraira et al., 2017). Lamina V-VI neurons share similar dendritic morphology where their dendrites extend dorsoventrally. These dorsal and ventral extensions appear to be symmetrical (Schoenen & Faul, 2004).

While morphological and physiological properties may be used to broadly classify neurons of one lamina over another; they are less reliable identifiers of individual cell types because many of the neurons that share electrophysiological features show different morphologies. There is also a significant proportion of lamina II neurons that are “unclassified” in terms of their morphology as they do not fit any of the criteria (Grudt & Perl, 2002). Additionally, there are inconsistencies in the morphological classes of the superficial dorsal horn reported across species when compared to Grudt and Perl’s classification scheme of the hamster dorsal horn (Beal & Cooper, 1978; Gobel, 1978; Price et al., 1979). For example, in the human substantia gelatinosa, islet cells were identified along with filamentous, curly and stellate cells in the sagittal plane. (Schoenen, 1982). Thus, additional features such as the chemoarchitecture of the neurons can be used to define neuron populations.

1.5.2 General Features of Excitatory and Inhibitory Interneurons

Excitatory neurons account for nearly 74% of the total neurons in laminae I-II and 62% of those in lamina III in the rodent (Polgar et al., 2013). Additionally, all excitatory neurons in the dorsal horn are glutamatergic and express VGLUT2 (Oliveira et al., 2003). In lamina II, excitatory interneurons predominantly have vertical or radial morphology (Lu & Perl, 2005; Peirs et al., 2020).

Inhibitory neurons in the dorsal horn use γ-amino butyric acid (GABA) and/or glycine. GABAergic inhibitory interneurons are distributed mainly in laminae II-III, while glycinergic neurons are found in lamina I and laminae III-V (Zeilhofer et al., 2012). There are however, neurons in lamina III that utilize both GABA and glycine (Powell & Todd, 1992). A majority of islet cells are GABAergic, but there are also some central, radial and vertical cells that have been shown to be GABAergic (Maxwell et al., 2007; Zeilhofer et al., 2012). A few islet cells in lamina III are reportedly glycinergic (Maxwell et al., 2007). In short, though all islet cells are inhibitory and display tonic firing patterns; not all inhibitory neurons are islet cells or have tonic firing properties.

The expression of certain transcription factors in the developing spinal cord plays an important role in determining the excitatory versus inhibitory phenotype of dorsal horn neurons. Some of these continue to express in adult such as the paired box gene 2 (PAX2), gastrulation brain homeobox 1 (GBX1), T-cell leukemia homeobox protein 3 (TLX3) and the LIM homeobox transcription factor 1 beta (LMX1B) (Del Barrio et al., 2013). PAX2-expressing neurons co-express genes found in GABAergic neurons such as glutamate decarboxylase 1 and 2 (*Gad1* and *Gad2*), and vesicular inhibitory amino acid transporter

(VIAAT encoded by *Slc32a1*). TLX3- and LMX1B- expressing neurons are glutamatergic as they co-express VGLUT2.

Lu and Perl proposed that a modular organization for dorsal horn neurons exists in which particular combinations of neurons are frequently synaptically connected to amplify, modulate or integrate primary afferent input (Lu & Perl, 2005). From whole-cell recordings in sagittal slices, they observed unidirectional excitatory connections between transient central cells of lamina II_i to vertical cells of lamina II_o. Interestingly, they also observed functional excitatory connections between the vertical cells of lamina II_o to lamina I neurons, thereby confirming previous assumptions obtained from morphological and physiological correlations. (Bennett et al., 1980; Gobel, 1978; Lu & Perl, 2005).

1.5.3 Non-overlapping Classes of Neuropeptides and Other Populations

Examination of genes differentially expressed between excitatory and inhibitory mouse dorsal horn neurons show that apart from those related to neurotransmitter synthesis and signaling (*Slc17a6*, *Gad1*, *Gad2* etc.), there is an enrichment of genes encoding neuropeptides, particularly in excitatory neurons (Das Gupta et al., 2021). In total, 13 neuropeptide genes were found to be specifically enriched in excitatory neurons and 3 in inhibitory neurons. These include adenylate cyclase activating polypeptide (*Adcyap1*), *Cck*, *Crh*, gastrin releasing peptide (*Grp*), *Nmb*, neuropeptide FF (*Npff*), neuromedin S (*Nms*), neuromedin U (*Nmu*), neurotensin (*Nts*), *Tac1*, *Tac2*, thyrotropin releasing hormone (*Trh*), urocortin 3 (*Ucn3*) among the excitatory neurons and prepronociceptin (*Pnoc*), neuropeptide Y (*Npy*) and prodynorpin (*Pdyn*) among the inhibitory neurons. Interestingly, *Cck*, *Tac1, Grp, Tac2, Npff,* and *Nts* show largely

non-overlapping mRNA expression profiles that are spatially restricted to one or two dorsal laminae from *in situ* hybridization experiments (Das Gupta et al., 2021). In contrast, other genes – *Adcyap1*, *Crh*, *Nmb* and *Nms* show widely distributed but weak or no mRNA expression *in situ*. Thus, this review will focus instead on what is known about the neurons that express the remaining 12 neuropeptide genes, in addition to other classically studied populations of the mouse dorsal horn.

1.5.3.1 CCK Neurons

CCK is expressed predominantly by interneurons and as a recent study discovered, is also expressed by a small population of projection neurons (Abraira et al., 2017; Gutierrez-Mecinas, Bell, Shepherd, et al., 2019; Peirs et al., 2021; Wercberger et al., 2021). These neurons are concentrated in laminae II_i-IV (Gutierrez-Mecinas, Bell, Shepherd, et al., 2019; Peirs et al., 2021). CCK neurons display a unique combination of morphological and physiological features that distinguish them from other interneurons present in laminae II_i-IV (Abraira et al., 2017). They reportedly show phasic and regular spiking action potential discharge patterns from whole-cell patch clamp recordings of sagittal slices, and receive Aδ-LTMR and Aβ-LTMR primary afferent input, in addition to descending cortical and local interneuron input (Abraira et al., 2017; Liu et al., 2018; Peirs et al., 2021). Genetic ablation of CCK neurons resulted in a reduction in paw withdrawal response to noxious stimuli (pinprick stimulation) as well as innocuous stimuli (evoked by brush) (Gatto et al., 2021). A single-cell RNA-seq study of the mouse dorsal horn assigned *Cck* as a major marker gene of a population of excitatory neurons (Haring et al., 2018). This population could be further split into three

subsets (Marked by *Cpne4*, *Maf* or *Trh* expression) based on the similarity of their gene expression profiles (Haring et al., 2018). Interestingly, chemogenetic silencing of the *Cpne4* and *Maf* subsets of CCK neurons resulted in a reversal in static and dynamic mechanical allodynia produced by inflammatory or neuropathic injury (Peirs et al., 2021). Furthermore, activation of these same neurons produced a marked decrease in the paw withdrawal latency in the Hargreaves thermal assay, suggestive of a role in heat hypersensitivity (Peirs et al., 2021). A study by Liu et al showed that corticospinal inputs descending from S1/S2 somatosensory cortex potentially facilitate mechanical allodynia by providing excitatory synaptic input to CCK interneurons (Liu et al., 2018).

A sub-population of CCK neurons express VGLUT3 transiently (tVGLUT3) during development. Ablation of VGLUT3-lineage neurons resulted in an increase in baseline mechanical threshold measurements and a decrease in response to dynamic brush stimuli (Cheng et al., 2017). Chemogenetic silencing of tVGLUT3 neurons did not affect acute somatosensory behaviors except for a shorter latency to the sticky tape assay, similar to what was seen with CCK neurons (Peirs et al., 2021). Under inflammatory or nerve injury, chemogenetic silencing of tVGLUT3 neurons reversed dynamic allodynia but not static allodynia. Importantly, this behavioral phenotype appears to be mediated primarily by the *Maf* subset of CCK neurons (Peirs et al., 2021). Of note, pharmacological disinhibition using inhibitory antagonists- strychnine and bicuculline in transverse spinal cord slices of global VGLUT3 KO mice abolished polysynaptic EPSCs in lamina I NK1R projection neurons (Peirs et al., 2015). Thus, both tVGLUT3 as well as CCK neurons play an important role in converting touch to pain through dorsally directed polysynaptic pathways.

1.5.3.2 TRH Neurons

TRH neurons are sparsely distributed in lamina II_i and the dorsal region of lamina III (Gutierrez-Mecinas, Bell, Shepherd, et al., 2019; Peirs et al., 2021). Nearly 85% of *Trh*-expressing neurons overlap with *Cck*; however, only a small population of *Cck* neurons co-express *Trh* with *in situ* hybridization (Das Gupta et al., 2021; Gutierrez-Mecinas, Bell, Shepherd, et al., 2019). The *Trh* subset of CCK neurons was not chemogenetically targeted in the behavioral experiments conducted in CCK^{Cre} mice by Peirs et al, thus the functional role of these neurons remains to be characterized (Peirs et al., 2021). However, almost all TRH neurons (91%) co-express protein kinase c gamma (PKCγ).

1.5.3.3 PKCγ Neurons

Early studies recognized PKCγ interneurons as a distinct excitatory population since PKCγ immunoreactivity showed a concentrated plexus consisting of cell bodies and their dendrites in lamina II_i and III, with sparse labeling in lamina I and deeper laminae of the rodent dorsal horn (Mori et al., 1990; Polgar et al., 1999). Subsequent characterization of these interneurons, especially by transcriptomic studies, revealed that these neurons were more diverse than originally assumed, and therefore composed of multiple sub-populations (Abraira et al., 2017; Gutierrez-Mecinas et al., 2016; Haring et al., 2018). However, a consensus has not been reached in the classification of PKCγ neurons. Haring et al detected *Prkcg* mRNA across several of the dorsal horn excitatory clusters while Sathyamurthy et al highlighted a single

cluster (DE-4) containing nuclei with high and specific expression of *Prkcg* along with calbindin (*Calb1*) (Haring et al., 2018; Sathyamurthy et al., 2018). A recently conducted meta-analysis merged six published transcriptomic datasets of the postnatal mouse spinal cord which includes the Haring and Sathyamurthy datasets, in order to reconcile the differences arising from the studies (Russ et al., 2021). The meta-analysis assigned two clusters (Excit 03-04) to a family that was defined by *Prkcg* expression and this *Prkcg* family contains nuclei that also express neuropeptide genes- *Cck*, *Trh*, *Sst* and *Nts* in varying proportions. This analysis is further complicated by results from a different study in which ~25% of PKCγ neurons overlap with PPTB (Encoded by *Tac2*) (Gutierrez-Mecinas et al., 2016). Thus, it remains to be seen how the different neuropeptide subsets of the larger PKCγ population coordinate to contribute to sensory processing within the dorsal horn.

As expected, PKCγ neurons show diverse morphological features with a majority being central cells but radial, vertical, unclassified and even islet cells have been observed, indicative of a small population of inhibitory PKCγ neurons (Peirs et al., 2021; Wang et al., 2020). PKCγ neurons display tonic, phasic, irregular, as well as delayed spiking patterns in response to current injection (Abraira et al., 2017; Peirs et al., 2021; Wang et al., 2020). They receive input from Aβ-, Aδ-, and C-LTMR primary afferents, other excitatory and inhibitory interneurons, and also from descending serotonergic pathways (Abraira et al., 2017; Alba-Delgado et al., 2018; Lu et al., 2013; Peirs et al., 2021; Peirs et al., 2015; Wang et al., 2020).

Interestingly, mice with a deletion in the gene that encodes for PKCγ show normal acute nociceptive behavior, but a reduction in mechanical and thermal hypersensitivity following partial nerve injury (Malmberg et al., 1997). Mechanical allodynia induced by strychnine was reversed by intracisternal administration of a PKCγ inhibitor in rats, providing further evidence for the involvement of the PKCγ enzyme in allodynia (Miraucourt et al., 2007). In 2013, Lu et al demonstrated that PKCγ interneurons receive subthreshold Aβ fiber input under

physiological conditions but are gated by feedforward inhibition from lamina III glycinergic interneurons using patch-clamp recordings (Lu et al., 2013). However, disinhibition by application of strychnine or following peripheral nerve injury, Aβ fiber activation produces action potential firing in PKCγ interneurons (Lu et al., 2013; Wang et al., 2020). Furthermore, they proposed that in the onset of injury, the PKCγ interneurons provide excitatory synaptic input to lamina II transient cells which synapse on to vertical cells and eventually activate NK1R projection neurons (Lu et al., 2013). Additionally, inhibitory interneurons which express the receptor tyrosine kinase (RET) in laminae III-V early in development are thought to provide fee-forward glycinergic input to PKCγ neurons (Cui et al., 2016). Peirs et al demonstrated for the first time that acute inhibition of the PKCγ interneurons themselves reverses static and dynamic allodynia following neuropathic injury but not inflammatory injury in mice (Peirs et al., 2021; Peirs et al., 2015). Thus, there is overwhelming evidence showing that PKCγ interneurons are critical to the allodynia circuitry and that neuronal populations belonging to this circuitry are differentially recruited depending on the injury type (Peirs et al., 2020; Peirs et al., 2021).

1.5.3.4 NTS neurons

As mentioned above, NTS neurons form a sub-population of PKCγ neurons (~90% co-express PKCγ) and are primarily found in lamina II_i and III (Das Gupta et al., 2021; Gutierrez-Mecinas et al., 2016). Though this population has not been specifically targeted in persistent pain models, we could speculate that it shares functional features with the larger PKCγ population. One study demonstrated that NTS-lineage neurons are sufficient for wind-up in

lamina I spinoparabrachial neurons (Hachisuka et al., 2018). Wind-up is defined as a type of facilitation that causes the response to repetitive stimulation of peripheral C-fibers to increase with each stimulus (Herrero et al., 2000). Studies have speculated that in the context of injury, wind-up or amplification of dorsal horn neurons to nociceptive input, could contribute to central sensitization leading to hyperalgesia. However, these mechanisms are poorly understood. Activation of NTS-lineage neurons resulted in an increase in paw withdrawal response to brush stimulus; but ablating these neurons had no effect on paw withdrawal responses to pinprick or brush assays (Gatto et al., 2021). It should be noted however, that the neurotensin-lineage neurons capture a broader population than what has been observed by NTS protein expression in adult mice (Gutierrez-Mecinas et al., 2016).

1.5.3.5 TAC1 Neurons

TAC1 neurons are found primarily in the superficial dorsal horn, and to a lesser extent in the deeper dorsal horn (Dickie et al., 2019; Gutierrez-Mecinas et al., 2018). They are predominantly excitatory neurons but a small proportion of inhibitory neurons have also been observed to express *Tac1* or the protein it encodes- substance-P (Gutierrez-Mecinas et al., 2018; Haring et al., 2018; Sathyamurthy et al., 2018). A majority of substance-P expressing neurons in the superficial dorsal horn are radial cells with delayed firing patterns (Dickie et al., 2019). Interestingly, apart from interneurons and anterolateral tract projection neurons, there are substance-P expressing excitatory neurons that provide propriospinal input to the LSN (Gutierrez-Mecinas et al., 2018). As mentioned earlier in the review under projection neurons, the role of TAC1 neurons has been broadly investigated in the context of acute or sustained

pain (Gutierrez-Mecinas et al., 2018; Huang et al., 2019). The presynaptic inputs to and postsynaptic targets of TAC1 neurons also remain to be identified, though there is some evidence suggesting that substance-P expressing neurons receive synaptic input mainly from other excitatory interneurons, and to a lesser extent from descending input and/or unmyelinated nociceptive fibers (potentially a subset of TRPV1 fibers) (Gutierrez-Mecinas et al., 2018; Haring et al., 2018).

1.5.3.6 GRP Neurons

Grp is expressed by excitatory neurons (90% of *Grp* neurons overlap with VGLUT2) in lamina II with sparse distribution in lamina III (Das Gupta et al., 2021; Sun et al., 2017). They are predominantly central cells with transient or single-spiking firing patterns (Albisetti et al., 2019; Dickie et al., 2019). Studies surrounding GRP neurons and neurons expressing its associated receptor-GRPR have challenged how itch versus pain is coded. Evidence for labeled-line transmission can be seen from the existence of a class of itch-specific unmyelinated neurons that respond to multiple chemical pruritogens (chloroquine, BAM 8-22 and SLIGRL), and express *MrgprA3* (Han et al., 2013; Liu et al., 2009). Additionally, these *MrgprA3* primary sensory neurons form synapses with GRPR neurons in the dorsal horn (Han et al., 2013). Ablation of *MrgprA3* primary sensory neurons or GRPR dorsal horn neurons reduce or completely abolish itch response but spares pain response (Han et al., 2013; Sun et al., 2009). One study challenged the view of *MrgprA3* as a labeled-line for itch since at the cellular level these primary sensory neurons are polymodal, and they proposed instead that these neurons recruit different ion channels and engage divergent spinal cord pathways

depending on the nature of stimulation (Sharif et al., 2020). *Grp* dorsal horn neurons receive monosynaptic input from *MrgprA3* primary afferents as well as other nociceptors (Sun et al., 2017). Another study observed that in GRP::eGFP mice which express eGFP only in a subset of *Grp* neurons, eGFP expressing cells receive excitatory synapses from *MrgprA3*, *Mrgprd* and *VGLUT3* (for cells in lamina II_i) expressing primary afferents (Bell et al., 2020). Sun et al demonstrated using mice where TRPV1 was exclusively expressed by *Grp* dorsal horn neurons, that increasing doses of intrathecal capsaicin (Acts through TRPV1) prolong the duration of pain and itch response; however, pain responses decrease at very high capsaicin doses while itch responses reach a plateau (Sun et al., 2017). Thus, they postulated a 'leaky gate' model in which GRP neurons positively code for itch whereas high-intensity stimulation of these neurons evokes a feedforward inhibition through enkephalin release to dampen pain transmission. However, partial ablation of GRP neurons reduced itch responses but did not alter thermal or mechanical nociceptive responses (Albisetti et al., 2019). Therefore, while GRP neurons show a potential involvement in the spinal relay of itch signals, the circuitry underlying this mechanism requires further investigation.

1.5.3.7 UCN3 Neurons

Ucn3 interneurons overlap extensively with *Cck* and *Trh* and are present in lamina III (Das Gupta et al., 2021). Ucn3-lineage neurons co-express PKCγ, calbindin, calretinin and NPY receptor (NPY1R) in varying proportions (Pan et al., 2019). Additionally, a majority of these neurons displayed initial bursting firing patterns. Mechanically evoked itch which has been observed in humans as well as in mice is distinct from chemical itch (Akiyama et al.,

2012; Fukuoka et al., 2013). Genetic silencing of dorsal horn *Ucn3*-lineage neurons attenuated mechanical itch responses without affecting touch, thermal or pain sensation (Pan et al., 2019). These neurons reportedly receive synaptic input from TLR5 expressing Aβ-LTMRs and are gated by NPY inhibitory interneurons (Pan et al., 2019).

1.5.3.8 TAC2 and NMU Neurons

Single-cell and single-nucleus RNA-sequencing studies of the mouse dorsal horn combined with *in situ* hybridization identified two distinct populations of *Tac2* neurons- those that co-express *Nmu* and those that don't (Haring et al., 2018; Sathyamurthy et al., 2018). Both populations are present in lamina II and to a lesser extent in lamina III. *Tac2*-lineage neurons in lamina II_i which may include the *Nmu* subset, display delayed firing, initial firing, tonic firing and phasic firing patterns and chiefly receive Aδ and C-fiber input. In contrast, *Tac2*-lineage neurons in lamina III mostly show phasic-bursting firing and receive Aβ-fiber input (Chen et al., 2020). These lineage neurons are thought to be involved in mechanical itch transmission under naïve as well as dry itch conditions (Chen et al., 2020). It is likely that that the developmental *Ucn3* neurons and *Tac2* neurons are engaged in the same spinal circuitry to drive mechanical itch; however, it is less clear if there is redundancy in their functional roles.

Moreover, it has been reported that nearly 84% of neurokinin B (NKB – encoded by the *Tac2* gene) neurons in laminae I-II show calretinin immunoreactivity (Gutierrez-Mecinas, Davis, et al., 2019). Excitatory calretinin neuron neurons have been shown to be important for the transmission of mechanical allodynia induced by inflammatory pain (Peirs et al., 2021; Peirs et al., 2015). Ablation of *Tac2*-lineage neurons did not alter acute somatosensory

phenotypes nor pain behavior following nerve injury; however, it remains to be seen if *Tac2* neurons relay touch-evoked pain in inflammatory pain conditions (Duan et al., 2014).

1.5.3.9 Calretinin Neurons

Calretinin neurons are mostly excitatory (~85%) and account for 30-40% of the total neurons in the superficial dorsal horn (Gutierrez-Mecinas, Davis, et al., 2019; Smith et al., 2015; Smith et al., 2016). This population is molecularly heterogeneous and thus could be classified into molecular subsets based on overlap with TAC1, NKB, GRP or PKCγ (Gutierrez-Mecinas, Davis, et al., 2019). Alternatively, Smith et al described two distinct subsets of calretinin neurons based on their morphological and electrophysiological properties; the excitatory subset consisting of central, vertical or radial cells with predominantly delayed firing patterns, and the inhibitory subset consisting mainly of islet cells with tonic firing patterns (Smith et al., 2015). In general, calretinin neurons receive Aδ- and C-fiber input (Peirs et al., 2021). Additionally, the excitatory calretinin neurons receive GABAergic and glycinergic inhibitory input and respond to noradrenaline and serotonin, while inhibitory calretinin neurons mainly receive glycinergic input and respond to enkephalin (Smith et al., 2016). Calretinin neurons are thought to be involved in several polysynaptic pathways or microcircuits (Peirs et al., 2021; Smith et al., 2019). There is circumstantial evidence showing that calretinin neurons receive excitatory input from deep dorsal horn neurons, and either directly or through polysynaptic pathways involving somatostatin-expressing neurons recruit lamina I projection neurons (Peirs et al., 2015; Smith et al., 2019). Optogenetic and chemogenetic activation of calretinin neurons *in vivo* evoked nocifensive behavior (Peirs et al., 2015; Smith et al., 2019).

Viral inhibition of calretinin neurons had no effect on acute somatosensory behaviors but produced a significant reversal in static and dynamic allodynia induced by inflammatory injury but not nerve injury (Peirs et al., 2021).

1.5.3.10 NPFF Neurons

NPFF is exclusively expressed by excitatory interneurons in laminae I and II_o (Gutierrez-Mecinas, Bell, Polgar, et al., 2019). Approximately ~38% of *Npff* neurons overlap with *Grp* and 85.3% with somatostatin (Gutierrez-Mecinas, Bell, Polgar, et al., 2019). Though poorly characterized, NPFF neurons do reportedly show p-ERK immunoreactivity (suggestive of activation) in response to noxious stimuli (Gutierrez-Mecinas, Bell, Polgar, et al., 2019).

1.5.3.11 SST Neurons

Single-cell and single-nucleus RNA-sequencing studies show that *Sst* mRNA is detected in virtually all excitatory clusters and may also be expressed by some inhibitory neurons (Chamessian et al., 2018; Haring et al., 2018; Sathyamurthy et al., 2018). Consequently, SST neurons are heterogeneous and composed of several of the populations already discussed above. Genetic ablation of somatostatin-lineage neurons dramatically reduced acute pain responses and mechanical (both static and dynamic) allodynia following

inflammatory and nerve injury (Duan et al., 2014). SST neurons may also be involved in chemical itch transmission (Fatima et al., 2019).

1.5.3.12 NPY Neurons

Inhibitory dorsal horn neurons have traditionally been divided into 5 largely non-overlapping populations based on their expression of neurochemical markers – NPY, parvalbumin (PV), DYN, calretinin, and neuronal nitric oxide synthase (nNOS) (Boyle et al., 2017). NPY neurons are thought to account for ~33% of inhibitory neurons in laminae I-II and 25% of those in lamina III. A majority of *Npy*-lineage neurons display tonic firing patterns (Bourane et al., 2015). Another study used NPY-GFP mice to characterize the morphological properties of NPY neurons (Iwagaki et al., 2016). However, in these mice GFP immunoreactivity overlapped with only 33% of NPY neurons in laminae I-II but overlapped with ~82% of NPY neurons in lamina III, thus it marks only a subset of NPY neurons. Surprisingly, the GFP expressing neurons showed unique morphological features that did not fit into any of the standard classes and hence may be grouped under the 'unclassified' class (Iwagaki et al., 2016). Ablation and chemogenetic silencing of *Npy*-lineage neurons in mice resulted in scratching evoked by low-threshold mechanical stimuli (Bourane et al., 2015). It did not however alter baseline mechanical thresholds or increase mechanical allodynia following inflammatory injury. Yet another study attempted to target the NPY neurons using a custom virus (AAV9.NpyP.tdTomato) approach in rats (Tashima et al., 2021). However, only ~40% of the tdTomato reporter-expressing cells showed NPY immunoreactivity. Thus, while there is some evidence implicating a role for NPY neurons in gating mechanical itch and

perhaps mechanical allodynia, specific and efficient targeting of these neurons must be achieved before meaningful conclusions can be drawn.

1.5.3.13 PV Neurons

PV interneurons can be found in laminae II_i and III with a vast a majority of them (~70%) containing GABA and glycine (Abraira et al., 2017). Diverse approaches such as a sophisticated classifier based on morphological features or Brainbow-labeling have been applied to distinguish between the morphological characteristics of excitatory and inhibitory PV interneurons (Abraira et al., 2017; Gradwell et al., 2021). Inhibitory PV neurons reportedly have a larger soma and dendritic arbors that extend further along the rostro-caudal axis than their excitatory counterpart (Gradwell et al., 2021). PV interneurons mainly exhibit tonic firing and, in some cases, initial bursting firing patterns (Gradwell et al., 2021).

Of note, inhibitory PV interneurons form a significant number of axoaxonic contacts with myelinated LTMRs (Except C-LTMRs) from glabrous as well as hairy skin (Abraira et al., 2017; Boyle et al., 2019; Hughes et al., 2012). Optogenetic activation of PV neurons in slices taken from PV;Ai32 mice result in monosynaptic as well as polysynaptic optogentically-evoked postsynaptic currents (Gradwell et al., 2021). Interestingly, for inhibitory PV neurons, bath application of bicuculline ($GABA_AR$ antagonist) diminished some optically-evoked inhibitory postsynaptic currents (oIPSCs); while application of strychnine (GlyR antagonist) reduced most of the oIPSCs, indicating that postsynaptic inhibition is mediated predominantly by glycine. There is also circumstantial evidence showing that PV interneurons provide convergent inhibition of vertical cells either directly or through presynaptic inhibition of

myelinated primary afferents (Boyle et al., 2019). Collectively, these findings suggest that PV interneurons gate innocuous and noxious input under physiological conditions. Indeed, chemogenetic activation of PV neurons in PV::Cre;tdTomato mice increased baseline mechanical thresholds and attenuated mechanical allodynia following nerve injury (Petitjean et al., 2015). Ablation of these neurons with intrathecal administration of saporin induced mechanical allodynia. While Petitjean et al speculated that this could be due to loss of inhibitory control of PKCγ neurons and reported a reduction in the number of contacts between PV terminals and PKCγ cell bodies following nerve injury, further studies are needed to investigate if functional connections exist between both neuron populations (Petitjean et al., 2015). Interestingly, optogenetic activation of excitatory PV neurons, many of which co-express *Cck* (74.5%), resulted in cFos (neuronal activity marker) expression in lamina I-II_o neurons, which suggests that excitatory PV neurons engage nociceptive circuits in the superficial dorsal horn (Gradwell et al., 2021).

1.5.3.14 DYN Neurons

DYN neurons are mainly present in laminae I-II, and a majority are GABAergic though a glycinergic subset has also been detected (Boyle et al., 2017; Duan et al., 2014). Most galanin cells are found to co-express DYN (Boyle et al., 2017). Surprisingly, excitatory dynorphin neurons are restricted to the medial half of the dorsal horn in the L4 segment, which receives input from glabrous skin (Boyle et al., 2017). In the rat however, excitatory dynorphin neurons are distributed mediolaterally (Sardella et al., 2011). As expected DYN inhibitory neurons display tonic firing patterns (Duan et al., 2014). DYN neurons in lamina I and II_o reportedly

receive monosynaptic and polysynaptic Aβ fiber input. Additionally, there are vertical cells expressing DYN that send dendrites to laminae III-IV, where they may receive direct Aβ fiber input (Duan et al., 2014). Ablation of inhibitory DYN neurons in the dorsal horn and in the hindbrain Sp5 nucleus resulted in development of static and dynamic mechanical allodynia (Duan et al., 2014). The functional role of excitatory DYN neurons is not clear, though there is some evidence indicating that these neurons may be involved in regulating acute phase hyperalgesia (Sapio et al., 2021; Varga et al., 2021).

The transcription factor BHLHB5 is expressed in several dorsal horn neuron populations during embryonic and early postnatal development (Ross et al., 2010). Approximately 33% of the BHLHB5 expressing neurons were identified as excitatory (Ross et al., 2010). *Bhlhb5* knockout mice developed skin lesions and exhibited heightened scratching behavior in responses to pruritic agents (Ross et al., 2010). Of note, the inhibitory subset of BHLHB5 neurons were thought to be responsible for the itch phenotype. The same study reported that baseline somatosensory responses and development of mechanical allodynia induced by an inflammatory agent (carrageenan) were unaffected in the *Bhlhb5* knockout mice. Investigation of the neurochemical markers co-expressed by BHLHB5 neurons revealed that a significant proportion show immunoreactivity to the somatostatin receptor sst_{2A}, galanin/dynorphin and nNOS, implicating a role for these sub-populations in mediating itch (Kardon et al., 2014). Indeed, a more recent study showed that chemogenetic inhibition of DYN dorsal horn neurons in mice results in spontaneous itch (Nguyen et al., 2021). Nguyen et al proposed that intrathecal administration of morphine causes itch through disinhibition of DYN neurons. Thus, the exact mechanisms through which DYN neurons inhibit nociceptive and/or itch circuits remain unknown.

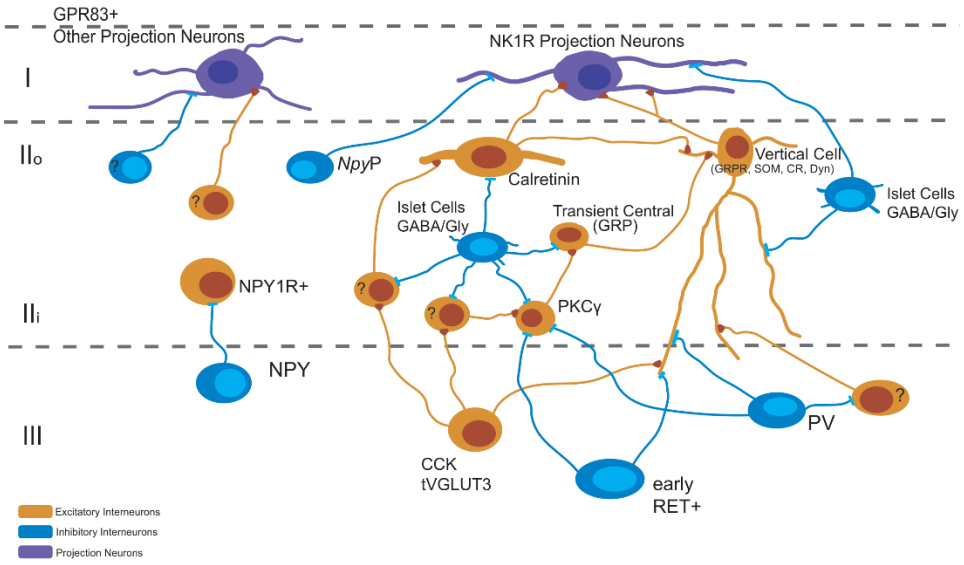

Figure 2. Schematic Representation of Dorsal Horn Excitatory Neuron Populations Important for Pain Transmission.

Neurons that express calretinin (CR), tachykinin 1 (TAC1), tachykinin receptor 1 (TACR1), G-protein-coupled receptor 83 (GPR83), cholecystokinin (CCK), protein kinase c gamma (PKCγ) and neurotensin (Nts) are found within the dorsal horn of spinal cord. CR neurons are found primarily in outer lamina II. Tac1 and Tacr1 are expressed in both interneurons as well as projection neurons while Gpr83 projection neurons are present mainly in lamina I. PKCγ neurons situated in inner lamina II and lamina III mostly co-express CCK or NTS. Circles depict interneurons and squares depict projection neurons. Circles with two colors represent overlap between the two respective populations.

1.5.4 Other Classification Schemes

Several other classification schemes for dorsal horn neurons have been proposed in addition to what has been described above. One study identified 11 interneuron populations including those expressing CCK, Calretinin, PKCγ and PV located in lamina II_i-IV, based on their unique combination of morphological, electrophysiological and synaptic properties

(Abraira et al., 2017). Another study proposed that sensorimotor reflex modules follow a laminar organization in which laminae I-II neurons are involved in protective scratch responses, laminae II-III neurons contribute to paw withdrawal behavior, and laminae III-IV neurons are involved in corrective motor movements (Gatto et al., 2021).

1.6 Summary

The molecular diversity and functional complexity of the dorsal horn neurons highlight the numerous potential targets available for the treatment of chronic pain and itch conditions. Yet we have seen in the Introduction that many of the neuron populations that have been characterized are defined by a neurochemical marker that labels a heterogeneous population (E.g., PKCγ neurons) or a developmental population that shows restricted or no expression in the adult (E.g., *Ucn3* neurons). Thus, a consensus in molecularly distinct dorsal horn cell-types and their organization is required to reliably determine whether these molecularly discrete cell types function as labeled-lines or work together to form functional modules along the dorsoventral axis of the dorsal horn. Also, of consequence for translational utility, is an understanding of the cellular and molecular organization of the primate dorsal horn. Transcriptomic studies of human and non-human primate DRG neurons revealed important differences in gene expression compared to mouse DRG neurons (Kupari et al., 2021; Middleton et al., 2021; Ray et al., 2018).

Thus, a goal of my thesis is to perform snRNA-seq of the Rhesus macaque dorsal horn to identify the major cell types present as well as their laminar organization. A subsequent goal is to compare the identified macaque neuronal cell types with the mouse meta-analysis derived cell types to develop a species-independent cellular and molecular classification scheme of dorsal horn neurons (Russ et al., 2021). I also examined the laminar distribution of neuropeptides in macaque and human dorsal horn to see if a neuropeptide code such as that observed in mouse dorsal horn exists (Das Gupta et al., 2021).

While there has been great advancement in our ability to manipulate specific populations using transgenic mice and Cre-dependent viral strategies, there are still limitations in targeting select populations with specificity (Arokiaraj et al., 2022). Additionally, to translate mouse dorsal horn findings to non-human primate for proof-of-principal studies, we require Cre-independent tools that can efficiently target distinct neuron populations. Thus, a third goal of my thesis is to establish a resource of potential regulatory elements (REs) present in the biologically active regions of the genome using single nuclear Assay for Transposase-Accessible Chromatin combined with sequencing (snATAC-seq) (Buenrostro et al., 2015). Putative REs can then be used in future experiments to drive gene expression in specific dorsal horn neuron populations across species, and in a Cre-independent manner using viral vectors for delivery.

2.0 Single Nuclear RNA-sequencing of the Macaque Dorsal Horn

2.1 Introduction

The spinal cord dorsal horn is a principal site for somatosensory integration and transmission not only for normal sensory processing but also for maladaptive states such as chronic pain (Hughes & Todd, 2020; Koch et al., 2018; Peirs & Seal, 2016). Classification schemes to describe neurons in the dorsal horn were initially based on major nuclear groups that were organized in a dorsoventral orientation starting with the most dorsal edge, also known as the marginal layer, followed by the substantia gelatinosa, the nucleus proprious and the Dorsal Nucleus of Clarke. Bror Rexed in the early 1950's, took into account the lamination pattern of the neuronal cytoarchitecture, and redefined the classification as layers or laminae that likewise extended dorsoventrally (Rexed, 1952).

Consistent with a laminar organization underlying a functional organization, central terminals of functionally distinct classes of primary afferent fibers terminate within specific laminae. Unmyelinated or lightly myelinated primary sensory neurons that sense temperature or noxious stimuli terminate primarily in laminae I-II but some also send fibers to lamina V (Al-Chaer et al., 1999; Al-Khater et al., 2008; Christensen & Perl, 1970; Lima et al., 1993; Lima & Coimbra, 1986). Unmyelinated primary sensory neurons that transmit information related to itch or innocuous mechanical stimuli terminate in lamina II, while myelinated fibers that carry innocuous, tactile information terminate in inner lamina II to V, also known as the

low threshold mechanoreceptor-recipient zone (LTMR-RZ) (Abraira et al., 2017; Arcourt et al., 2017; Bai et al., 2015; Koch et al., 2018; Li et al., 2011; Light et al., 1979). Lastly, myelinated afferent fibers that are primarily involved in proprioceptive pathways terminate in the deeper dorsal horn which includes lamina VI in cervical and lumbosacral enlargements, and in the ventral horn (Maxwell & Bannatyne, 1983; Maxwell & Riddell, 1999; Mears & Frank, 1997). Thus, each lamina of the dorsal horn receives distinct modalities of sensory input (Gatto et al., 2021).

Within the Rexed laminae are diverse types of interneurons and projection neurons that make up the spinal microcircuits. The precise classification of individual cell types is critical for delineating how the dorsal horn processes sensory information. Historically, interneurons have been classified by their location, morphology, neuronal connectivity, neurotransmitter and neurochemical type, and action potential firing patterns (Abraira et al., 2017; Boyle et al., 2017; Chisholm et al., 2021; Graham & Hughes, 2020; Grudt & Perl, 2002; Gutierrez-Mecinas et al., 2016; Lima et al., 1993; Lima & Coimbra, 1986; Maxwell et al., 2007; Todd, 2017). However, even taking into consideration these features, the neurons remain highly heterogeneous.

To determine the molecular cell types of the primate dorsal horn, we generated a high-resolution single-nucleus transcriptomic map from Rhesus macaque. Owing to their close evolutionary relationship to humans, nonhuman primates constitute an attractive animal model for research. This work therefore provides an essential resource for fundamental mechanistic investigations of non-human primate somatosensory processing as well as for translational studies.

2.2 Methods

2.2.1 Macaque spinal cord samples

All lumbar spinal cord samples used in this study were obtained from *Macaca mulatta* provided by Dr. David Lewis at the University of Pittsburgh. The macaques were cared for under the guidelines of the National Institute of Health. No prior manipulations to the spinal cord were conducted in these macaques. Three 3-year-old male macaques (Identifiers: 93-17, 94-17, and 95-17) were used for single nuclear RNA-sequencing. Male and female macaque lumbar spinal cord samples (Identifiers: 93-17, 94-17, 95-17, 337-16: Female-5 years, 328-16: Female-5 years, 338-16: Female-4 years, 88-17: Male-4 years, 89-17: Male-4 years) were utilized for *in situ* hybridization studies. Though we did not observe sex differences for any of the genes using *in situ* hybridization, there is not enough statistical power to confidently assess if there are sex differences due to the limited availability of macaque tissue.

2.2.2 Nuclear isolation and dissociation

Snap-frozen lumbar spinal cord segments were removed from -80ºC storage and placed into separate Petri dishes containing a cold slurry of dissection buffer consisting of 1x Phosphate Buffered Saline (PBS, ThermoFisher Scientific; AM9625), 10% Dithiothreitol (DTT, Sigma; 43816-50ML). From each animal, transverse sections (~50-75 mg) were made

using a sterile razor blade. Three sections were selected for further dissection and the rest were discarded. The sections were cut in the coronal plane at the middle of the spinal cord to obtain dorsal and ventral halves. Any residual meningeal membranes were removed. The three dorsal halves were retained and the ventral halves discarded. Nuclei were isolated according to Martelotto with some modifications (Martelotto, 2020).The dorsal halves for each animal were transferred into separate Dounce homogenizers (Sigma) containing 1 mL of ice-cold homogenization buffer consisting of EZ Nuclei Lysis Buffer (Sigma; NUC101-1KT) with 0.5% RNasin Plus (Promega; N2615), 0.5% SUPERase-In (ThermoFisher; AM2696) and 1mM DTT. The samples were homogenized on ice using 20 strokes of Pestle A followed by 20 strokes of Pestle B. Any residual meningeal membrane was removed before switching pestles. The homogenate was filtered through a 50 μm filter (Sysmex; 04-004-2327) into a 2 mL microcentrifuge tube (Eppendorf; 022431048). An additional 0.5 mL of homogenization buffer was used to wash the Dounce homogenizer and filter. The sample was then placed on ice while the remaining samples were processed. The sample was centrifuged at 500g at 4ºC for 5 min to obtain a crude pellet containing spinal nuclei. The supernatant was removed and discarded, being careful to not disturb the pellet. The pellet was resuspended in 1.5 mL of Homogenization Buffer and allowed to sit on ice for 5 mins. The samples were again centrifuged at 500g, 4ºC for 5 min. The supernatant was removed and the pellet was resuspended in 1 mL of Nuclei Resuspension Buffer (NRB) consisting of 1x PBS, 1% Bovine Serum Albumin (BSA, Sigma; 2905-5GM) and 1% SUPERas-In followed by centrifugation at 500g, 4ºC for 5 mins. This wash step was repeated twice more for a total of 3 washes. The final pellet was resuspended in 0.5 mL of NRB containing 6 μM 4′,6-diamidino-2-phenylindole, dihydrochloride (DAPI, ThermoFisher; D1306). The suspension was filtered through a 20 μm filter (Sysmex; 04-004-2325) into a polypropylene tube and kept on ice.

Fluorescence Activated Nuclear Sorting (FANS) was performed to purify nuclei from debris on a FACSAria II (BD). Gates were set to isolate $DAPI^+$ singlet nuclei based on forward scatter and side scatter as well as fluorescence intensity. The instrument was set to 40 pounds per square inch (psi) of pressure and a 70 µm nozzle was used, with sterile PBS sheath fluid. Nuclei were sorted into a 1.5 ml microcentrifuge tube containing 15 µl of NRB at 4ºC. For each sample, 18,000 events were sorted into the collection tube. The sorted nuclei and NRB total volume were approximately 45 µl, allowing for the entire loading of the suspension into the Chromium Single Cell 3' v3 solution (10x Genomics) without any further manipulation. 10x libraries were processed according to the manufacturer's instructions. Completed libraries were run on the Novaseq 6000 (Illumina).

2.2.3 Data and Statistical Analysis

2.2.3.1 Alignment

Bcl files were converted to fastq format using the *cellranger mkfastq* command line tool. Fastq reads were then aligned to Mmul10 genome and quantified into a raw UMI count matrix using the STAR aligner with the -solo option (Dobin et al., 2013). A custom transcriptome annotation that we previously developed was also given as input to the STAR aligner (He et al., 2021).

2.2.3.2 Quality control filtering

Each biological replicate underwent a separate but standardized quality control (qc) filtering, whereby empty droplets were removed using the *defaultDrops* function, which is a quantile filtering approach based on number of UMIs, with default parameters in the DropletUtils package (Lun et al., 2019). Doublet filtering was also performed using the *cxds_bcds_hybrid* function, which uses a hybrid approach utilizing artificial generated doublets and unlikely coexpression pairs, with a cutoff of 1.0 in the SCDS package (Bais & Kostka, 2020). After both rounds of filtering 12,243 cells were left across all 3 replicates.

2.2.3.3 Normalization

The filtered digital gene expression (DGE) matrices were then loaded into Scanpy to perform the preclustering needed for Scran normalization (Lun, McCarthy, et al., 2016; Wolf et al., 2018). Each biological replicate DGE was then normalized with log counts per million normalization, and denoised using iterative pca with 50 components. The actual preclustering was done via the Leiden community detection algorithm using Scanpy's Leiden function (Traag et al., 2019). All 3 biological replicates were then co-normalized using the *computeSumFactors* function in Scran and *normalize* function in Scuttle with the preclusters as input (McCarthy et al., 2017). The size factor normalization that was used was chosen for its ability to handle sparse single cell data which may have cell types with different expression values (Lun, Bach, et al., 2016).

2.2.3.4 Integration of neuronal cells and clustering

Post normalization clustering was performed again using Scanpy's Leiden function (Traag et al., 2019). The clusters were classified into oligodendrocytes 1 and oligodendrocytes 2, neurons, astrocyte 1 and astrocyte 2, oligodendrocyte precursor cells, microglia, meninges, ependymal cells and Schwann cells based on the expression of established marker genes. Neuronal clusters were then selected using the marker gene *RBFOX3*, which left a total of 2,698 cells across replicates. Data integration across biological replicates and neuron filtered gene expression matrices were performed using the integrate_scanpy function in Scanorama, which uses a panoramic stitching algorithm to integrated datasets by producing a batch corrected cell-cell distance graph (Hie et al., 2019). Leiden community detection was then performed with a resolution of 1.0 on the batch corrected cell-cell distance graph to get an initial integrated clustering (Traag et al., 2019). It is important to note that while the Scanorama batch corrected data was used for clustering and integration, the 'un-corrected' data was used for marker gene and differential expression analysis to reduce possible bias that may have occurred during batch correction. Our initial clustering was organized into a dendrogram using ward hierarchical clustering. Further refinement of these clusters was performed by splitting clusters that had both excitatory and inhibitory markers (*SLC17A6* and *SLC32A1* respectively). We computed a midVentral and dorsal score for each cluster based on the average z-score scaled expression of genes that have a high discriminative ability (AUROC) between the spinal cord regions as computed by previous studies (Sathyamurthy et al., 2018). Two of the macaque clusters were thus grouped into a single cluster labeled midVentral. This cluster is excluded from our analysis of the dorsal horn populations as it lies outside our region of interest. The final list of dorsal horn clusters included 11 excitatory clusters and 5 inhibitory clusters.

2.2.3.5 Marker gene selection

A combination of methods was used for the marker gene selection for the clusters. A binary matrix was constructed by thresholding the normalized gene expression values at a threshold of 0.2. The binary matrix was then used to compute the precision and sensitivity of each gene for each cluster. In addition, the top differentially expressed genes were computed using the *rank_gene_groups* function in Scanpy, and Wilcoxon rank-sum (Mann-Whitney-U) test. From this list, we removed genes that were co-expressed in non-neuronal cells if possible.

2.2.4 RNAscope® in situ hybridization

Fresh frozen lumbar spinal cord tissue samples were harvested from 3-year-old male and female macaques perfused with aCSF. The tissue was immediately placed in OCT and frozen on dry ice. L4-L6 lumbar spinal cord was sectioned using a cryostat at 20 μm thickness on to Superfrost-charged slides and stored in -80ºC until the start of the assay. *In situ* hybridization was performed according to the Multiplex v2 Fluorescent (Advanced Cell Diagnostics) protocol for fresh frozen tissue after fixing the slides with cold 4% paraformaldehyde (PFA) for thirty minutes (Ferreira et al., 2022; Wang et al., 2012).The probes were designed and purchased from Advanced Cell Diagnostics. Signal amplification was carried out using the TSA Fluorescin, Cyanine 3 and Cyanine 5 reagents from Akoya Biosciences at 1:1500.

Combinations:

GLUT1	*CRHR2* (452041-C1); *COL13A1* (865661–C2)
GLUT2	*NMUR2* (582881-C1)
GLUT3	*TAC3* (520901-C1); *NMU* (837871-C2)
GLUT4	*COL5A2* (866291-C1); *PAX2* (837981-C3)
GLUT5	*COL24A1* (865991-C1); *NMBR* (821681-C2)
GLUT6	*TAC1* (837891-C1); *ANOS1* (866021-C2)
GLUT7	*COL21A1* (865681-C1); *MAF* (865691-C2)
GLUT8	*MAFA* (865701-C1); *RBFOX3* (486781-C3)
GLUT9	*ADAMTS16* (865791-C1); *TLL2* (865801-C2)
GLUT10	*OTOGL* (865981-C1)
GLUT11 and GABA5	*PDYN* (838041-C1); *PAX2* (837981-C3)
GABA1	*MASP1* (866041-C1); *PAX2* (837981-C3)
GABA2	*GDNF-AS1* (866051-C1); *RREB1* (866331-C2)
GABA3	*NPY* (535471-C1); *RREB1* (866331-C2)
GABA4	*MET* (546191-C1); *PTN* (866131-C2)

2.2.4.1 Image acquisition and quantification

For macaque spinal cord experiments, representative images were acquired at 10X magnification using the Nikon A1R and Nikon's NIS-Elements imaging software and processed with ImageJ. Images taken for quantitative analysis were acquired using Nikon Eclipse 800. Laminar boundaries for the images were drawn with the Canvas X software using Atlas of the Spinal Cord: Mouse, Rat, Rhesus, Marmoset and Human as a reference. The

substantia gelatinosa of the primate dorsal horn is also easily recognizable due to its translucent nature and hence was used to demarcate the boundary between laminae II and III. For the quantitative analysis, cells with more than three puncta were manually counted as positive. In order to account for the presence of lipofuscin in the macaque spinal cord tissue, the 488 channel was left blank i.e., no probe or fluorophore was added, and this was used for background subtraction.

2.2.5 Data and code availability

The code and Jupyter notebooks used for the analysis of the macaque snRNA-seq has been made available at Github repository https://github.com/pfenninglab/dorsal_horn_snrnaseq. Additionally, the macaque dataset can be accessed through an R shiny application (https://seallab.shinyapps.io/dorsalhornseq/). This Shiny application was created using a Shiny Cell package (Ouyang et al., 2021).

2.3 Results

2.3.1 Major cell types of the macaque dorsal horn

To determine the cellular and molecular organization of the macaque dorsal horn, we performed single-nuclear RNA sequencing (snRNA-seq) on lumbar tissue (L4-5) harvested from young adult (3-year-old) male Rhesus macaques (n=3) using the 10X Genomics Chromium platform. For the isolation of the dorsal horn nuclei, the spinal grey matter of each animal was dissected, transected at the central canal and mechanically dissociated (**Figure 3A**). Deep sequencing of the single cell libraries produced an average of ~50M reads per animal. To optimize alignment of the reads to the macaque genome (Mmul10), we employed a custom annotation method that resulted in 91% of the reads mapping to genes (He et al., 2021). After the removal of doublets and mitochondrial reads, 12,243 nuclei were retained for further analyses. The three biological replicates were then co-normalized to remove cell-specific read sampling biases using Scran and subsequently integrated and batch-corrected with Scanorama (**Figure 4A**) (Hie et al., 2019; Lun, McCarthy, et al., 2016). Nuclei were assigned to their cell type based on the expression of well-established marker genes and we detected on average 1,720 genes and 3,700 UMIs per cell type (**Figure 4B-C**) (Sathyamurthy et al., 2018). For example, 2,698 neurons were identified by the expression of RNA Binding Fox-1 Homolog 3 (*RBFOX3*), and thus comprised ~22% of the total number of nuclei (**Figures 3B-C**). Oligodendrocytes, identified by the gene encoding Myelin Basic Protein (*MBP*), comprised the largest class (~39%). These cells could be further sub-clustered into two groups based on the expression of quinoid dihydropteridine reductase (*QDPR*) in one case and Dpy-19 like C-

mannosyltransferase 1 (*DPY19L1*) together with S100 calcium binding protein B (*S100B*) in the other (**Figures 3B-C**). Astrocytes were present in about the same numbers as neurons and were also sub-clustered into two groups based on high (Astrocyte 1) or low (Astrocyte 2) expression of Glial fibrillary acidic protein (*GFAP*). Oligodendrocyte precursor cells, microglia, meninges, ependymal cells and Schwann cells all made up smaller individual clusters.

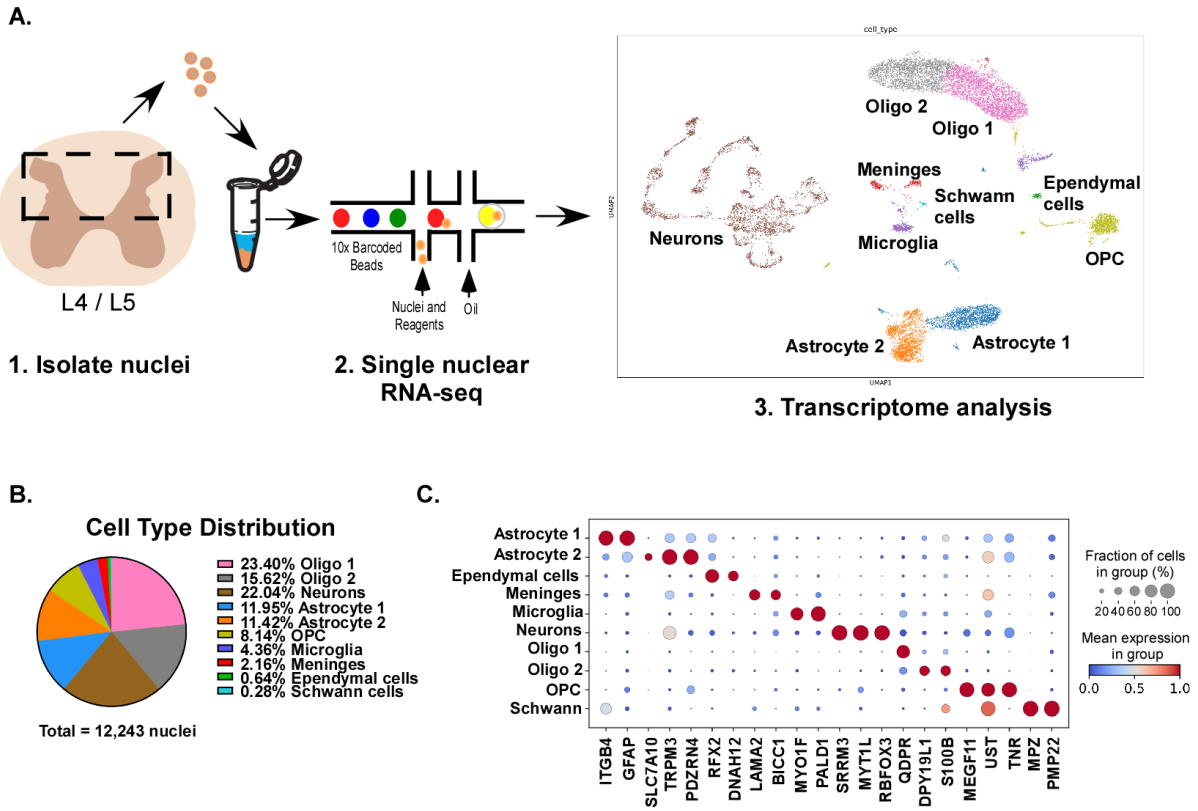

Figure 3: Major cell types of the macaque dorsal horn

A. Schematic overview of the single-nuclear RNA-sequencing (snRNA-seq) experimental workflow of the macaque lumbar dorsal horn. **B.** Pie chart representation of the contribution of each major cell type present in the macaque dorsal horn which includes oligodendrocytes, neurons, astrocytes, oligodendrocyte precursor cells (OPC), microglia, meninges, ependymal cells and Schwann cells. **C.** Heatmap of the normalized mean expression of key marker genes used to identify each major cell type. The size of the circles depicts the percentage of cells within each cluster that express the gene.

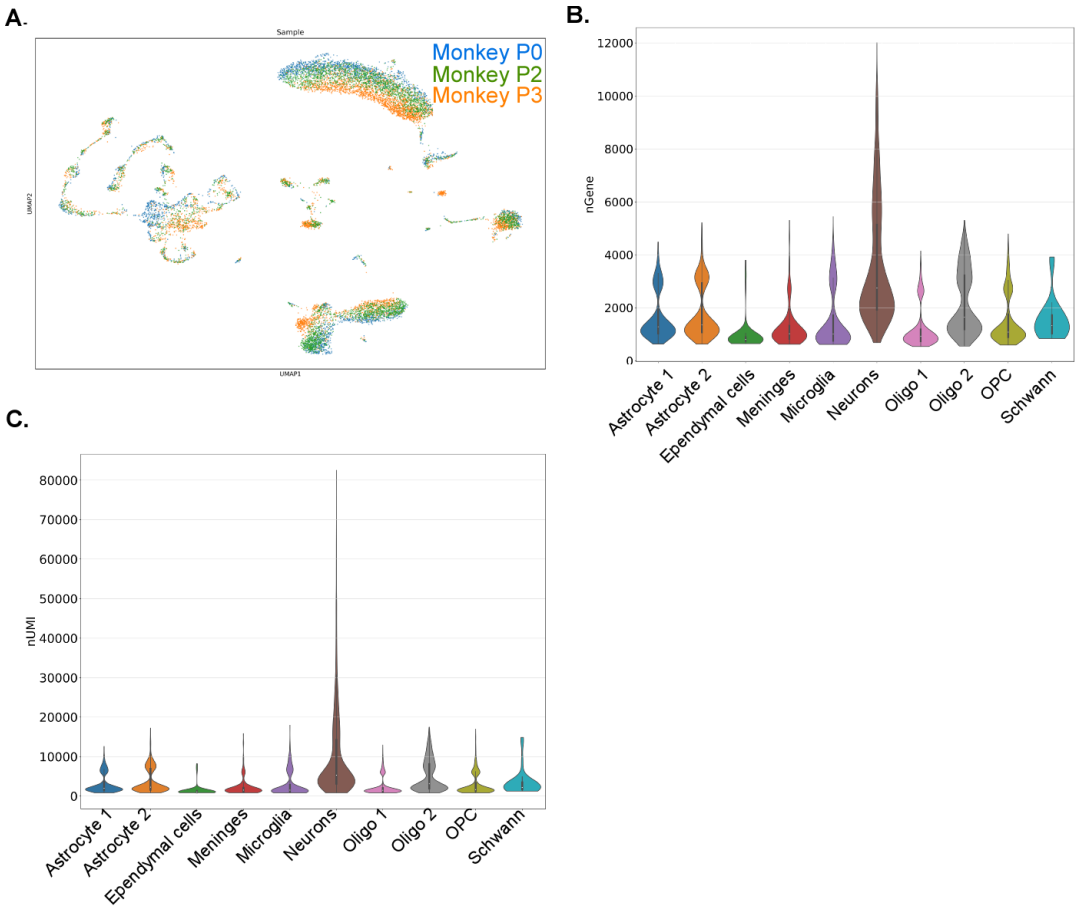

Figure 4: Quality metrics for nuclei obtained from three biological replicates

A. UMAP visualization of the dorsal horn nuclei from three biological replicates after co-normalization. **B.** Violin plot showing the number of genes across the major cell types. **C.** Violin plot showing the number of UMIs across the major cell types.

2.3.2 Transcriptomically defined neuronal clusters

To analyze the neurons in more detail, we sub-clustered them into sixteen finer resolution clusters (Wolf et al., 2018). The resulting clusters could be broadly categorized as either excitatory or inhibitory using the known markers, vesicular glutamate transporter 2 gene

(*SLC17A6*) or vesicular inhibitory transporter (*SLC32A1*). Two clusters were unusual in that they each contain a substantial number of neurons that are either excitatory or inhibitory, but that otherwise have computationally indistinguishable gene expression profiles (**Figure 5A**). This is characteristic of clusters previously identified to be a part of the intermediate and ventral regions of the spinal cord (Laminae VI-VII) (Sathyamurthy et al., 2018). Because of the challenge of assigning these nuclei to distinct clusters and our interest specifically in laminar regions involved primarily in somatosensation (Laminae I-V), we combined these nuclei into one midVentral domain (midVen) cluster (**Figure 5B**). Clusters were then manually inspected for highly enriched genes that could serve as cluster markers. Those that lacked such genes were merged to create fewer, larger clusters with well-defined marker genes. Our final dataset, excluding the midVen, consisted of 1,954 nuclei, out of which 64% were classified as excitatory and 36% as inhibitory (**Figure 6A-B**). These nuclei formed 11 excitatory clusters (GLUTs 1-11) and 5 inhibitory clusters (GABAs 1-5) with an average of 139 nuclei per cluster (Range is from 49 to 222 nuclei per cluster) (**Figure 6B-C**). On average, approximately 4,000 genes and 10,000 UMIs were detected per cluster (**Figure 6D**). Relationships between individual clusters were visualized using the Ward's hierarchical clustering method together with the correlation matrix (**Figure 5C and 6E**) and, as expected, the largest distance in the resulting dendrogram occurred between the excitatory and inhibitory clusters, indicating that the gene expression profiles of these two groups are the least similar. To define each neuronal cluster, we selected a marker gene(s) that had to be both highly expressed and uniquely enriched within the cluster. The ability of markers to ideally represent more than 20% of the cells within a cluster, often required using a combination of marker genes (**Figures 6E-F**).

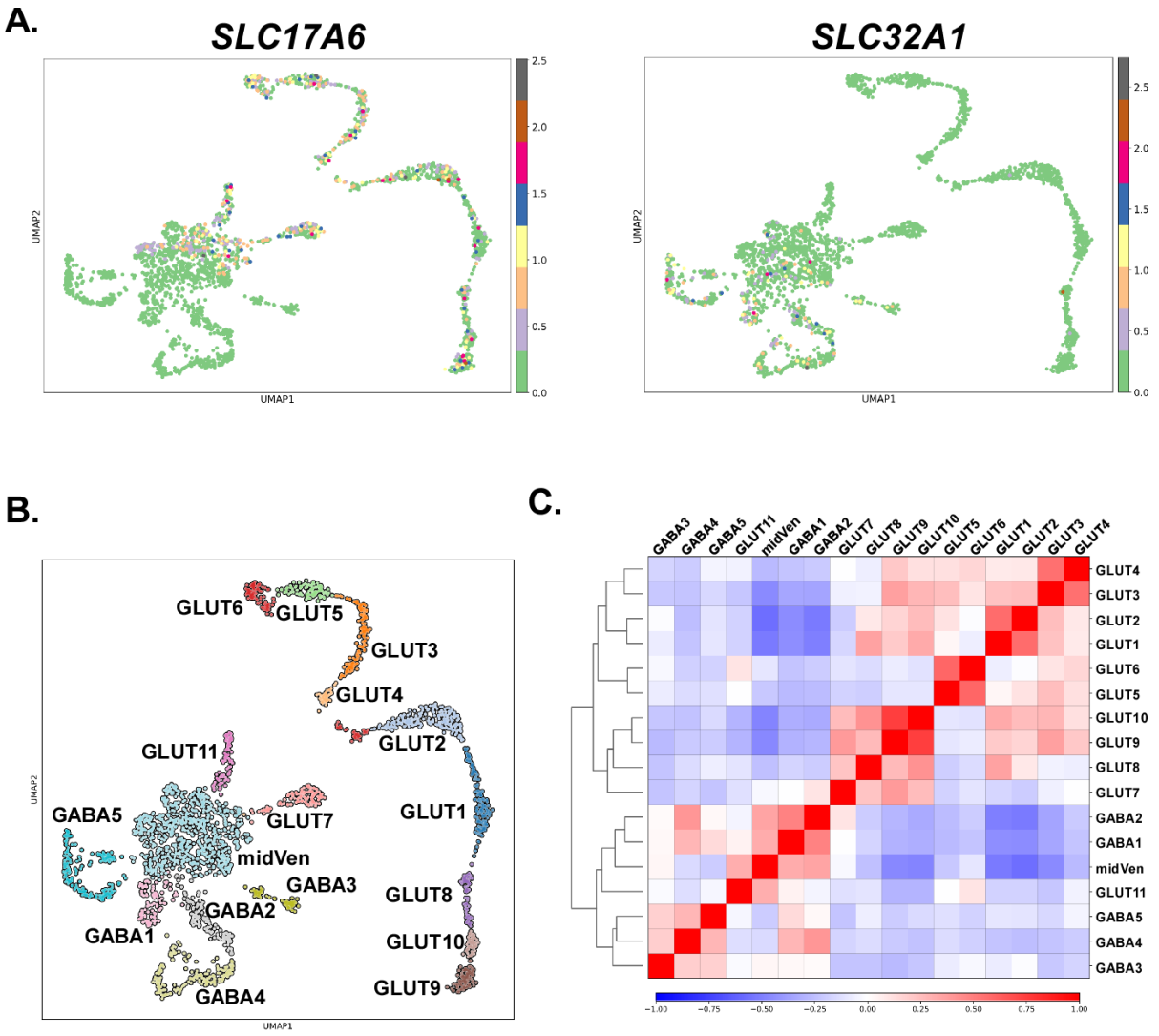

Figure 5. Neuronal clusters with the midVentral domain

A. UMAPs showing vesicular glutamate transporter 2 (SLC17A6) and vesicular inhibitory amino acid transporter gene (SLC32A1) expression. **B.** Two clusters with overlapping gene expression profiles were assigned to a single cluster named midVentral (midVen) domain as depicted in the UMAP showing neurons colored according to their cluster identity. **C.** Correlation matrix highlighting the relationship among the clusters using Pearson's correlation.

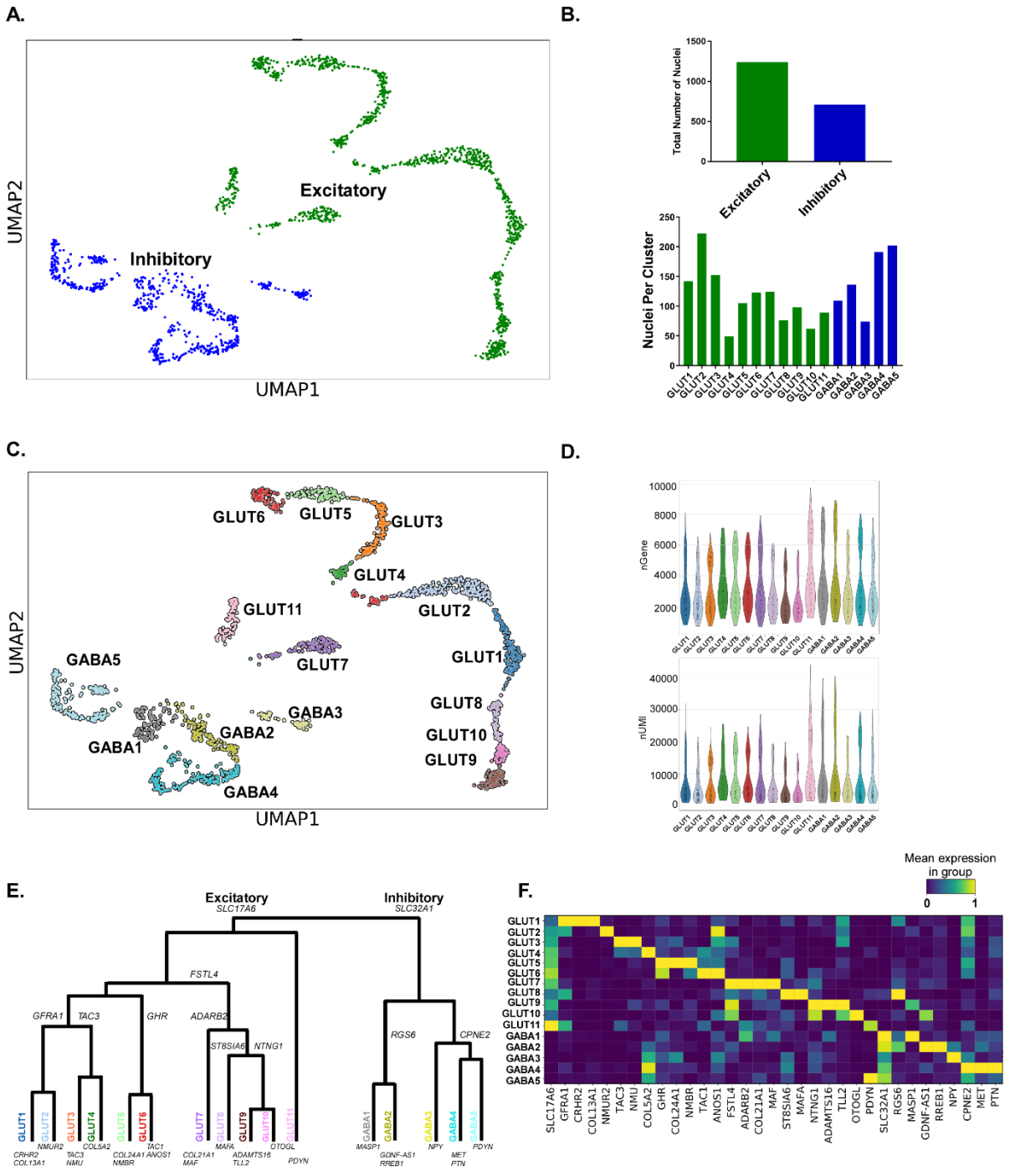

Figure 6. Classification of macaque dorsal horn neurons

A. UMAP visualization plot of the neuronal clusters broadly classified as either excitatory (green) or inhibitory (red) based on their neurotransmitter identity. **B.** Bar graphs of (top) the total number of nuclei that are excitatory (1,355 nuclei) or inhibitory (870) and (bottom) the number of nuclei per cluster. **C.** UMAP visualization of the 2,225 neuronal nuclei that are colored based on their cluster identity from Louvain clustering. Excitatory clusters are prefixed with GLUT and inhibitory clusters with GABA. **D.** Violin plots depicting the number of genes (top

panel) and UMIs (bottom panel) in each neuronal cluster. **E.** Neuronal clusters were hierarchically clustered as shown in the dendrogram. Marker genes for each major branch point of the dendrogram are listed. E.g., Neurons belonging to the GLUT1 cluster express SLC17A6, GFRA1, CRHR2 and COL13A1. **F.** Heatmap of the normalized mean expression of marker genes (mentioned in the dendrogram) for the neuronal clusters.

2.3.3 Laminar Distribution of Marker Genes

To determine how the transcriptomically defined clusters are distributed within the Rexed laminae, we performed RNAscope® fluorescence *in situ* hybridization in lumbar spinal cord slices taken from both male and female macaques using the selected marker genes (**Figure 7**) (Wang et al., 2012). GLUT1 neurons were visualized using either Corticotropin-releasing hormone receptor 2 (*CRHR2*) or Collagen, type XIII, alpha 1 (*COL13A1*) as markers. Of the 320 nuclei showing expression of either gene, 72.81% were located within laminae I-II. The GLUT2 cluster was identified using Neuromedin U receptor 2 (*NMUR2*), GLUT5 by the overlap of Collagen Type XXIV Alpha 1 Chain (*COL24A1*) and Neuromedin B receptor (*NMBR*), GLUT6 by the overlap of Tachykinin precursor 1 (*TAC1*) and Anosmin 1 (*ANOS1*), GLUT8 by the overlap of MAF BZIP Transcription Factor A (*MAFA*) and *RBFOX3*, and GLUT11 by excitatory prodynorphin (*PDYN*) expression. Interestingly, all five of these clusters are also enriched in the superficial laminae (I-II). Neurons belonging to the GLUT3 cluster, identified by expression of both Tachykinin precursor 3 (*TAC3*) and Neuromedin U (*NMU*), are located along the lamina II/III boundary, but reside primarily within lamina III. Other clusters that showed a similar enrichment in lamina III include GLUT9 which was detected by expression of both Tolloid like 2 (*TLL2*) and ADAM Metallopeptidase with Thrombospondin Type 1 Motif 16 (*ADAMSTS16*) as well as GLUT10 which was marked by

Otogelin-like (*OTOGL*) gene. The GLUT7 neurons, identified by the overlap of Collagen Type XXI Alpha 1 Chain (*COL21A1*) and *MAF* genes, are largely located within laminae III and IV. Lastly, since Collagen Type V Alpha 2 Chain (*COL5A2*) which is a marker for GLUT4, is also expressed by Paired box 2 (*PAX2*)-expressing inhibitory neurons, we probed for neurons that are positive for *COL5A2* and negative for *PAX2*. These cells are distributed across the entire dorsal horn without any particular laminar enrichment in contrast to the other clusters. All cluster markers showed a similar distribution in males and females. The inhibitory clusters were similarly analyzed (**Figure 8**). Neurons in the GABA5 cluster, identified by the expression of *PDYN* along with *PAX2*, are located primarily within laminae I-II (**Figure 8**). GABA4 inhibitory neurons marked by tyrosine-protein kinase *MET* and pleiotrophin (*PTN*) expression are enriched in lamina III. Neurons belonging to GABA1 were visualized by the overlap of MBL Associated Serine Protease 1 (*MASP1*) and *PAX2* and to GABA2 by expression of both GDNF antisense RNA 1 (*GDNF-AS1*) and ras responsive element binding protein 1 (*RREB1*). All of these markers were mainly located in laminae III-IV. Neuropeptide Y (*NPY*) expressing neurons are found in GABA2 as well as GABA3, we therefore identified the distribution of GABA3 neurons by probing for *NPY* neurons that did not also express *RREB1*. These neurons are distributed across all dorsal laminae. Overall, a majority of the clusters show enrichment within particular laminae laying a foundation for the molecular and cellular as well as a potential functional organization of the macaque dorsal horn.

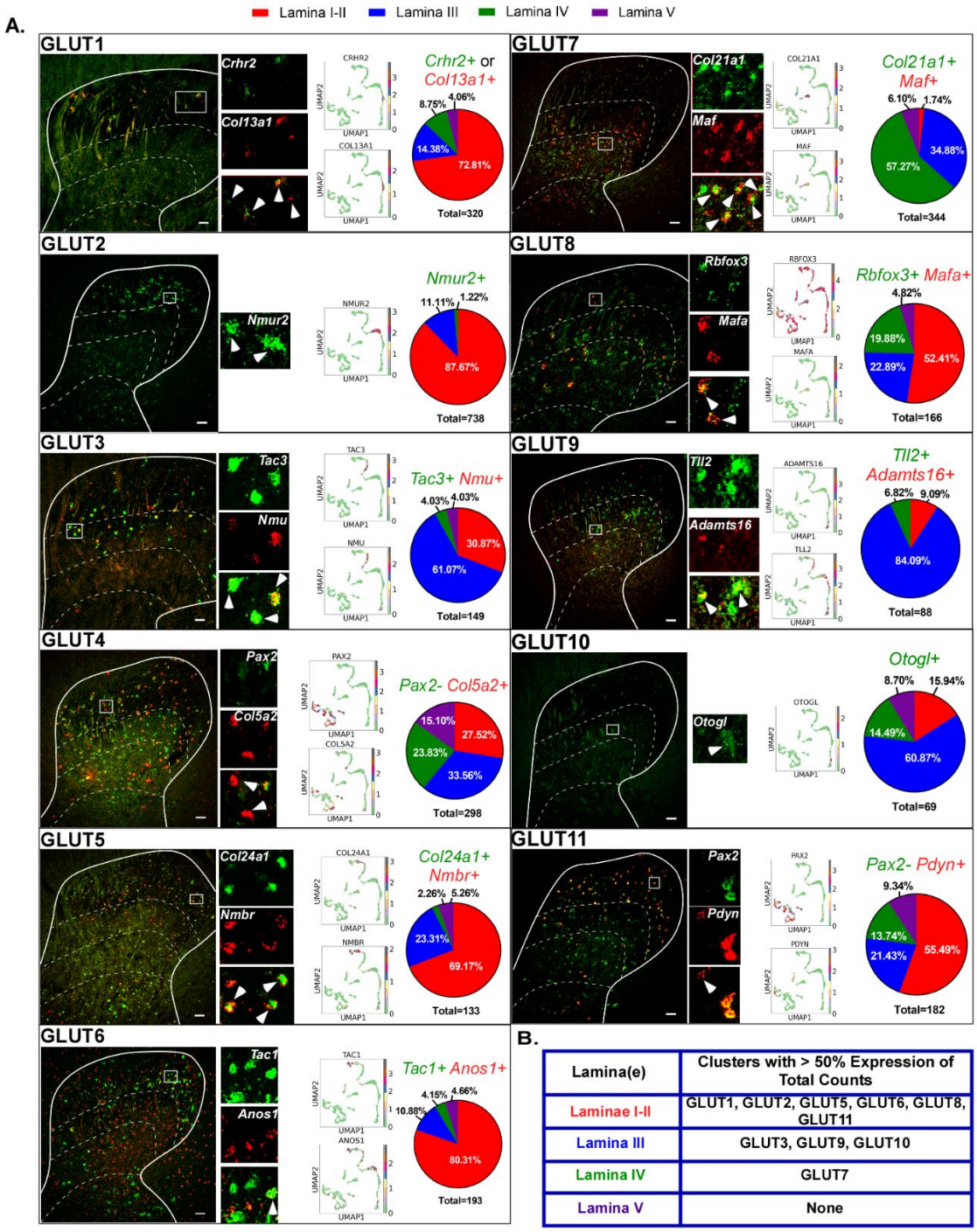

Lamina(e)	Clusters with > 50% Expression of Total Counts
Laminae I-II	GLUT1, GLUT2, GLUT5, GLUT6, GLUT8, GLUT11
Lamina III	GLUT3, GLUT9, GLUT10
Lamina IV	GLUT7
Lamina V	None

Figure 7. *In situ* validation of excitatory cluster markers

A. Panels depict *in situ* hybridization of marker gene combinations used to detect each excitatory cluster. Dorsal horn images are taken at 10X with the smaller insets showing a magnified image (20X) of the individual gene(s) as well as the merged image. Laminar boundaries (dashed lines) are drawn between II/III, III/IV and IV/V. White

arrows point to positive cells belonging to the respective cluster. UMAPs of the marker genes used in the in situ are shown. Pie charts show the percentage of cells expressing the cluster marker genes across laminae I-V. n=6 spinal cord sections from N=2-3 macaques. Scale bar = 100 µm **B.** Summary table showing laminar enrichment of excitatory clusters.

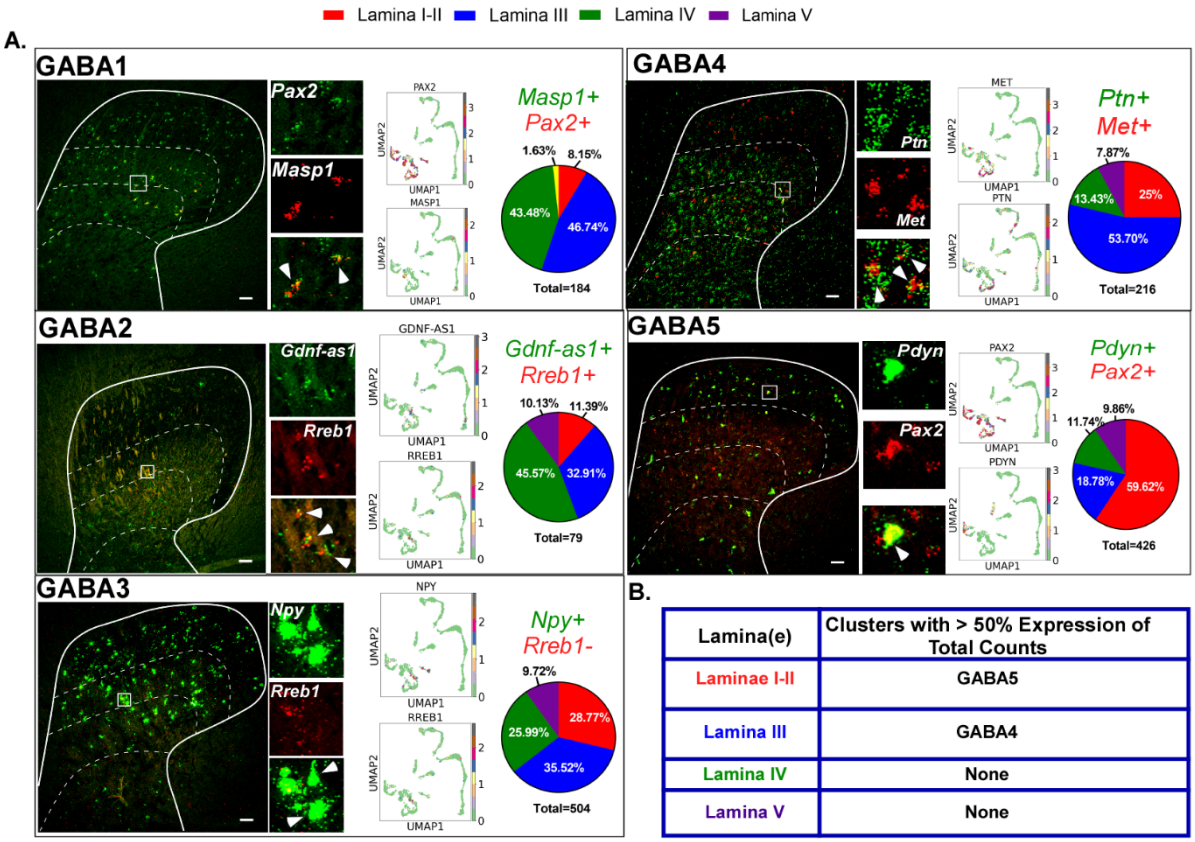

Lamina(e)	Clusters with > 50% Expression of Total Counts
Laminae I-II	GABA5
Lamina III	GABA4
Lamina IV	None
Lamina V	None

Figure 8. *In situ* validation of inhibitory cluster marker profiles

A. Panels depict *in situ* hybridization of marker gene combinations used to detect each inhibitory cluster. Representative dorsal horn images are taken at 10X with the smaller insets showing a magnified image (20X) of the individual gene(s) as well as the merged image. Laminar boundaries (dashed lines) are drawn between II/III, III/IV and IV/V. White arrows point to positive cells belonging to the respective cluster. UMAPs of the marker genes used in the in situ are shown. Pie charts show the percentage distribution of cells expressing the cluster marker genes across laminae I-V. n= 6 spinal cord sections from N=2-3 macaques. Scale bar = 100 µm **B.** Summary table showing laminar enrichment of inhibitory clusters.

2.4 Discussion

Understanding the cellular and molecular organization of the dorsal horn is essential for determining how the molecularly distinct neuronal populations form functional circuits to process somatosensory information. Our work provides a high-quality snRNA-seq dataset of the non-human primate dorsal horn neurons categorized into 16 distinct cell types. The gene expression profiles for each cell type can easily be probed through this interactive database https://seallab.shinyapps.io/dorsalhornseq/ . In addition to identifying the cell types, we determined that they have largely restricted laminar patterns and also, intriguingly, that in many cases, clusters that are hierarchically close to one another show a similar laminar distribution. GLUTs1-2, 5-6, 8, 11 and GABA5 all showed enrichment in the superficial laminae (I-II); GLUT3 and GABA4 in lamina III and GLUTs9-10 and GABAs1-2 in laminae III-IV. The similar spatial organization of highly related clusters may point to a common developmental origin as well as clues to their potentially related functional roles. Moreover, this study highlights the molecular diversity of the macaque dorsal horn neurons similar to what has been observed for neurons of the mouse dorsal horn (Haring et al., 2018; Sathyamurthy et al., 2018).

3.0 Comparative Analysis of the Mouse and Macaque Dorsal Horn Transcriptomes

3.1 Introduction

Single cell transcriptomic studies of embryonic and adult mouse spinal cord have added a higher level of specificity in identifying molecularly distinct cell types (Delile et al., 2019; Haring et al., 2018; Rosenberg et al., 2018; Sathyamurthy et al., 2018; Zeisel et al., 2018). A meta-analysis, performed subsequently, further aligned these transcriptomic based populations (Russ et al., 2021). Nevertheless, the generality of this classification scheme particularly across species remains unresolved, despite the fact that fundamental studies of the spinal cord as well as the validation of targeted therapeutics, depend on it. To address this, we compared the macaque cell types (From Chapter 2) to the mouse meta-analysis derived cell types, to produce a unified classification scheme that is based, in large part, on cross-species conservation (Russ et al., 2021). To resolve the classification scheme further, we also compared the laminar distributions of identified cell types from each species, including validation of certain genes in human. Species-specific differences in the expression of salient genes, which may reflect evolutionary changes that could influence functional phenotypes and translatability, were also identified.

3.2 Methods

3.2.1 Comparison of macaque and mouse meta-analysis clusters

To identify orthologous genes across species, each mouse gene symbol was matched to the corresponding ENSEMBL ID using BioMart (v101). BioMart was used to identify the orthologous human gene, filtering for one-to-one orthologs to avoid potential false positives. The macaque genome was annotated with orthologous human genes as previously described (He et al., 2021; Schneider et al., 2017; Warren et al., 2020). The resulting datasets frame for macaque and mouse contained 15,157 one-to-one orthologs.

Orthologous genes of two of the mouse family markers, *RORB* and *ADAMTS5*, showed separation in the macaque UMAP, but were not independently clustered. GABA2 and GABA4 clusters were re-clustered using Leiden clustering (resolution 0.3) (Traag et al., 2019). Three of the identified clusters represented *RORB* populations while the remaining two populations represented *ADAMTS5*.

A straightforward scoring approach was used for the cross-species comparisons to improve the interpretability. We identified the top 100 most enriched and most-depleted makers for each of the mouse cell classes (Excitatory, Inhibitory, and midVentral). Mouse and macaque markers for comparison were selected using the Wilcoxon rank sum approach in the "rank_genes_groups" function (Wolf et al., 2018). The relative levels of those markers, weighted by their cluster enrichment scores, created a score that we could use to annotate each cell in the macaque population for each of the major cell classes. These enrichment scores corresponded strongly with the individual marker-based annotation of the macaque cell classes.

These scores were then used to identify significant shifts across the population using a t-test. The t-statistic confirms the broad differences in the distribution of the enrichment scores, with the exception of cluster GLUT11, which has features of midVentral neurons, but that we verify is highly similar to a specific sub-population of mouse excitatory neurons.

The same procedure was used to score each macaque cell for its cluster identity relative to its cell class (Excitatory or Inhibitory). We used the 50 most enriched and depleted markers, rather than 100, because the strength of enrichment declined more quickly down the ranked list for subtler differences that exist between subtypes of excitatory and inhibitory neurons in comparison to the strong differences that exist across those populations. Again, the annotation of cell clusters based on a t-test showed a strong match to annotation based on the most confident individual mouse markers.

To find genes specialized in a particular species, the mouse cells used were limited to the Sathyamurthy dataset from the meta-analysis (Russ et al., 2021; Sathyamurthy et al., 2018). Rather than the processed data, where low variance genes are removed, we used an unfiltered version of the mouse dataset. This allowed us to identify potential examples where the gene is specialized in macaque, but not mouse. Log fold differences were calculated using the procedure described above for both the mouse and macaque for each cell class relative to the others and for each family relative to the cell class. The family-level comparison was chosen to maximize the number of cells available for a rigorous identification in the differences in markers. We manually filtered out genes that exhibited a strong difference across species based on log2 fold change, but had very low abundance and were not significant. The orthologous marker genes of orthologous populations of cells were correlated with each other in their overall pattern (Pearson's R ranging from 0.058 to 0.21; p-value from $1*10^{-9}$ to $7*10^{-142}$). These correlations provide further support for our assignment of cell type families. The broad range reflected the relative abundances of the cell types rather than the lack of a strong match. To

determine species-specific markers, we required a gene to have an adjusted p-value of $< 10^{-5}$ and a log2 fold difference of greater than 2. In addition, we required that the orthologous gene have a log2 fold difference of less than 0 in the other species. This highly stringent procedure may miss candidates, but the remaining ones are likely to be high quality.

3.2.2 Human spinal cord samples

All human spinal cord procurement procedures were approved by the Institutional Review Boards at the University of Texas at Dallas. Donor information is provided in **Appendix A (Table 3)**. The human spinal cords were gradually embedded in OCT in a cryomold by adding small volumes of OCT over dry ice to avoid thawing. All tissues were sectioned at 20 μm onto SuperFrost Plus charged slides using a cryostat. Sections were only briefly thawed in order to adhere to the slide but were immediately returned to the -20°C cryostat chamber until completion of sectioning. Again, due to the limited availability of human donor tissue, not enough samples were assessed for sex differences at the gene level.

3.2.3 RNAscope® in situ hybridization

The *in situ* protocol as described in Chapter 2 was followed for macaque and mouse spinal cord sections (L4-L6 segments). For *in situ* hybridization experiments conducted with human lumbar spinal cord, samples were fixed with cold 4% paraformaldehyde (PFA) for 15

minutes. The Multiplex v2 Fluorescent (Advanced Cell Diagnostics) protocol for fresh frozen tissue was followed with a 2-minute protease IV digestion. The Fluorescin, Cyanine 3 and Cyanine 5 reagents from Akoya Biosciences were used for probe visualization. Probes used in this chapter include: *PIEZO2* (macaque, 1051051-C1), *CPNE4* (macaque, 801111-C2), *Piezo2* (mouse, 400191-C2), *Cpne4* (mouse, 474721-C1), *TAC1* (macaque, 837891-C1), *TAC1* (human, 310711-C2), *GRP* (macaque, 1079131-C2), *GRP* (human, 465261-C1), *CCK* (macaque, 461721-C3), *CCK* (human, 539041-C2), *NTS* (macaque, 837851-C2), *NTS* (human, 512561-C3), *TAC3* (macaque, 520901-C1), *TAC3* (human, 507301-C3), *NMU* (macaque, 837871-C2), *NMU* (human, 520051-C1), *NPY* (macaque, 535471-C1), *NPY* (human, 416671-C2), *PDYN* (macaque, 838041-C1), *PDYN* (human, 507161-C2), *PAX2* (macaque, 837981-C3), *PAX2* (human, 442541-C1).

3.2.4 Image Acquisition and Quantification

For mouse and macaque spinal cord experiments, representative images were acquired at 10X magnification using the Nikon A1R and Nikon's NIS-Elements imaging software and processed with ImageJ. Laminar boundaries for the images were drawn with the Canvas X software using Atlas of the Spinal Cord: Mouse, Rat, Rhesus, Marmoset and Human as a reference. The substantia gelatinosa of the primate dorsal horn is also easily recognizable due to its translucent nature and hence was used to demarcate the boundary between laminae II and III.

For human spinal cord experiments, multiple 10X images were acquired of the dorsal horn starting from the substantia gelatinosa to lamina 10. The acquisition parameters were set

based on guidelines for the FV3000 provided by Olympus. The 10x images were stitched together manually using anatomical landmarks (particularly lipofuscin) that were common between images. For the quantitative analysis, cells with more than three puncta were manually counted as positive. In order to account for the presence of lipofuscin in the macaque/human spinal cord tissue, the 488 channel was left blank i.e., no probe or fluorophore was added, and this was used for background subtraction.

3.2.5 Data code and availability

The code and Jupyter notebooks used for the analysis of the macaque snRNA-seq has been made available at the Github repository https://github.com/pfenninglab/dorsal_horn_snrnaseq. Additionally, the macaque dataset can be accessed through an R shiny application (https://seallab.shinyapps.io/dorsalhornseq/). This Shiny application was created using a Shiny Cell package (Ouyang et al., 2021).

The mouse meta-analysis pipeline is publicly available through the Github repository https://github.com/ArielLevineLabNINDS/SeqSeek_Classify_Full_Pipeline .

3.3 Results

3.3.1 Cross-species comparison of mouse and macaque dorsal horn neuron clusters

A meta-analysis that unified six single cell sequencing datasets from mouse, put forward an atlas of dorsal horn neuronal clusters organized as distinct families (Russ et al., 2021). To determine the extent of molecular and cellular conservation between macaque and mouse dorsal horn neurons, we compared our macaque dataset to this ~10,000 neuron mouse dorsal horn atlas. Specifically, we scored each macaque cell across each major cell class (excitatory, inhibitory or midVentral) based on the top 100 marker genes from the mouse meta-analysis. Based on these analyses, we found a remarkably high correlation across species for both the excitatory and inhibitory clusters (**Table 1 and Figure 9A**). Additionally, nuclei assigned to the midVentral cluster in macaque show the highest correlation to the midVentral clusters in mouse (**Figure 9A**). The macaque nuclei were then assigned a score depending on how similar their gene expression profiles were to the individual mouse clusters, rather than to the major cell classes. From this, a striking correspondence was observed between the nuclei of the individual macaque and mouse clusters, with the exception of GABA2 and GABA4 clusters, which did not correspond to any of the mouse clusters, and Excit-07 and Excit-17 which did not correspond to any of the macaque clusters (**Figure 10A**). This latter observation is not surprising given that these two clusters contain neurons only from the Rosenberg dataset which analyzed early postnatal mouse spinal cord (P2 and P11) (Rosenberg et al., 2018; Russ et al., 2021).

Neurons in the mouse meta-analysis were sub-clustered to a higher degree than in the macaque dataset, resulting in a greater number of smaller clusters. For this reason, we also compared the macaque clusters with higher-order clusters of the mouse, also known as families (**Figure 10A-B**). In this case, the orthologous genes of key markers from each of the mouse families were plotted onto the newly generated macaque UMAP (**Figure 10B**). From this, we observed that GLUT1 and GLUT2 clusters correspond to the *Reln* family; GLUT3, GLUT4, GLUT5 and GLUT6 to the *Sox5* family; GLUT7 to the *Maf* family; GLUT8 to the *Cpne4* family; GLUT9 and GLUT10 to *Prkcg* family; GLUT11 to the *Rreb1* family; GABA1 to the *Cdh3* family; GABA3 to the *Npy* family and GABA5 to the *Pdyn* family. However, GABA2 and GABA4 again did not correspond directly to the mouse families. Upon closer examination, we saw in the UMAP that orthologous genes of two of the mouse family markers, *RORB* and *ADAMTS5*, showed an interesting separation within both GABA2 and GABA4 clusters (**Figure 10C**). To investigate, we re-clustered GABA2 and GABA4 and found that sub-clusters GABA2_1 and GABA4_1 correlated with the mouse *Rorb* family and GABA2_2 and GABA4_2 correlated with the *Adamts5* family. To get a better idea of how well the markers represent clusters across species, we also plotted the distribution of mouse family markers in the macaque clusters and the macaque cluster markers in the mouse families as dotplots (**Figure 9B**).

We next wanted to determine whether the laminar organization of the macaque clusters and the corresponding mouse families are conserved. Comparing the distributions of the macaque clusters, as shown in Figure 7 and 8, with what was reported for the families in the meta-analysis, we reveal that the dorsoventral locations of the clusters are indeed remarkably conserved across species (**Figure 10D**) (Russ et al., 2021).The molecular and spatial alignment of macaque clusters with the mouse families that we report here provides a valuable framework for how dorsal horn neurons are organized at the molecular and cellular level across species.

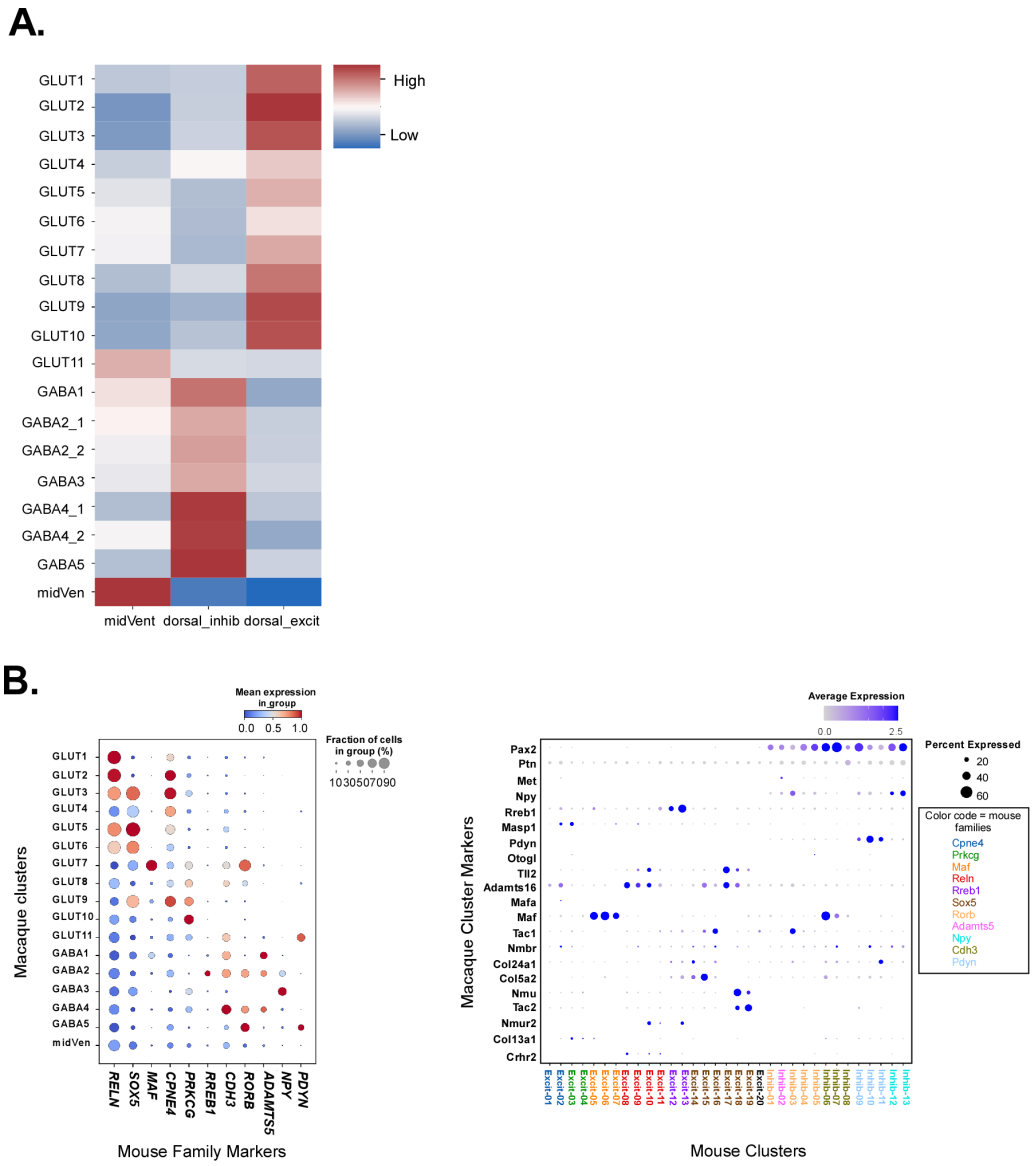

Figure 9. Comparison of clusters from the macaque with the major classes of the mouse meta-analysis

A. Heatmap showing high correlation of the macaque excitatory, inhibitory and midVentral clusters (vertical axis) to the excitatory, inhibitory, and midVentral clusters of the mouse respectively (horizontal axis). **B.** Dotplots depict the average gene expression of orthologous genes of mouse family markers across the macaque clusters (left) and average gene expression of macaque cluster markers (right) across the mouse dorsal horn clusters. Diameter of the circles represent the percentage of cells/nuclei within each cluster expressing the gene. Dotplot on the right generated through https://seqseek.ninds.nih.gov/.

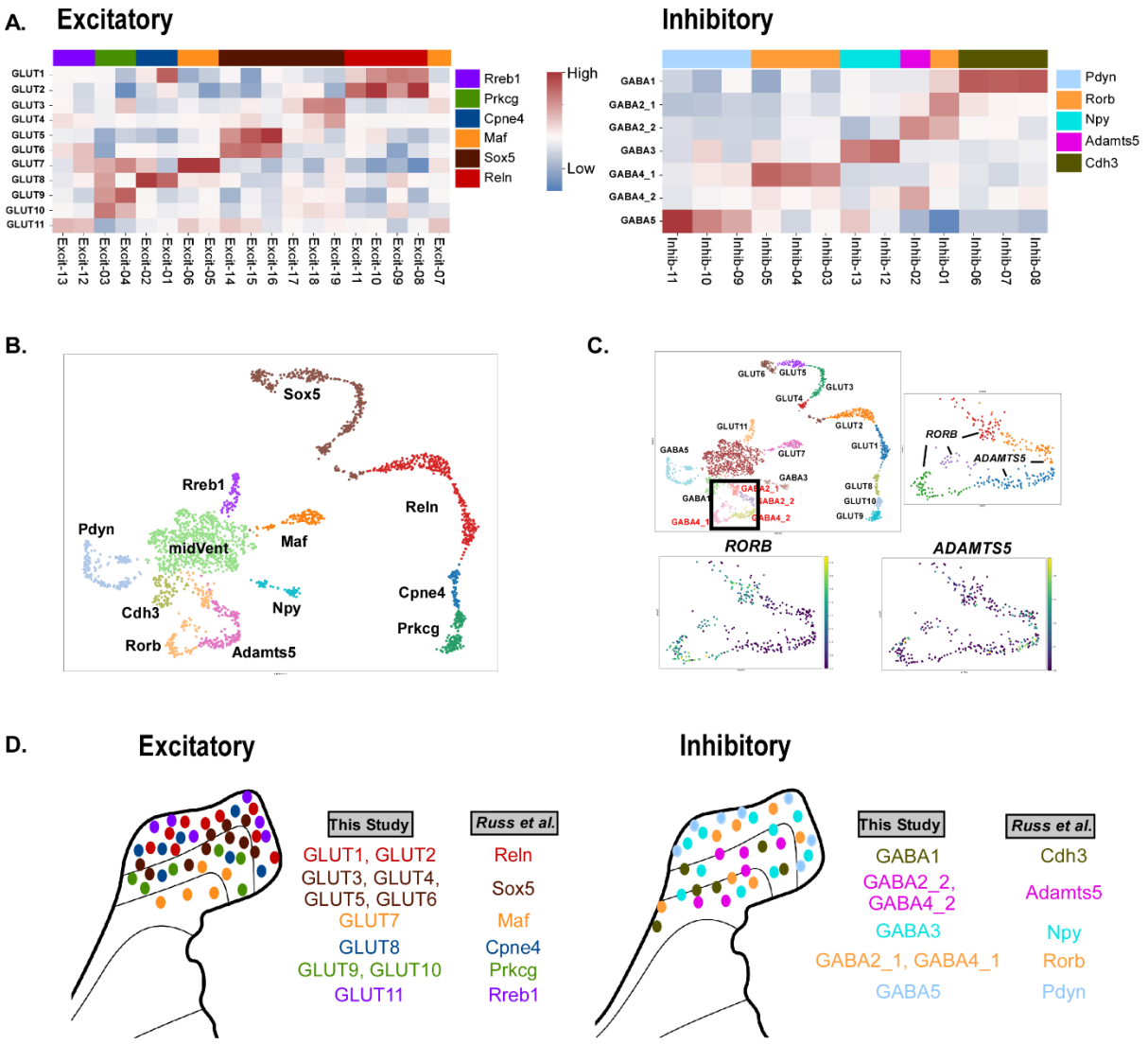

Figure 10. Cross-species comparison of marker genes across mouse and macaque

A. Heatmap of macaque nuclei clustered based on their correlation to the mouse excitatory (left) and inhibitory clusters (right) and families from Russ et al., 2021 adult dataset. **B.** UMAP visualization of the macaque dorsal horn neurons colored and annotated based on the mouse families from Russ et al., 2021 (left). **C.** UMAP showing dorsal horn clusters along with GABA2 and GABA4 subclusters. Leiden re-clustering of GABA2 and GABA4 (top right). Visualization of *RORB* and *ADAMTS5* gene expression within the GABA2 and GABA4 clusters (bottom). **D.** Dorsal horn schematic of the laminar distribution of excitatory (left) and inhibitory clusters (right) organized by mouse families.

Table 1. Correlation between the macaque and mouse classes

Classes	R	p value
dorsal_excit	0.212710994	7.39E-142
dorsal_inhib	0.204071153	2.65E-129
midVent	0.18044691	1.42E-103
excit_Reln	0.195537331	4.91E-109
excit_Sox5	0.12224756	2.04E-45
excit_Maf	0.206464754	1.94E-119
excit_Cpne4	0.114924579	3.63E-32
excit_Prkcg	0.121390648	1.59E-39
excit_Rreb1	0.057928031	1.00E-09
inhib_Cdh3	0.131176623	3.30E-49
inhib_Rorb	0.091241634	9.70E-26
inhib_Npy	0.148185954	2.98E-57
inhib_Adamts5	0.087809576	7.36E-22
inhib_Pdyn	0.144183776	7.71E-60

3.3.2 Laminar distribution of neuropeptides in macaque and human

In a mouse ontology study, genes related to neuropeptide signaling were found to be overrepresented in excitatory neurons of the dorsal horn (Das Gupta et al., 2021). Further, the laminar distribution of the neuropeptide genes such as cholecystokinin (*CCK*), neurotensin (*NTS*), gastrin releasing peptide (*GRP*), neuropeptide FF-amide peptide precursor (*NPFF*),

thyrotropin releasing hormone (*TRH*), *TAC1*, *TAC2* and *NMU* show expression patterns restricted to one or two dorsal laminae (Das Gupta et al., 2021; Peirs et al., 2021). Several of these neuropeptides have been targeted for study in the rodent dorsal horn and have been shown to be important for pain or itch. We were therefore interested to see if their dorsal horn distributions are conserved across species including in human (**Figures 11A-B and Table 2**). Both *TAC1* and *GRP* expressing neurons are located mainly within lamina II of macaque and human dorsal horns, as was reported for mouse. Similarly, *TAC3* (*Tac2* homolog in primate), *NMU* and *NTS* neurons also show a conserved laminar distribution with mice, as *TAC3* and *NMU* are located predominantly in laminae II and III and *NTS* is enriched in lamina III. Interestingly, while *CCK* expressing neurons are abundant in laminae III and IV of the macaque dorsal horn, similar to mouse, the neurons in human show greater enrichment in the superficial laminae in addition to their presence in deeper laminae. We also examined the distribution of two other neuropeptide genes which are markers of inhibitory clusters in both macaque and mouse, *NPY*, and *PDYN* (**Figure 11B**). The *NPY* gene is exclusively expressed by inhibitory neurons distributed across all dorsal horn laminae of macaque and human, similar to what is observed in mouse (Haring et al., 2018; Iwagaki et al., 2016; Russ et al., 2021). With respect to the *PDYN* gene, the neurons are primarily inhibitory and reside in laminae I-II in all three species. Interestingly in mouse, a significantly greater number of excitatory dynorphin neurons are present in the medial part of the L4 segment which receives glabrous skin input, compared to the L2 segment which only receives hairy skin input (Boyle et al., 2017; Huang et al., 2018). Such a restricted distribution along the mediolateral axis of the lumbar enlargement is not observed for excitatory *PDYN* neurons in primate. Nevertheless, the overall laminar distribution of neuropeptide genes is highly conserved across species.

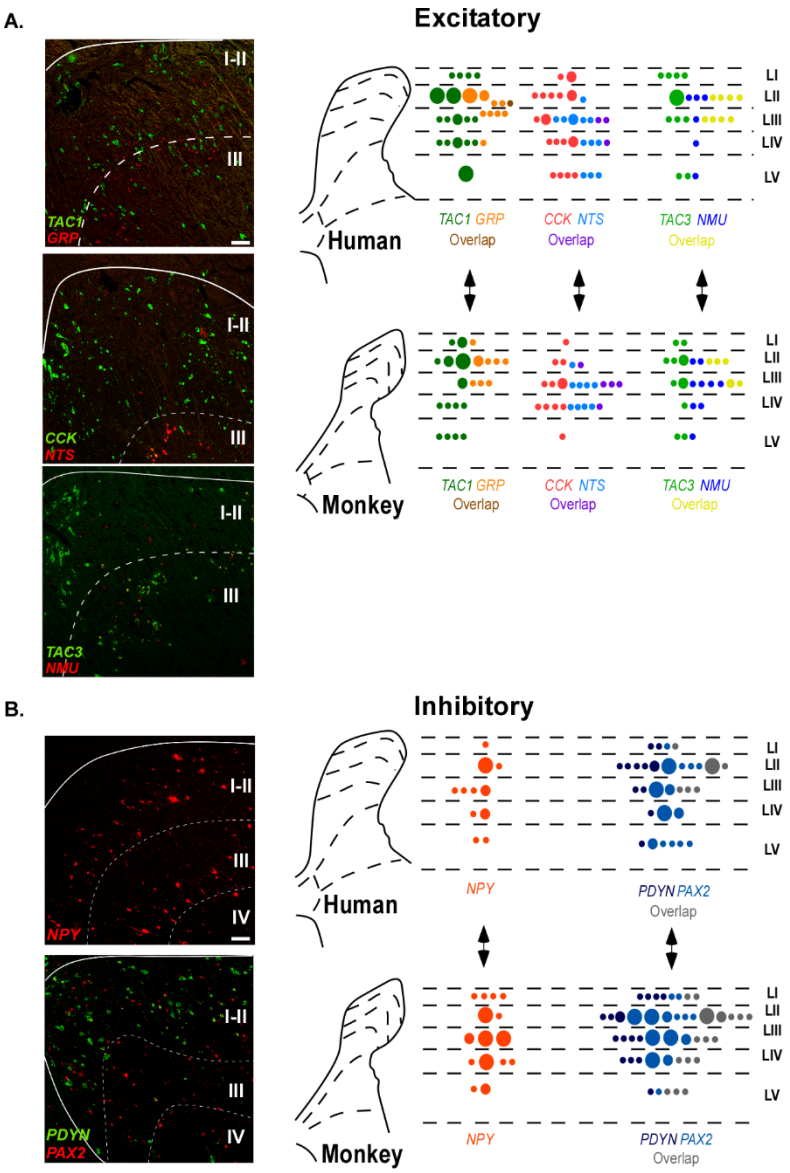

Figure 11. Cross-species comparison of neuropeptides across macaque and human

A. Representative human dorsal horn *in situ* images of excitatory neuropeptides – *TAC1*, *GRP*, *CCK*, *NTS*, *TAC3*, and *NMU* after background subtraction to remove lipofuscin (left). All images were taken at 10X. Scale bar = 100 µm. *In situ* hybridization counts of neuropeptides (right) averaged from 6 hemi sections (N= 2-3 macaque/human donors) to represent a single spinal cord section (2 hemi sections, 20 µm thickness) of macaque and human lumbar dorsal horn. Smallest circle = 2 cells, medium circle = 10 cells, large circle = 20 cells. **B.** Representative human dorsal horn *in situ* images of inhibitory neuropeptides – *NPY*, *PDYN* and *PAX2* after background subtraction to remove lipofuscin (left). Parameters similar to **A**.

Table 2. Distribution of neuropeptides in macaque and mouse meta-analysis clusters

Gene	Macaque Clusters	Mouse Meta-analysis Clusters
CCK	GLUTs 5,7,9 and 11	Excit-01-03; Excit-05
GRP	GLUTs 1,3 and 5	Excit-08-10; 15, 18-19
NMU	GLUTs 3 and 9	Excit-18
NTS	GLUTs 7 and 9	Excit-04
TAC1	GLUTs 5-6 and 11	Excit15-16
TAC2	GLUTs 3-4 and 11	Excit18-19

3.3.3 Comparisons of select functionally relevant genes between mouse and macaque

Cells belonging to 11 principal progenitor domains in the developing mouse spinal cord are defined by specific combinations of transcription factors, which govern neuronal cell-type specification along the dorsoventral axis of the mature spinal cord. Six of these domains (dI1-6), as well as two late-born domains (dILA and dILB) give rise to post-mitotic dorsal horn interneurons (Alaynick et al., 2011; Lai et al., 2016). Given that some of these embryonic transcription factors continue to express in major cell classes (i.e., excitatory or inhibitory groups) in adult, we sought to examine if a similar correspondence between cell types and transcription factors exists in the macaque spinal cord (Del Barrio et al., 2013). The dI5 and late born excitatory neurons are defined by the expression of Lim homeobox transcription factor 1-beta (*LMX1B*) while gastrulation brain homeobox 1 (*GBX1*) is required for the development of a subset of *PAX2* inhibitory neurons (Buckley et al., 2020; Del Barrio et al.,

2013; Ding et al., 2004; Gross et al., 2002; Muller et al., 2002). A similar separation exists in the macaque where *LMX1B* is widely expressed among the excitatory clusters and *GBX1* is found specifically in *PAX2* expressing inhibitory clusters (**Figure 12B**). Interestingly, we find that the BRN3A transcription factor (also known as POU class 4 homeobox 1 - POU4F1) which is a marker of excitatory populations- dI1-3 and dI5 during development, is still expressed in the macaque GLUT4 and GLUT11 clusters (Zou et al., 2012). The MAF group of transcription factors (MAFA, MAFB and c-MAf) are largely expressed by neurons in laminae II-IV of the mouse dorsal horn at postnatal ages as well as in adult (Del Barrio et al., 2013). In the macaque, MAFB is not detected in the dorsal horn but MAF and MAFA serve as marker genes of GLUT7 and GLUT8, respectively (**Figure 12B**). Moreover, as in mouse, *MAF* expression was restricted to laminae III-IV while *MAFA* expression was visualized in lamina II as well as in deeper laminae (**Figure 7**). Zinc finger homeobox 3 (ZFHX3), is a transcription factor that was recently shown to be expressed ventrolaterally by excitatory and inhibitory interneurons from embryonic stages into adulthood, in the mouse spinal cord (Osseward et al., 2021). Additionally, different types of long-range projection neurons were found to express *Zfhx3* (Osseward et al., 2021). The orthologous gene in macaque- *ZFHX3*, is present in several excitatory and inhibitory clusters, with high expression in GLUT1, GLUTs7-10 and GABA3 (**Figure 12B**). As inhibitory projection neurons have not been observed in the mouse dorsal horn, it is likely that the aforementioned excitatory clusters may consist of projection neurons in addition to local interneurons.

We also looked at the distribution of channels and receptors across the macaque clusters. Overall, their expression patterns correspond to what has been reported in the mouse. With respect to the voltage-gated sodium channels, the most commonly studied include Nav1.7 (*SCN9A*), Nav1.8 (*SCN10A*) and Nav1.9 (*SCN11A*) due to their role in pain in peripheral sensory neurons of mice and humans (Akopian et al., 1996; Baker & Nassar, 2020; Cox et al.,

2010; Emery et al., 2016). *SCN9A* is distributed across several clusters as in mice while *SCN10A* and *SCN11A* are lowly expressed in both species (**Figure 12C**) (Haring et al., 2018; Sathyamurthy et al., 2018). The TTX-resistant Nav1.5 channel, encoded by *SCN5A* is highly specific to the macaque GLUT8, similar to its expression in the corresponding mouse *Cpne4* cluster (Excit -01) (**Figure 12C**). As in mice, we notice that most of the calcium and transient receptor potential (TRP) channels of the subfamily C and M are present in a number of clusters while the TRP channels of the V subfamily are sparsely expressed (**Figure 12D-E**) (Haring et al., 2018; Russ et al., 2021).

Similarly, with respect to receptors, we find that the Gamma aminobutyric acid reporter subunit alpha-1 (*GABRA1*) is highly expressed in GLUT7 and GLUT9 clusters and to a lower extent in GABA4 (**Figure 13D**). This correlates well with its expression in the corresponding clusters of the mouse. Most nicotinic acetylcholine receptors are not expressed or sparsely expressed in the macaque and mouse dorsal horn. However, we do detect high levels of *CHRNA7* across several of the macaque clusters (**Figure 13F**). The serotonin receptor encoding gene 5-Hydroxytryptamine Receptor 2A (*HTR2A*) is highly expressed in GLUT10, similar to its high expression in the corresponding mouse *Prkcg* family of clusters (**Figure 13G**). Polymorphisms in the *HTR2A* gene have been associated with chronic low back pain and fibromyalgia in human patients (Nicholl et al., 2011; Yildiz et al., 2017).

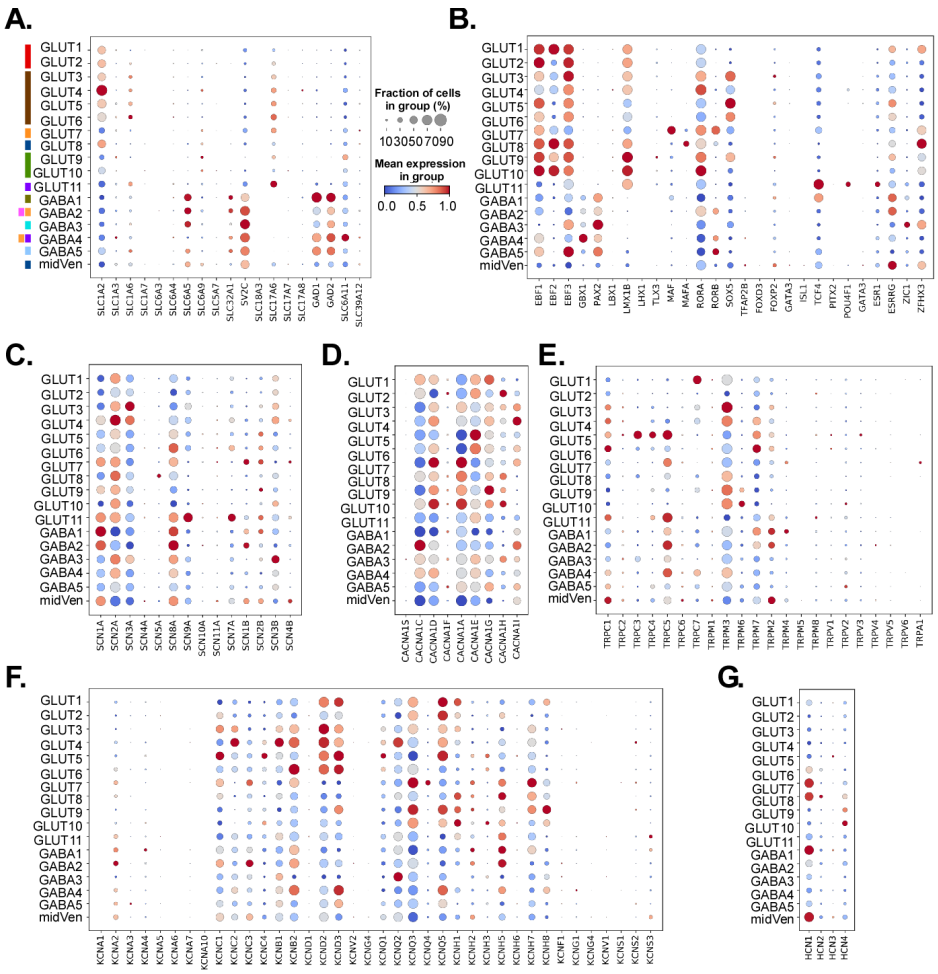

Figure 12. Expression of neurotransmitter-related enzymes, transporters, transcription factors and channels across the macaque clusters

A. Dotplot showing mean expression (by circle color) of neurotransmitter-related enzymes and transporters and the percentage of nuclei (by circle diameter) that express the specific genes in a cluster. Color bars on the vertical axis refer to the corresponding families from the mouse meta-analysis. From top to bottom: Reelin, Sox5, Maf, Cpne4, Prkcg, Rreb1, Cdh3, Rorb and Adamts5, Npy, Pdyn and midVentral. **B.** Dotplot showing mean expression of transcription factors. **C.** Dotplot showing mean expression of sodium channels. **D.** Dotplot showing mean expression of calcium channels. **E.** Dotplot showing mean expression of transient receptor potential (TRP) channels. **F.** Dotplot showing mean expression of potassium channels. **G.** Dotplot showing mean expression of hyperpolarization-activated cyclic nucleotide (HCN) channels.

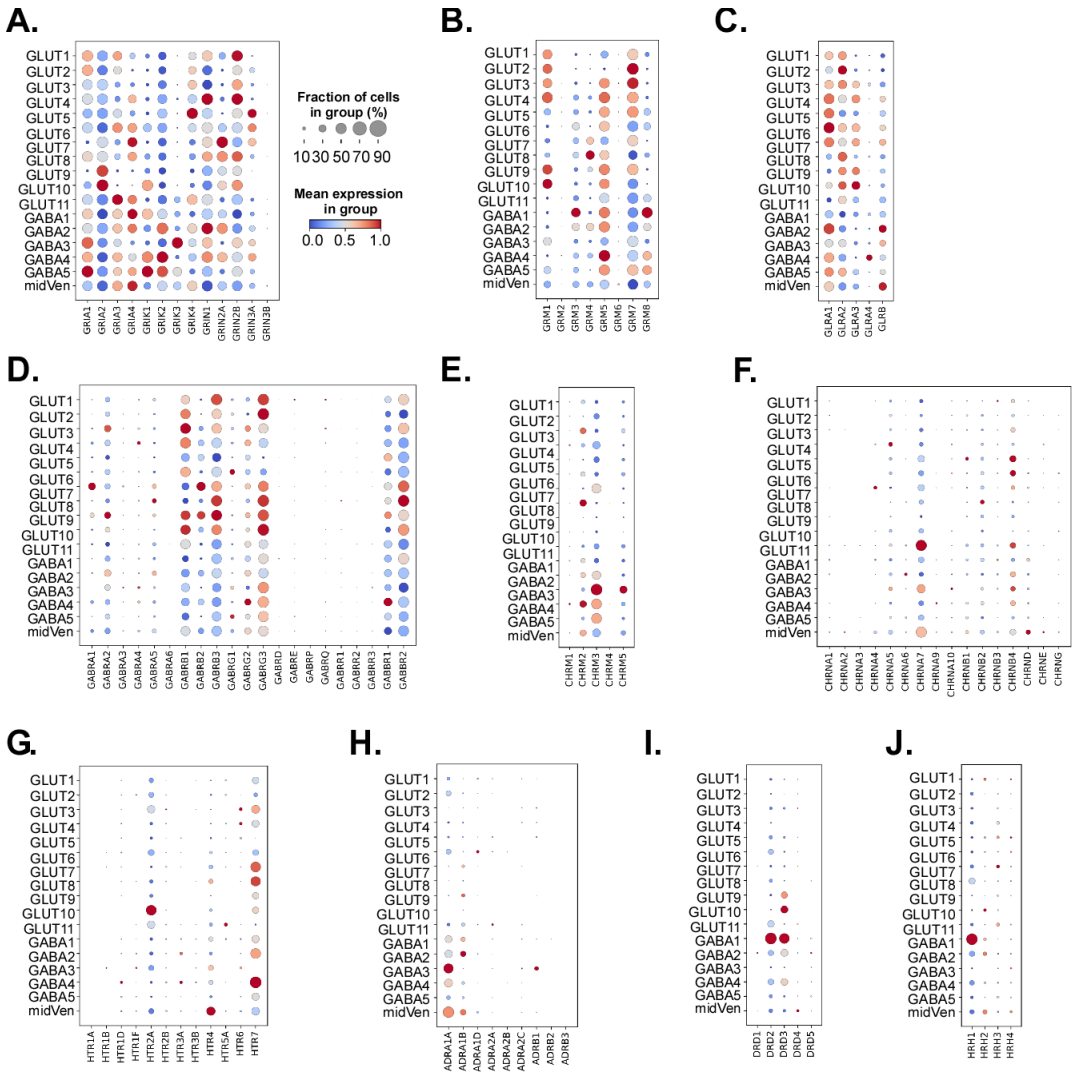

Figure 13. Expression of neurotransmitter- related receptors across the macaque clusters.

A. Dotplot showing mean expression of ionotropic glutamate receptors, (**B.)** metabotropic glutamate receptors, (**C.)** glycine receptors, (**D.)** GABA receptors, (**E.)** muscarinic acetylcholine receptors (**F.)** nicotinic acetylcholine receptors, (**G.)** serotonin receptors, **(H.)** adrenergic receptors, (**I.)** dopamine receptors, and (**J.)** histamine receptors.

3.3.4 Genes differentially expressed between macaque and mouse transcriptomes

Although the expression profiles of genes within cell populations are conserved enough to identify strong cluster relationships between the mouse and macaque, species-specific differences do exist. To find species-specific enrichment of genes across gene families, we first identified differentially expressed genes separately across each of the corresponding macaque and mouse cell type families using a Wilcoxon Rank Sum test (Russ et al., 2021). To avoid confounds from development or the isolation of whole cells versus nuclei, we only used nuclei isolated from adult mice in the meta-analysis. Highly significant genes of each cluster were considered as those that are $p < 10^{-5}$ and have a log-fold-change greater than 2 relative to their expression in the other excitatory or inhibitory families. Second, the expression of the gene in the corresponding family of the other species had a log-fold-change less than 0 relative to the other clusters of that species (**Figure 14, Appendix B**). We identified fifteen genes that are enriched in the macaque excitatory clusters compared to the mouse (**Figure 14A, Left**). Conversely, only carbonic anhydrase 12 (*CA12*) is found to be enriched in the mouse excitatory clusters in comparison to the macaque (Figure 11A, Right). A number of genes (12) are found to be enriched in the macaque inhibitory clusters compared to the mouse, among these include *MET* and *PTN*, which are marker genes for GABA4 (**Appendix B**). Surprisingly, *CPNE4* is not enriched in the cluster corresponding to the mouse *Cpne4* family (GLUT8) (**Figure 14B**). However, one of the genes enriched in GLUT8 is the Piezo- type mechanosensitive ion Channel component 2 (*PIEZO2*). Consistent with this result, the number of *PIEZO2* positive cells detected in the macaque dorsal horn is significantly higher than in mouse, as visualized by in situ hybridization (**Figure 14C**). *PIEZO2* expressing primary sensory neurons have been studied for the critical role they play in mechanotransduction so their significantly larger

presence in the macaque dorsal horn poses a question of how they may influence or be critical to the function of these neuronal populations (Chesler et al., 2016; Coste et al., 2010; Ranade et al., 2014; Woo et al., 2015). Interestingly, different collagen genes are found to be specifically enriched in several of the macaque excitatory clusters, thereby serving as useful marker genes (data not shown). The finding raises the question of what role(s) collagen proteins and specifically each type plays in dorsal horn function.

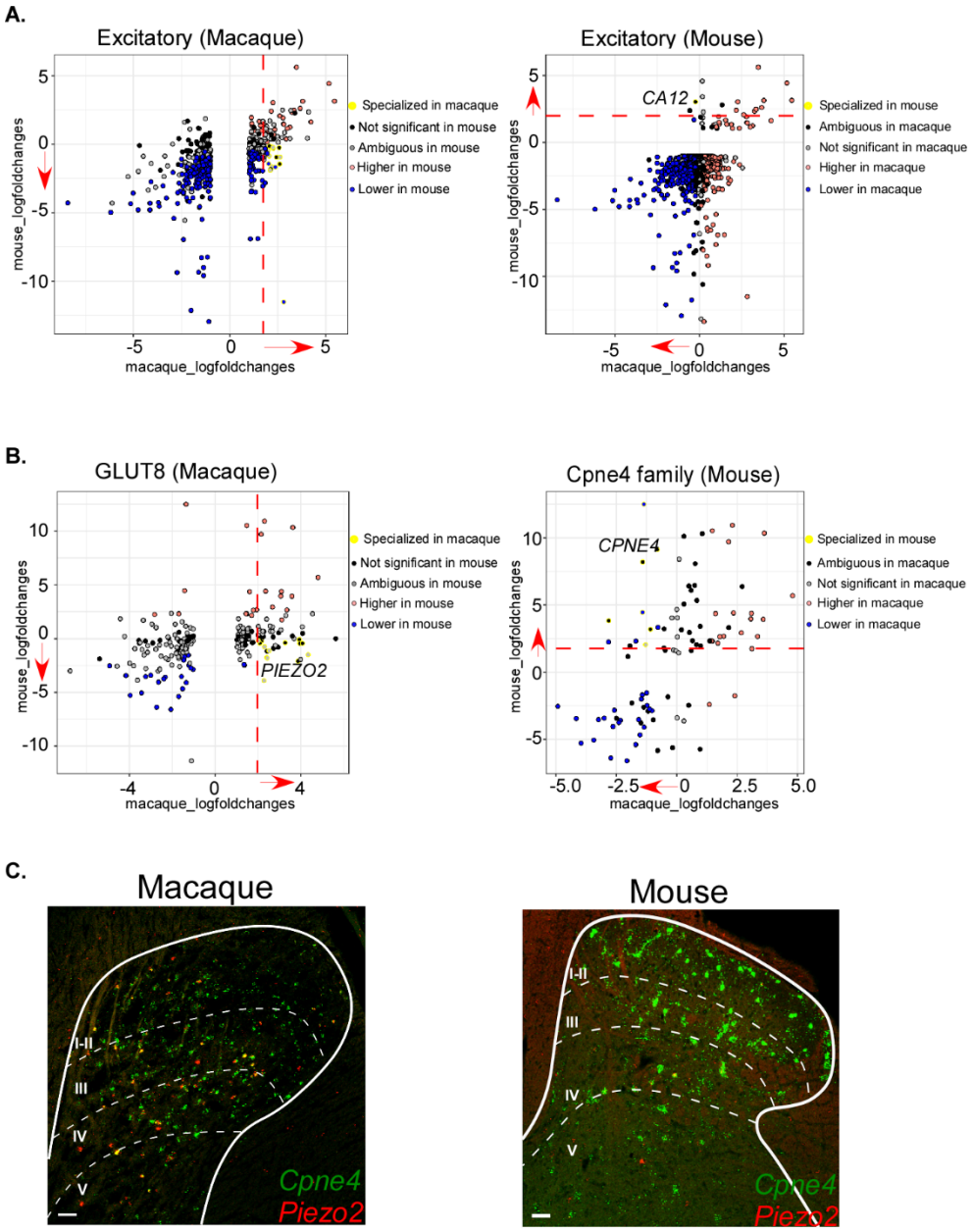

Figure 14. Macaque and mouse-specific gene enrichment

A. Correlation plots of genes specialized in the macaque excitatory clusters (left panel) compared to the adult mouse excitatory clusters. Significant genes (black circles) within each cluster show $p < 10^{-3}$ and log-fold-change > 1 relative to other clusters of the macaque. Among these, genes are species-specific or specialized (yellow circles) if they show enrichment scores of $p < 10^{-5}$ and log-fold-change (lfc) > 2 (compared across other clusters of that species) and the orthologous genes in the other species show lfc < 0 (compared across other clusters of that species). Specialized genes in mouse excitatory clusters are in yellow (right panel). All significant genes are plotted (black circles). **B.** Correlation plot of genes specialized in the macaque cluster GLUT8 (left pl. *PIEZO2* is enriched in GLUT8 but not in the corresponding clusters of the *Cpne4* family of mouse (mac lfc = 3.6774378,

mouse lfc = -0.46002). *Cpne4* is enriched in the mouse *Cpne4* family of clusters but not in the corresponding GLUT8 cluster of macaque (mac lfc = -0.1435162, mouse lfc = 9.116846). All significant genes are plotted (black circles). C. Macaque dorsal horn (left) *in situ* hybridization of *CPNE4* (green) and *PIEZO2* (red). Mouse dorsal horn (right) *in situ* hybridization of *Cpne4* (green) and *Piezo2* (red). Representative images are 10X. Scale bar = 100 μm.

3.4 Discussion

3.4.1 Similarities between mouse and macaque transcriptomes

Overall, our comparative analyses between clusters of the macaque and mouse show that the underlying molecular organization is largely conserved between the two species. Analysis of features that have been classically used to describe cell types such as their neurotransmitter phenotype, transcription factors, and channel expression show a high congruence with what has been reported in the rodent dorsal horn. Confidently identifying macaque-mouse conserved cell types and molecular signatures provides an important resource for the community, especially considering the high degree of cell type heterogeneity and the difficulty of harmonizing them within species (Russ et al., 2021). We find numerous examples which highlight that this molecular conservation likely points toward a functional conservation. For instance, glycinergic neurons, which through pharmacogenetic activation in mice have been shown to alleviate neuropathic injury-induced hyperalgesia and also block chloroquine-

and histamine-induced itch, are prevalent in deeper laminae of the mouse dorsal horn (Foster et al., 2015). We similarly find that the GABA1-3 clusters of macaque, which show high expression of the glycine transporter 2 (*SLC6A5*) are also enriched in the deeper laminae (III-IV). Similarly, the hyperpolarization-activated cyclic nucleotide-gated cation channel HCN4, which has been implicated in mechanical allodynia (touch-evoked pain) under neuropathic conditions due to its presence on PKCγ neurons, is enriched in macaque clusters GLUT9 and GLUT10 which correspond to the mouse *Prkcg* family (Nakagawa et al., 2020).

Initially, two of the macaque clusters - GABA2 and GABA4 did not show a strong correspondence with any of the mouse families. However, we noted that both *RORB* and *ADAMTS5*, orthologs of markers of distinct families in the mouse meta-analysis, were expressed in both clusters. Re-clustering GABA2 and GABA4 with a finer resolution revealed sub-populations showing a strong correspondence with both the mouse *Rorb* and *Adamts5* families. We suspect that this may be due to a higher degree of similarity in the molecular profiles of the *Rorb* and *Adamts5* families during embryonic/developmental ages than in the adult. Alternatively, it is possible that evolutionary differences in gene expression resulted in GABA2 and GABA4 clusters becoming more molecularly distinct in the macaque. Interestingly, both the GABA4_1 sub-cluster, and its corresponding subset from the mouse *Rorb* family (Inhibitory 03-05), show high expression of calretinin (*Calb2*) (https://seqseek.ninds.nih.gov/#/genes). Calretinin inhibitory neurons are largely concentrated in lamina II of the mouse dorsal horn and make up ~25% of the inhibitory neurons in this area (Gutierrez-Mecinas, Davis, et al., 2019). Thus, the GABA4_1 cluster may represent a more superficially located population of the *RORβ* neurons than GABA2_1. A study involving the neuronal activity marker, phosphorylated extracellular signal related kinase (pERK), reported a role for inhibitory calretinin neurons in processing noxious mechanical information and to a lesser extent, noxious chemical stimulation (Smith et al., 2015).

Other classically studied non-overlapping inhibitory populations, apart from calretinin, include galanin (*Gal*) which co-expresses dynorphin in the mouse dorsal horn, neuronal nitric oxide synthase (*Nos1*), parvalbumin (*Pvalb*) and *Npy* (Boyle et al., 2017). These genes are largely segregated among the 5 GABA clusters with *NOS1* enriched in GABA1, *NPY* in GABAs 2 and 3, *PVALB* in GABA4 and *PDYN* in GABA5. *GAL* is detected at low levels in the macaque dorsal horn and so its overlap with dynorphin is minimal. We observe high expression of *NOS1* and *PVALB* in excitatory clusters as well as the inhibitory clusters, similar to the mouse (Boyle et al., 2017; Gradwell et al., 2021; Hughes & Todd, 2020). *PVALB* is present in GLUT7, whose nuclei show laminar enrichment in laminae III-IV. This corresponds with *PVALB* expression in deeper laminae of the mouse dorsal horn (Boyle et al., 2017; Hughes et al., 2012). Neuronal nitric oxide synthase (nNOS)-expressing neurons in mice show minimal overlap with *PVALB* or *NPY*, however 82% of inhibitory nNOS-expressing inhibitory neurons were reported to overlap with *PDYN* across development (Boyle et al., 2017). It is thus possible that the GABA5 cluster of inhibitory *PDYN* neurons in macaque also expresses NOS1, however from computational analysis, we find that this overlap appears to be less than 1%.

3.4.2 Distribution of potential projection neurons across excitatory macaque clusters

Projection neurons located in lamina I and in the deeper laminae III-VI transmit modality-specific somatosensory information to multiple brain regions (Todd, 2010; Todd et al., 2000). Similar to spinal interneurons, these neurons are molecularly diverse, however, their identification is more challenging, as it requires back-labeling from distinct brain regions coupled with single cell sequencing or histology using cell-type markers. Such studies have

been performed to an extent in rodents but would be a major undertaking in macaque. Nevertheless, it is an important question that should be addressed in future studies. Extrapolating what is known in rodents to our macaque database, we can speculate on which clusters contain projection neurons in the macaque. Studies in rodents have focused primarily on spinoparabrachial projection neurons. Those expressing neurokinin 1-receptor (*NK1R*) are thought to account for the majority of lamina I projection neurons (~80% in mouse and 90% in rat) (Cameron et al., 2015; Spike et al., 2003; Todd, 2010). NK1R projection neurons are activated by noxious stimuli and innocuous cooling and have been shown to be important for the generation of hyperalgesia under inflammatory or neuropathic pain conditions (Andrew, 2009; Bester et al., 2000; Han et al., 1998; Willis et al., 1974). A subset of the NK1R neurons may also be involved in spinal itch mechanisms (Carstens et al., 2010). The *TACR1* gene which encodes the NK1 receptor is expressed in macaque GLUT 4, 6, 7 and 11 clusters. Häring et al identified an excitatory cluster – GLUT15 that consisted of spinoparabrachial neurons marked by the expression of *Lypd1* and *Elavl4* (Haring et al., 2018). We noted that orthologs of these two mouse genes, *LYPD1* and *ELAVL4* are expressed together with *TACR1* in GLUT7 and GLUT11, but also in GABA1 and in deeper midVen clusters. A more recent study by Wercberger et al analyzed the molecular signatures of spinoparabrachial projection neurons that are not NK1R+, and identified a small proportion of projection neurons that expressed either *Cck*, neuronal pentraxin 2 (*Nptx2*) or neuromedin B (*Nmb*) many of which reside outside lamina I (Wercberger et al., 2021). While *CCK* is expressed in several macaque excitatory clusters including GLUT7 and GLUT11 as seen with *TACR1*, *NPTX2* and *NMB* show restricted expression in GLUT8 and GLUT9 respectively. Thus, we speculate that GLUTs 4, 6, 7, 8, 9 and 11 may contain sparse populations of projection neurons in addition to interneurons.

3.4.3 Differences between mouse and macaque transcriptomes

Several species-specific differences are also observed at the gene level. This was initially noted when assigning marker genes to the macaque clusters. While some marker genes such as *NMUR2*, are unique and highly expressed in correlating clusters of both mouse and the macaque, this was not seen for all clusters. For example, we now provide novel molecular markers such as *CRHR2* and *COL13A1*, which are not present in the mouse dorsal horn, as better candidates for the targeted study of their respective cell types in the macaque.

Another notable difference in gene expression was observed with *PDYN* in excitatory neurons which are more prominent in the primate dorsal horn compared to the mouse. Sathyamurthy et al study assigned the excitatory dynorphin neurons to the DE-15 cluster whereas they were not reported in the Haring et al study or in the meta-analysis (Haring et al., 2018; Russ et al., 2021; Sathyamurthy et al., 2018). Immunohistochemical studies in mice suggest excitatory dynorphin neurons are primarily located within the medial portion of lumbar segment L4, which receive input from glabrous skin (Boyle et al., 2017; Huang et al., 2018). Discrepancies in the reporting of these cells therefore may reflect their low abundance outside the lumbar enlargement in mice. Interestingly, in the rat lumbar dorsal horn, approximately ~50% of the dynorphin neurons in lamina I and 20% of those in lamina II were reported to be excitatory and to span the mediolateral axis (Sardella et al., 2011). In the primate, we observe 60-70% of the dynorphin neurons in lamina I and 30-40% of those in lamina II to be excitatory. Here also, the expression was not restricted to the medial dorsal horn. The excitatory dynorphin neurons are of interest, as a transcriptomic study conducted in mice showed a unilateral upregulation of genes specifically in these neurons in the superficial laminae ipsilateral to the site of surgical incision or carrageenan inflammation (Sapio et al., 2021). Additionally, another

study showed that excitatory dynorphin neurons are implicated in noxious heat-induced burn injury (Varga et al., 2021). Taken together, the excitatory dynorphin neurons may potentially be involved in acute phase hyperalgesia (Serafin et al., 2021).

3.4.4 Organization of neuropeptides in the primate dorsal horn

A lot of work has been done in mice to understand the role of neuropeptide-expressing excitatory dorsal horn neurons and their receptors. Several of these neuropeptides show modality-specific functions with respect to pain or itch processing and restricted laminar expression patterns (Das Gupta et al., 2021). *GRP* neurons in the macaque belong to GLUT1, GLUT3 and GLUT5 clusters which corresponds to their inclusion in the mouse meta-analysis families - *Reln* (Excit 08-10) and *Sox* (Excit15, 18-19). In the rodent dorsal horn, *Grp* neurons present in lamina II receive primary afferent input from *MrgprA3* pruritoceptors and are involved in spinal itch mechanisms (Albisetti et al., 2019; Pagani et al., 2019). The GRP receptor GRPR, found in laminae I-II of the rodent dorsal horn also transmits itch information conveyed by GRP from primary sensory neurons (Pagani et al., 2019; Sun & Chen, 2007). Furthermore, GRPR neurons reportedly form synaptic contacts with projection neurons in lamina I (Bardoni et al., 2019). The macaque GLUT2 cluster contains neurons expressing GRPR as well as a subset of the somatostatin (SST) neurons- a population that has also been implicated in the itch circuitry in mouse (Huang et al., 2018). Interestingly, we find that the neuropeptide thyrotropin-releasing hormone (TRH) – expressing neurons belong to both GLUT1 and GLUTs 9-10 which correspond to the *Reln* and *Prckg* mouse families, respectively. Computationally, these neurons do not appear to overlap with the GRP population

which is also present in GLUT1. TRH neurons in the mouse dorsal horn have not been functionally investigated in the context of pain or itch, but as a subset of the larger PKCγ neuron population, they may be involved in the transmission of neuropathic pain (Gutierrez-Mecinas, Bell, Shepherd, et al., 2019; Peirs et al., 2021). Both GLUT3 and GLUT4 are characterized by *TAC3* expression which is expressed in laminae II-III similar to the mouse meta-analysis clusters Excit-18-19, which are marked by Tac2 expression. *TAC3* is also minimally expressed in GLUT11. Ablation of TAC2 neurons did not affect acute somatosensation or mechanical thresholds after nerve injury in mice (Duan et al., 2014). However, there is evidence for a role for these neurons in mechanical itch (Chen et al., 2020). Additionally, 84% of TAC2 neurons express calretinin, which has been shown to be important for the transmission of mechanical allodynia under inflammatory conditions (Gutierrez-Mecinas, Davis, et al., 2019; Peirs et al., 2021; Peirs et al., 2015). Both GLUT5 and GLUT6 show high expression of *TAC1* similar to their mouse meta-analysis counterparts Excit- 15-16 and in both species, *TAC1* is distributed in laminae I-II as well as in deeper laminae IV-V. We also find lower levels of TAC1 expression in the macaque GLUT4 and GLUT11 clusters. Ablation of TAC1 dorsal horn neurons in mice did not alter reflexive-defensive behaviors but rather caused a deficit in nociceptive coping behaviors- suggestive of a role in the affective component of sustained pain (Huang et al., 2019). The neuropeptide *CCK* is detected in several clusters. It is expressed in GLUT7 and at lower levels in GLUT9 which correlates with *Cck* expression in the mouse meta-analysis clusters Excit-05 (Part of *Maf* family) and Excit-03 (Part of *Prkcg* family), respectively. We also observe high expression of *CCK* in GLUT5 which expresses TAC1. One study reported that ~20% of *Cck* neurons in laminae I-III overlap with *Tac1* in mouse using histological methods (Gutierrez-Mecinas, Bell, Shepherd, et al., 2019). Interestingly, we detected high expression of CCK in GLUT11 and this is not seen in the mouse meta—analysis counterpart. In mice, laminae III-IV CCK neurons are involved in the transmission of

mechanical allodynia and heat hypersensitivity following inflammatory injury and transmission of mechanical allodynia following neuropathic injury (Peirs et al., 2021). It is notable that the distribution of *CCK* was different in the human spinal cord, where it is more highly expressed in the outer laminae. Given the differences in nociceptor primary afferent termination in humans, these neurons may play a specialized role in pain transmission in clinical pain disorders (Shiers et al., 2021). GLUT7 and GLUT9 express the neuropeptide-*NTS* which corresponds with what is seen in the mouse meta-analysis clusters Excit-03-05. Activation of NTS- lineage neurons in laminae II_i-III of the mouse dorsal horn resulted in an increase in withdrawal response to brush stimulation (Gatto et al., 2021). Dorsal root stimulation of NTS-lineage neurons was sufficient to evoke wind-up in lamina I spinoparabrachial neurons (Hachisuka et al., 2018). Overall, the expression of neuropeptides in distinct clusters shows a strong correlation between the mouse and macaque (Das Gupta et al., 2021). Furthermore, we show a striking conservation in their laminar distribution patterns across species including in human, suggestive of conserved somatosensory roles for these neuropeptides in the primate dorsal horn.

4.0 Identification of macaque dorsal horn cell-type specific regulatory elements

4.1 Introduction

Persistent pain is a public health epidemic that alters the quality of life for patients by negatively impacting their physical and emotional functioning. The spinal cord dorsal horn is a principal site for the investigation of pain processing as it receives nociceptive signals from the periphery, gates and modulates this information, and transmits to supraspinal sites. Resources such as genetic and viral tools have enabled researchers to target and manipulate specific dorsal horn populations in the mouse for circuit-based studies. For instance, using transgenic mouse lines and chemogenetic viral tools, we identified three different dorsal horn populations that are important for the transmission of mechanical allodynia (MA), a clinical feature associated with several persistent pain conditions, in which innocuous stimuli become painful (Peirs et al., 2021). The populations include calretinin expressing neurons which transmit MA following inflammatory injury and PKCγ expressing neurons which transmit MA following nerve injury. Interestingly, CCK expressing neurons were found to transmit MA induced by both types of injuries and are involved in the transmission of heat hypersensitivity following inflammatory injury (Peirs et al., 2021).

The ease of maintaining and breeding mice, coupled with available tools, have made them indispensable for the study of a number of complex human diseases including pain. However, species-specific differences can often affect the translatability of therapeutic targets

identified in the mouse. Rhesus macaques, which are 28 million years (MY) diverged from humans compared to rodents, which are 89 MY from humans, serve as an attractive animal model for proof-of-concept pain studies (Disotell & Tosi, 2007). Through a single-nucleus transcriptome study of the macaque dorsal horn, we identified the major neuronal cell types and their laminar organization (Chapters 2 and 3). Additionally, we report a conservation in the cell types and their laminar organization between the mouse and macaque, suggestive of a conservation in their functional organization. Unfortunately, the diverse genetic tools available in mouse and some rats do not exist to selectively target neuron populations in the non-human primate dorsal horn for anatomical or functional interrogation.

Here, we used single-nucleus Assay for Transposase-Accessible Chromatin with sequencing (snATAC-seq) to identify putative regulatory elements (REs) that are present in the open chromatin regions of select genes of interest in the macaque dorsal horn (Buenrostro et al., 2015; Cusanovich et al., 2015). Open chromatin regions show lower nucleosomal density or are nucleosome-free and contain transcription factor binding sites enabling them to flexibly modulate gene regulation based on the available transcription factors and chromatin landscape of a cell type (Long et al., 2016). Transcription of genes in a particular tissue is chiefly regulated by a combination of sequence-specific DNA binding transcription factors along with cis-regulatory elements (promoters and enhancers). Machine learning models can then be applied to identify the 'regulatory code' i.e., the combinatorial code of transcription factor binding sites and associated DNA sequences present in the cell-type's open chromatin region (Kelley et al., 2016; Zhang et al., 2020; Zhou & Troyanskaya, 2015). We leverage this strategy to identify REs that may be cell type specific by its chromatin accessibility in one cell type and not others, as well as its underlying DNA sequence predicted to contain the relevant regulatory code.

Viral vectors containing putative REs or orthologs of these REs can therefore be used to drive reporter or other transgene expression in a cell-type specific manner across species.

While such efforts are underway in targeting neurons of different brain regions, the dorsal horn remains largely unexplored (Dimidschstein et al., 2016). Thus, this work will serve as a valuable resource for the subsequent development of viral tools to target and study conserved cell-types involved in the primate dorsal horn pain circuitry. Importantly, these viral tools can double as therapeutics through manipulation of specific dorsal horn populations involved in pain transmission.

4.2 Methods

4.2.1 Macaque Spinal Cord Sample

Fresh lumbar segment (L4-L6) tissue was harvested from a 3-year-old male Rhesus macaque (Provided by Dr. Leah Byrne at the University of Pittsburgh) for snATAC-seq. For euthanasia, the animal was initially sedated with ketamine (15 mg/kg IM), and then perfused through the circulatory system with 3-4 liters of ice cold artificial cerebrospinal fluid (ACSF; 124 mM NaCl, 5 mM KCl, 2 mM MgSO4, 2 mM CaCl2, 23 mM NaHCO3, 3 mM 524 NaH2PO4, 10 mM glucose; pH 7.4, osmolarity 290–300 mOsm).

4.2.2 Nuclei Isolation

Spinal cord grey matter was transected at the central canal under a dissection microscope and immediately placed in a glass dounce homogeneizer containing 1 ml NbActiv1. The 10X Genomics nuclei isolation protocol for scATAC-seq was followed. We homogenized tissue using approximately 30 strokes of a loose pestle. The nuclei were then filtered through a 40 µm strainer (EZFlow Cell Strainer, Foxx Life Sciences, Cat# 410-0001-OEM). 1 ml of NbActiv1 was passed through the strainer into the same collection tube. The nuclei were transferred to a 2 ml microcentrifuge tube and centrifuged at 500 rcf for 5 minutes at 4°C. After removing the supernatant, 100 µl of chilled 0.1x lysis buffer was added and mixed by pipetting up and down 5 times. The mixture was incubated on ice for 5 minutes. Then, 1 ml of chilled wash buffer was added to the lysed cells and mixed by pipetting up and down 5 times. This was followed by centrifugation at 500 rcf for 5 min at 4°C. The supernatant was removed and the nuclei were resuspended in chilled diluted nuclei buffer.

4.2.3 snATAC-seq

The Chromium single-cell ATAC-seq v1.1 kit was used for this work. Five technical replicates from the nuclei sample were pooled and loaded onto a Illumina Novaseq 6000 S2-100 flow chip. We sequenced samples to a depth of ~64,000 reads per nucleus.

4.2.4 Data analysis and processing

Raw bcl files were demultiplexed using the cellranger-atac workflow. The resulting fastq files were aligned to the rheMac10 genome using Chromap (Zhang et al., 2021). The aligned fragments files were then converted to arrow files to be analyzed using the snATAC-seq suite of analyses toolkit ArchR with a custom gene annotation file created for the rheMac10 genome (Granja et al., 2021; He et al., 2021). The custom gene annotation was necessary to supplement the minimally annotated macaque genome, which were previously shown to miss many untranslated elements of transcripts and non-coding transcripts (He et al., 2021). Briefly, we applied the liftOff tool of the human RefSeq gene annotation on the hg38 genome to identify orthologous rheMac10 gene annotation (Shumate & Salzberg, 2020).The ArchR pipeline was used for quality control pre-processing steps such as doublet detection and removal, dimensional reduction and clustering of nuclei, and transfer learning using Seurat v3 canonical correlation analysis of computed snATAC gene accessibility scores with our previously described snRNA-seq gene expression data.

4.3 Results

4.3.1 Chromatin accessibility of macaque dorsal horn

To identify transcriptionally active regions of specific dorsal horn cell-types, we harvested lumbar dorsal horn tissue from a young-adult (3-year-old) male Rhesus macaque for single nucleus Assay for Transposase-Accessible Chromatin using high-throughput sequencing (snATAC-seq) (Buenrostro et al., 2015). The nuclei were isolated from fresh homogenized tissue and five technical replicates were made for snATAC-seq. These snATAC-seq libraries were then deep sequenced using the Novaseq 6000 platform. Using the ArchR pipeline, we performed quality control metrics (Granja et al., 2021). Here, we found that each of the technical replicates consisted of ~10,000 nuclei with ~13,000 unique fragments per nucleus, which is above the lower limit of snATAC quality of 1,000 unique fragments. Additionally, the fragments exhibited the expected periodicity in their length i.e., depletion of fragments that that are multiples of the length of DNA wrapped around a nucleosome (~147 bp, ~296 bp etc.) (**Figure 15A**). All replicates also show a high signal at the transcription start site (TSS), indicative of fragments measured from intact nuclear chromatin (**Figure 15B**). Computationally detected doublets were inferred and also removed from the final dataset (**Figure 15C**). Overall, these pre-processing steps indicate that the snATAC-seq libraries are of high quality.

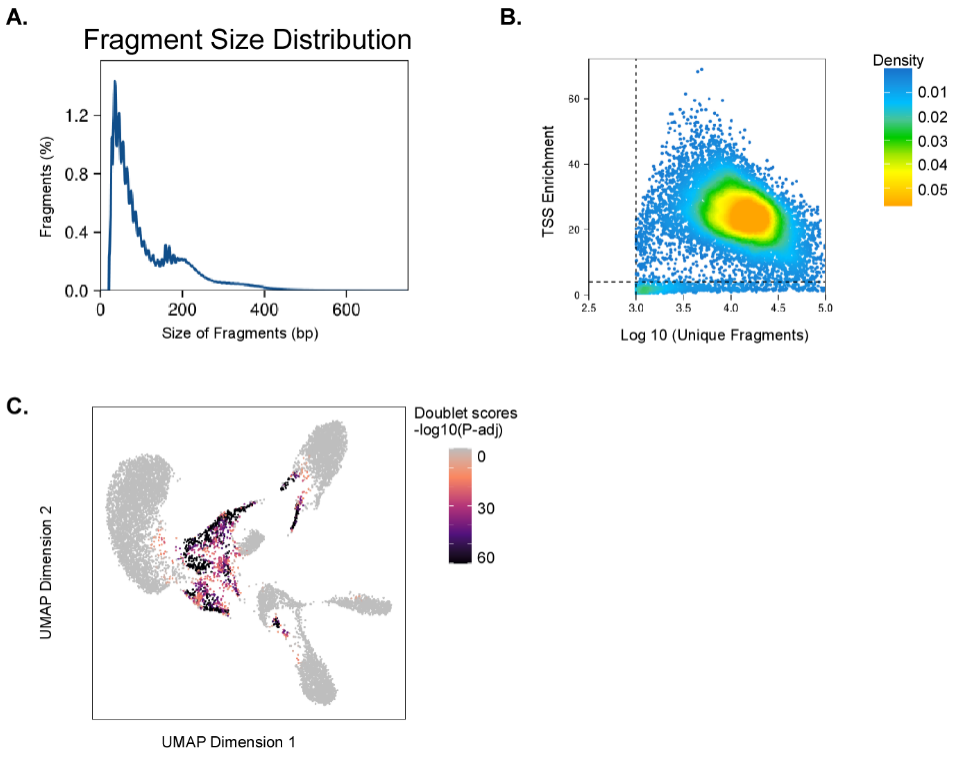

Figure 15. Quality control metrics performed on snATAC-seq libraries

A. Characteristic periodicity in fragment length distribution with dips at 147 bp and 296 bp marks. **B.** Dotted line indicate nuclei that pass the default thresholds (TSS score > 4 and containing more than 1000 unique fragments). **C.** In silico doublets are synthesized from the data and projected on to the UMAP to identify their nearest neighboring nuclei. These nuclei whose signal are similar to the synthetic doublets are subsequently removed. All plots are representative examples from technical replicate #1.

4.3.2 Integration of snRNA-seq and snATAC-seq data

Dimensionality reduction with UMAP and Louvain clustering were performed on the snATAC-seq data using ArchR (Granja et al., 2021). All nuclei from the five technical replicates were clustered together, and nuclei with high gene accessibility score around the *RBFOX3* gene were identified as neurons. Of note, the neuronal nuclei could be clustered into 11 excitatory and 5 inhibitory dorsal horn clusters as seen with snRNA-seq (**Figure 16A**)

(Chapters 2 and 3). Furthermore, we carried out high-dimension clustering of the snATAC to compute gene accessibility scores using the previously described snRNA-seq macaque dorsal horn gene expression data to align clusters from the two datasets together. We detect an average of 40 nuclei per cell type with ~20,000 – 25,000 fragments per cell, yielding more than 200 high-quality nuclei per neuronal cell type for cluster-level epigenomic analyses (**Figure 16B**). To visualize the higher-order relationship between the clusters, the snATAC-seq clusters were labeled by the corresponding meta-analysis derived families (**Figure 16C**).

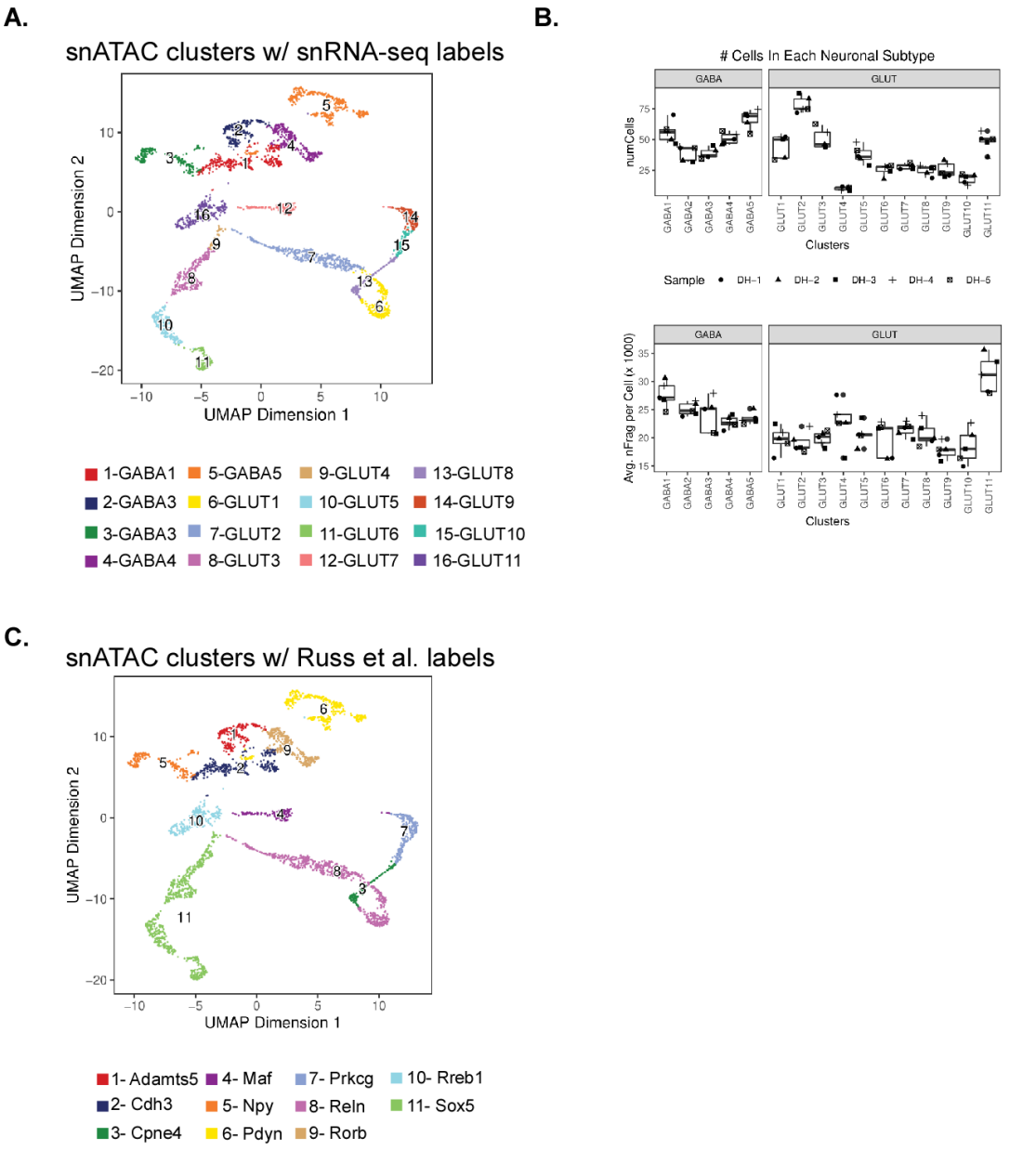

Figure 16. Representation of snATAC-seq fragments across all 16 dorsal horn cell types

A. UMAP showing snATAC-seq clusters annotated based on their correlation to the snRNA-seq clusters. **B.** Plots showing the number of cells (top) and average number of fragments (bottom) across the dorsal horn cell types from each technical replicate. **C.** UMAP showing snATAC-seq clusters annotated based on their correlation to the meta-analysis families.

4.4 Discussion

These data lay the groundwork for identifying the 'regulatory code' of individual dorsal horn cell types across species. Though this work is ongoing, here we show that clusters from the snATAC-seq align well with those from the snRNA-seq. Furthermore, approximately 200 high-quality nuclei per cell type are available, offering the scope to probe the chromatin accessibility of all 16 distinct cell types and compare it to the mouse. Additionally, fragments from glial cells, which have been shown to be important for dorsal horn pain mechanisms, were also clustered based on their accessibility scores to glial cell marker genes such as *GFAP* for astrocytes and *MBP* for oligodendrocytes (data not shown).

Classically, studies employed methods such as DNase-seq, MNase-seq or Chip-seq to understand the epigenetic structure and identify promotor regions of individual genes (Landt et al., 2012; Song & Crawford, 2010; Zaret, 2005). However, these methods require a high input cell number and the protocols are time-consuming. ATAC-seq in contrast, is a simple protocol that can be performed in a few hours with just 50,000 cells. Thus, we adopted this method to probe the transcriptional profiles of dorsal horn neuron populations. Additionally, while studies have attempted to achieve cell-type specific targeting in brain regions using promoters or enhancers delivered in viral vectors, there has been a lack of attention on the dorsal horn- a region with numerous candidate targets for pain therapeutics (Dimidschstein et al., 2016; Lawler et al., 2020; Mich et al., 2021). The work described in this chapter therefore attempts to reconcile this gap in knowledge. Importantly, the snATAC-seq analyses will be supplemented by analysis of the macaque ventral horn multiome (snRNA-seq+snATAC-seq) to ensure that candidate REs a5.re specific to genes of dorsal horn cell types and do not overlap with ventral horn populations.

5.0 General Discussion

5.1 Importance of a classification scheme

Through a large-scale transcriptomic analysis of the macaque dorsal horn (Chapter 2-4), several key features were observed. The macaque dorsal horn neurons are molecularly diverse. Similar transcriptomic analyses in the mouse spinal cord also highlighted this molecular diversity, particularly in comparison to ventral horn neurons (Russ et al., 2021; Sathyamurthy et al., 2018). This diversity is not only limited to the neurochemical profiles of dorsal horn neurons but also extends to their morphological and physiological features. Thus, it has been challenging to reach a consensus in their molecular and functional organization. Separate studies have looked at individual neuropeptide gene expression in monkey spinal cords using immunohistochemistry (Zhang et al., 1995; Zhang et al., 1993). However, using a combination of snRNA-seq with computational analyses (Chapter 2), we provide a more comprehensive atlas of the molecular profiles of all dorsal horn neurons. I show that the neurons can be clustered in to 11 excitatory clusters and 5 inhibitory clusters based on their distinct gene expression profiles. One of the main organizing principles of the spinal cord is the Rexed laminae, which divides the dorsal horn into different layers based on the cytoarchitecture (Rexed, 1952). As described in Chapter 1, the functional organization of the dorsal horn also appears to depend on this laminar organization. Thus, I examined the spatial distribution of neurons belonging to the 16 identified molecular cell-types using *in situ*

hybridization. Many of the excitatory cell-types show lamina-specific enrichment while inhibitory cell-types are distibuted across several dorsal laminae. I predict that this cellular organization may play an important role in allowing excitatory cell-types to differentially transmit pain, itch or touch information to supraspinal regions depending on if they are present in the superficial or deeper dorsal horn respectively, while inhibitory neurons share a common role in gating transmission of the various microcircuits formed by these excitatory cell types. However, further studies involving cell-type specific targeting as proposed in Chapter 4 are required to determine whether the discrete dorsal horn cell types perform functionally discrete roles, and how this compares to the ventral horn where neurons share largely overlapping gene expression profiles (Russ et al., 2021).

5.1.1 Conserved cellular and molecular organization between mouse and macaque

In Chapter 3, we performed a cross-species comparative analysis between the mouse meta-analysis and macaque dorsal horn cell types. We noticed that by grouping the macaque clusters according to their corresponding mouse families-which are higher-order clusters, a remarkable conservation in their laminar organization could be seen. Thus, there was a strong correspondence between both the cellular and molecular organization of the dorsal horn neurons. Briefly, as seen in the mouse dorsal horn, we find that glycinergic neurons (neurons expressing the *GLYT2* transporter) are primarily present in the deeper dorsal horn laminae. Channels and receptors that express in specific cell types in the mouse dorsal horn also appear to be present in the corresponding cell type of the macaque. For example, in mouse, HCN4 immunoreactivity was seen in PV and PKCγ expressing cells in the dorsal horn. We observe a

similar enrichment of this channel in cells expressing *PVALB* or *PRKCG.* Thus, we could predict that molecularly conserved cell types show conservation in their functional roles.

From comparative analyses, we could similarly predict which macaque clusters contain projection neurons based on the expression of molecular markers identified in the mouse. However, these are only correlations and further validation is required through retrograde tracing combined with histology or sequencing in the primate. Such viral tracing studies would again require a strategy for cell-type specific targeting.

In Chapters 1 and 3, I focused on the role of neuropeptides because neuron populations expressing these neuropeptides largely show a lamina(e) specific enrichment and their gene expression profiles are mostly distinct. The expression pattern of neuropeptide-expressing populations is also surprisingly conserved across mouse, macaque and human with slight differences. We have seen from rodent pain and itch studies, that these neuropeptide expressing neurons play important functional roles. Thus, they are good candidates for functional studies in the primate dorsal horn and may also be potential therapeutic targets.

5.1.2 Genes differentially expressed between mouse and macaque

Single-cell or nucleus transcriptomes of primary afferents and brain regions across species have shown important differences that must be considered for translational studies (He et al., 2021). In Chapter 3, we highlight several differences in gene expression between the mouse and macaque cell types that can be probed in future experiments. One such example is the expression of mechanosensitive ion channel *PIEZO2* which has been reported in primary sensory neurons and spinal cord ventral horn, but not in the dorsal horn (Ranade et al., 2014).

I speculate that cells expressing this channel in the macaque dorsal horn play an important role in conveying light touch information, however this requires further investigation.

Thus, the single nucleus transcriptomic analysis provides valuable insight into the organization of dorsal horn neurons in primate and importantly also offers several potential targets for further study.

5.2 Experimental Limitations

A primary limitation of the transcriptome studies described in Chapters 2-4 is that only male macaques were used. The challenge of obtaining fresh macaque spinal cord samples coupled with the cost of sequencing technology hampered us from running more biological replicates. However, in the *in situ* hybridization studies discussed in Chapter 2-3 I did not find any observable differences in the expression of genes probed between male and female macaques. Our future studies will commit to processing and analyzing spinal cords from female macaques, particularly for snATAC-seq. The chromatin landscape can vary not only across tissues but also between males and females, across development, and in disease conditions as reported by other studies (Gorkin et al., 2020; Liu et al., 2019; Wang et al., 2021). All of these are important considerations that must be taken into account when endeavoring to identify a reliable regulatory code for specific cell-types. In our snRNA-seq study, we used naïve young-adult macaques and while we did not directly compare their transcriptional profile to older adult macaques, we show that our proposed macaque clusters show a strong correlation to the

mouse meta-analysis-derived clusters which contained datasets ranging from embryonic to adult ages (Russ et al., 2021).

The RNAscope® technology is a qualitative assay. Variability between experimental runs or individual samples can affect the quality of mRNA expression making an accurate quantitative assessment difficult, thereby discouraging any statistical inference. Another confounding feature of primate tissue is the wide-spread presence of fatty deposits i.e., lipofuscin which look like positive *in situ* signal. To mitigate misinterpretation of the total neuropeptide counts of the specific genes probed in Chapters 3, I sampled sections taken from 2-3 macaque or human donor tissue samples and report normalized counts. We also used a background subtraction method to account for false positives arising from the presence of lipofuscin. Thus, though the counts may underrepresent the actual number of neurons expressing the different neuropeptides, it still provides a clear summary of which laminae show enrichment of individual neuropeptides.

For the snRNA-seq, we deep sequenced the samples and achieved ~50M reads per animal. Overall, we report a good representation of individual genes and cell types. However, there are a limited number of genes that are not represented in our dataset, such as *Sstr2 and Npff* which are expressed in the superficial part of the rodent dorsal horn (Das Gupta et al., 2021; Prasoon et al., 2015). The absence of these genes in our dataset is likely due to incomplete annotation of the macaque genome or insufficient number of reads captured from these genes. Indeed, I observed *Npff* mRNA expression through *in situ* hybridization in the superficial macaque dorsal horn (data not shown).

5.3 Future Directions

The main rationale for the experiments conducted in Chapters 2-4 is to establish an atlas for the primate dorsal horn which will enable functional and anatomical characterization of the molecularly discrete cell types and ultimately an understanding of the dorsal horn circuitry underlying somatosenation. As mentioned in section 5.2, a necessary next step is to sample more biological replicates for the snATAC-seq analysis with a separate analysis on differences in the chromatin landscape between male and female macaques. Furthermore, work is underway to perform a multiome analysis of the spinal cord ventral horn since our primary goal is to develop a strategy to selectively target individual genes of dorsal horn neurons and not ventral horn populations. Additionally, snATAC-seq of the primate DRG may also be necessary for the same reason. This will be challenging as several genes of interest such as *CCK* or *PVALB* are expressed in deeper spinal cord and DRG in primates. Strategies to restrict RE-driven transgene expression to the dorsal horn will likely require optimization of a number of factors such as viral serotype and method of delivery. Also, snATAC-seq data of the mouse dorsal horn may also be required to train the machine learning model to identify regulatory codes for specific genes that are conserved across species.

Candidate REs can be cloned into viral vectors along with a reporter transgene to assess their ability to drive expression efficiently and selectively in dorsal horn neuron populations of interest. The best candidates can then be used for subsequent experiments. An additional test would be to use the selected REs to drive Designer Receptor Exclusively Activated by Designer Drugs (DREADD) expression and perform behavioral assays before and after ligand administration. To validate the behavioral readout, this must be first tested with proper controls and in populations that have already been functionally characterized using transgenic Cre lines,

such as the CCK neurons (Acute viral inhibition of CCK neurons reverses mechanical allodynia following inflammatory and neuropathic pain) (Peirs et al., 2021).

Finally, the best candidate REs can be screened in the primate dorsal horn similar to the approach in mice, by assessing if reporter expression is specific to the cell type and the percentage of coverage obtained, using histological approaches. As mentioned in Chapter 1, the use of transgenic mice that mark developmental populations or the lack of specific Cre lines limit our interpretations and understanding of the dorsal horn neurons. The larger scope of our proposed strategy implies that REs that are species-independent can be used to achieve cell-type specificity in mice as well as in primates, to bridge our gap in understanding how dorsal horn neurons are connected and form microcircuits. The putative REs can be used for viral tracing studies to determine the molecular properties of projection neurons in the non-human primate dorsal horn and subsequently their morphological and physiological properties.

Genome-wide association studies (GWAS) is an approach in which genome regions are analyzed for genetic variants that may be associated with disease conditions or other phenotypes. Overlapping chromatin accessible regions with GWAS variants has helped identify single nucleotide polymorphisms located within specific genomic regions (Cano-Gamez & Trynka, 2020; Srinivasan et al., 2021). Thus, by comparing the snATAC-seq data (Chapter 4) with GWAS, future studies can examine any dorsal horn cell-type specific biases that occur for disease associated-traits.

While largely unexplored in my thesis, we identified through our snRNA-seq and snATAC-seq analysis a large proportion of glial cells and clustered them based on their expression of well-established marker genes. These data can be therefore be probed further to identify cross-species differences as well as to inform studies that require selective targeting of dorsal horn glial types for functional analysis.

Ultimately, future experiments can use selected REs to drive expression of designer receptors in the primate dorsal horn to activate or inhibit specific populations for functional interrogation and for therapeutics.

Appendix A Human Spinal Cord Tissue

As mentioned in Chapter 3, all human spinal cord procurement procedures were approved by the Institutional Review Boards at the University of Texas at Dallas. The following table provides additional information on the human donors.

Table 3. Human patient tissue information

Donor ID	Age	Sex	Race	COD	Medical History
AHLL052	64	M	White	CVA/Stroke	HTN; Diverticulitis and colon resection ~a year ago; 40 pack year smoking hx; Cataracts both eyes.
AHHJ227	44	F	Black	Anoxia/Cardiac Arrest	HTN, Obesity, Thyroid disease, Seizure and heart attack on this admission, Cesarean and Tubal only surgeries 20 and 17 years ago respectively
AHIB407	57	F	Black	CVA/Stroke	HTN, Previous Stroke; CAD; significant smoking history (60 pack years)

Appendix B Species-specific enrichment of genes

The following supplementary figures refer to **Section 3.3.4**. Data regarding the specialized genes are not shown here.

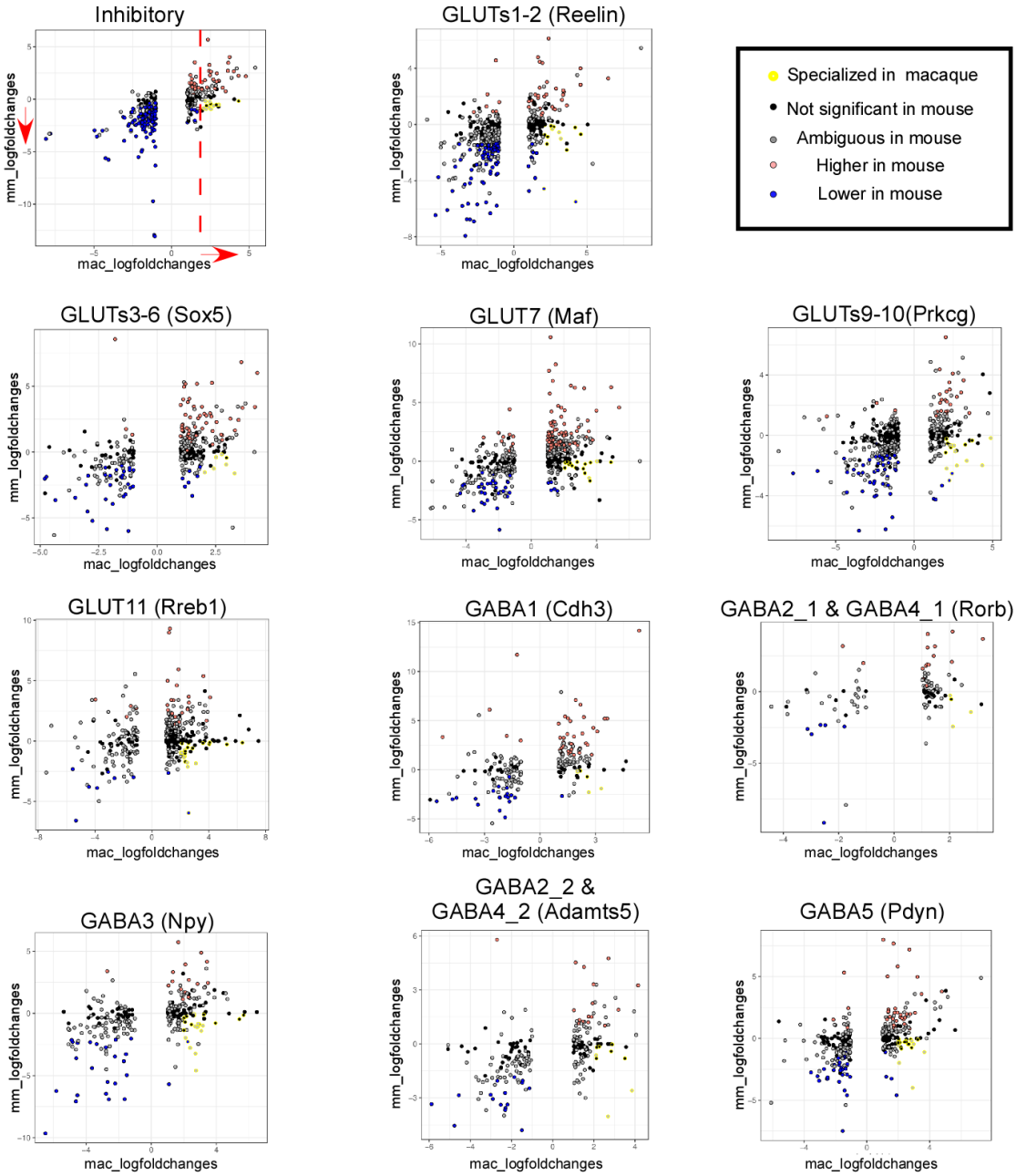

Figure 17. Macaque specific enrichment of genes across clusters

Correlation plots of genes enriched within defined clusters of the macaque. Significant genes (black circles) within each cluster show $p < 10^{-3}$ and log-fold-change > 1 relative to other clusters of the macaque. Among these, genes are macaque specific or specialized (yellow circles) if they show enrichment scores of $p < 10^{-5}$ and log-fold-change (lfc) > 2 (compared across macaque clusters) and the orthologous mouse gene shows lfc < 0 (compared across mouse clusters).

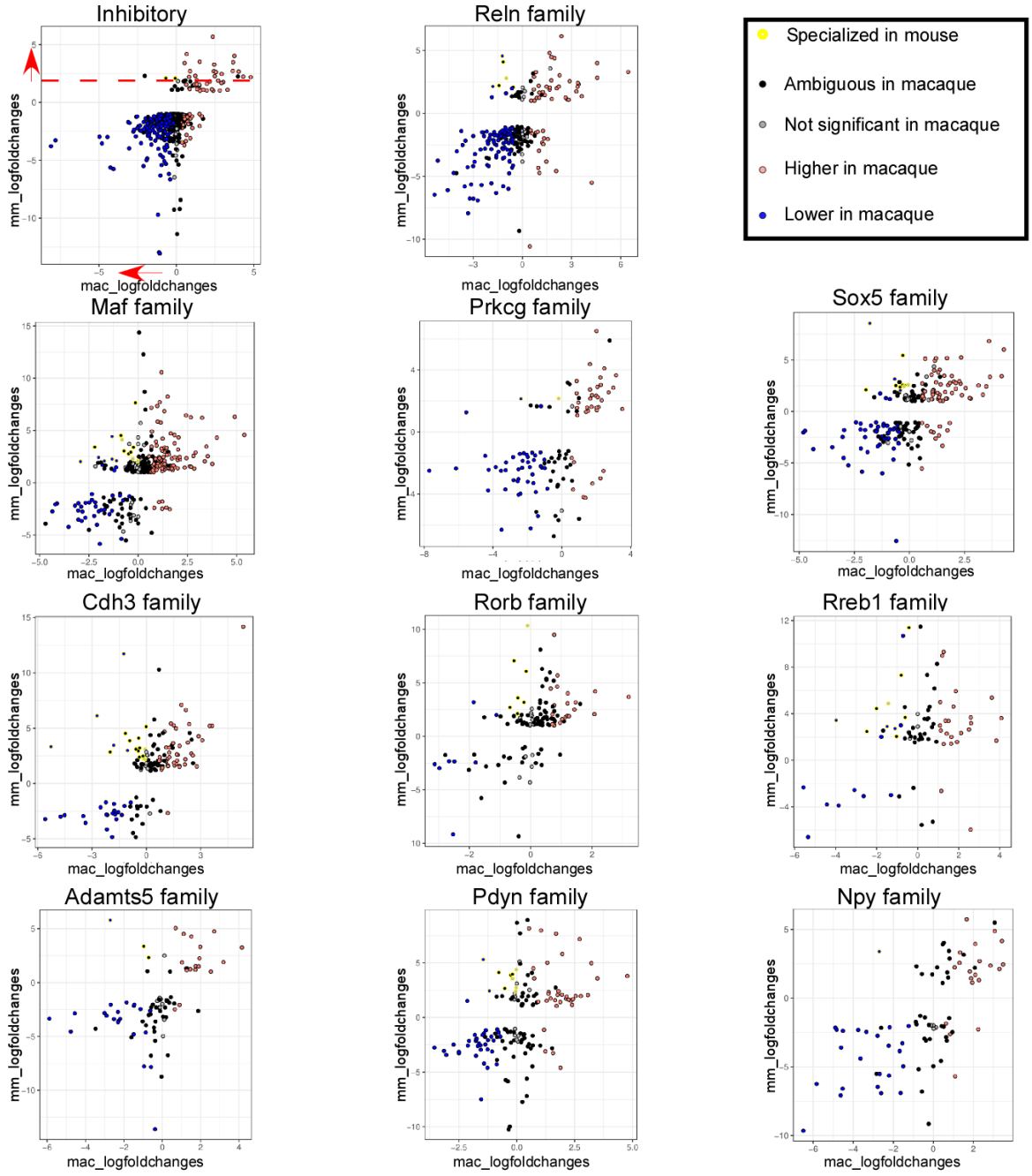

Figure 18. Mouse-specific enrichment of genes across clusters

Correlation plots of genes enriched within defined mouse clusters grouped by their family identity. Significant genes (black circles) within each cluster show $p < 10^{-3}$ and log-fold-change > 1 relative to other clusters of the mouse. Among these, genes are mouse specific or specialized (yellow circles) if they show enrichment scores of $p < 10^{-5}$ and log-fold-change (lfc) > 2 (compared across mouse clusters) and the orthologous macaque gene shows lfc < 0 (compared across macaque clusters).

Appendix C Identifying the role of CCK sub-populations in the allodynia circuitry

Identifying the molecular profiles of dorsal horn neurons and their classification can provide important insight into their functional role. To exemplify, I provide the following section summarizing from "Mechanical allodynia circuitry in the dorsal horn is defined by the nature of the injury" (Peirs et al., 2021). Briefly, chemogenetic inhibition of dorsal horn populations was achieved using the AAV8.hSyn.FLEX.PSAML141F-GlyR.IRES.EGFP virus which contains the designer receptor PSAM-GlyR. The authors targeted CCK, Calretinin, tVGLUT3 and PKCγ (using AAVDJ.pCAG.FLEX.PSAML141F-GlyR virus) neurons. Through behavioral assays, the authors report that i. CCK and PKCγ neurons are important for the transmission of mechanical allodynia following neuropathic injury, ii. VGLUT3 neurons transmit dynamic allodynia following both neuropathic and inflammatory injuries and iii. CCK and Calretinin neurons transmit mechanical allodynia following inflammatory injury.

To identify which sub-populations targeted by the virus mediates the observed phenotype, I performed intraspinal viral injections of AAV8.hSyn.Dio.EGFP into three different transgenic Cre lines (Cck, Vglut3 and Calretinin) and looked for the co-expression of markers (identified from Haring et al 2018 study) of their respective sub-populations through *in situ* hybridization. For example, "In the case of CCK, viral targeting of AAV8.hSyn.DIO.EGFP in the dorsal horn of P21 CCK^{Cre} mice labeled neurons located primarily in the deep dorsal horn (laminae III–IV), that did not include CR or PKCγ expressing neurons (**Figure 19A-B**). As predicted, $EGFP^{+}$ cells overlapped extensively with *Cck* and expressed *Cpne4* and/or *Maf*, but not *Trh* (**Figure 19C-F**).

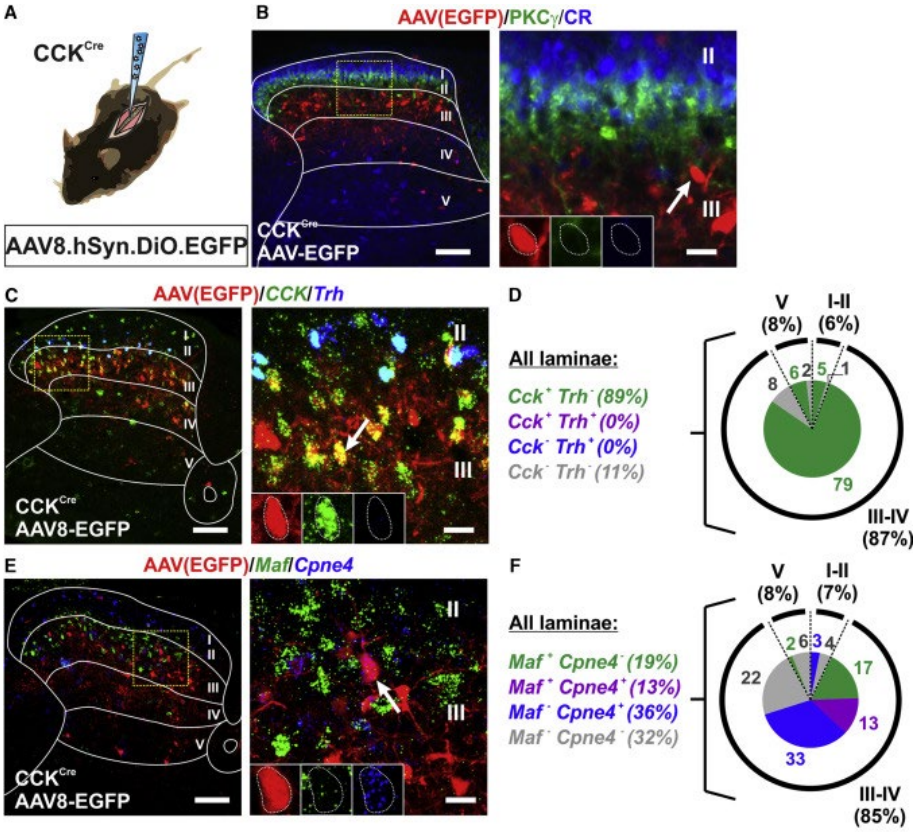

Figure 19. Molecular characterization of virally targeted CCK neurons

A and B. Schematic of CCK^{Cre} mice injected with AAV8.hSyn.DIO.EGFP virus. In the dorsal horn, EGFP+ neurons (red) are predominantly in lamina III with scattered cells in laminae II, IV, and V. Cells do not colocalize with PKCγ (green) or CR (blue). The yellow box shows the location of the inset. The arrow points to an example of an EGFP+ cell. Scale bars, 100 and 20 µm. **C and D**. Nearly all EGFP+ neurons (red) express Cck (green). Consistent with no PKCγ colocalization, none express Trh (blue). The values are percentages of the total EGFP+ neurons. The yellow box shows the location of the inset. The arrow points to an example of a colocalized cell. Scale bars, 100 and 20 µm. **E and F.** Most EGFP+ neurons (red) overlap with Maf (green) and/or Cpne4 (blue). The values are a percentage of the total EGFP+ neurons. The yellow box shows the location of the inset. The arrow points to an example of a colocalized cell. Scale bars, 100 and 20 µm.

Appendix D Multiplex *in situ* hybridization of the primate and rodent DRG and spinal cord

The following section is reprinted from a book chapter I co-authored for the book titled "Contemporary Approaches to the Study of Pain: From Molecules to Neural Networks" which is part of the Neuromethods series. Here, I provide a comprehensive description and protocol for the *in situ* hybridization technique employed in Chapters 2 and 3 of my thesis.

Introduction:

Fluorescence *in situ* hybridization (FISH) is a cytogenetic technique that allows spatial detection, localization and quantification of nucleic acids inside cells or tissues for the analysis and study of genomic sequences and transcriptomic expression profiles. This technique relies on the hybridization of sequence-specific probes to their complementary RNA or DNA target, and most recently it has been used in medical applications for the detection and diagnosis of cancer, syndromes and genetic abnormalities (Huber et al., 2018). It has also contributed to many areas of research, including gene mapping, gene expression, viral infection, and cytogenetics (Jensen, 2014).

Historically, the first *in situ* hybridization (ISH) was performed in 1969 using radioactively labeled probes (H^3 RNA probes) to study the binding of ribosomal RNA (rRNA) to the DNA which codes for it (rDNA) in a cytological preparation of oocytes (Pardue & Gall, 1969). Although radioisotope-labeled nucleotides were used as the gold standard for ISH; low sensitivity and resolution, high background, and long turn-around times were some of the disadvantages that led to the further development of non-radioisotopic labeling approaches in

the late 1970s including the use of hapten-labeled probes and enzymatically- or fluorescently-conjugated antibodies (Langer-Safer et al., 1982; Manning et al., 1975; Rudkin & Stollar, 1977). In the early 1980s, direct fluorescent detection and fluorescence-labeled probes were applied to in situ hybridization, marking the beginning of the modern era of fluorescence in situ hybridization (FISH), which was followed by growing technical advances in protocols that showed improved resolution and speed (Levsky & Singer, 2003). The improvements were mainly in probe design and labeling strategies, such as the synthetic oligonucleotide-based FISH probes, which can be specifically designed to detect splicing variants, single-nucleotide polymorphisms and for the simultaneous detection of multiple transcripts with high sensitivity and specificity in multiple types of biological samples (Beliveau et al., 2015; Kwon, 2013; Lubeck et al., 2014; Raj et al., 2008; Wang et al., 2012).

Until recently, the implementation of FISH required skilled personnel, protocol validation and procedures that needed to be optimized empirically for each experiment (probes, samples, etc.). However, many new technologies and validated protocols have emerged in the past few years, reducing the hands-on time and the need for experienced personnel, while increasing the consistency and reproducibility across different sample types and species. In this chapter, we will focus on RNAscope® (Wang et al., 2012), a cutting-edge ISH technology with a unique probe design strategy and a hybridization-based signal amplification system to simultaneously amplify signals and suppress background (Wang et al., 2012). It has become one of the most highly utilized techniques by the neuroscience field for the detection of target RNAs within intact cells and has become a promising platform for the translation of RNA biomarkers into molecular diagnostic assays. The field continues to rapidly evolve, including new methods to detect hundreds or thousands of expressed genes in situ with single-cell resolution (Waylen et al., 2020). This is a fast, reliable turnkey method for the common situation where a simple FISH with or without immunohistochemistry (IHC) is needed.

Technology:

The RNAscope® technology surpasses traditional ISH techniques by offering shorter protocol times, high sensitivity for the detection of even low-level expressed genes, and the ability to probe for multiple RNA targets simultaneously. Moreover, unlike past ISH strategies, the RNAscope® technology has been shown to work well in tissue perfused with a fixative, as well as in fresh frozen tissue. This technology utilizes a Z shaped probe, the bottom part is designed to be complementary and specific to the target RNA and is ~18-25 bases. The upper and bottom parts of the Z probe are separated by 14 base tail spacer sequence. There are 20 pairs of Z probes per target mRNA, but it is possible to achieve a minimum hybridization with 6 pairs of Z probes. Thus, mRNA targets of >300 bases can be detected, resulting in greater specificity. The signal amplification event is initiated by pre-amplifiers which detect and bind to the 28 base sequence formed by two adjacent Z probes. This is followed by a series of amplification steps in which pre-amplifiers are bound by amplifiers that contain binding sites for fluorophores or for chromogenic enzymes (Wang et al., 2012).

1. **Materials:**

The following items may be purchased directly from ACDBio:

- RNAscope® Multiplex v2 Fluorescent kit.
- HybEZ™ Hybridization System.
- Catalog Probes or Made-to-Order Probes. ACDBio can design custom probes provided you give them the exact sequence or nucleotide accession number from GenBank. For optimal results, the target sequence should be > 300 bases in length. If you plan to detect more than one gene at a time in the same slide, remember to assign different channels to each of the probes.
- Probe diluent.
- 3-plex control probes.

Items from other manufacturers:

- ImmEdge Hydrophobic Barrier PAP Pen (Vector Laboratories).
- TSA® or Opal Dyes – Fluorescein, Cy3 and Cy5 (Akoya Biosciences).
- Superfrost Plus microscope slides (Fisherbrand).

- ProLong™ Gold Antifade Mountant with DAPI (Invitrogen). **Note**: You can also purchase the mountant without DAPI if you want to use the DAPI that comes along with the Multiplex kit from ACDBio – recommended by the manufacturer.
- Coverslips.
- Fluorescent microscope that can visualize the fluorescein, Cy3 and Cy5 fluorophores.
- Water bath that can be set at 40°C.
- 20X Saline-sodium citrate buffer (Sigma-Aldrich).
- O.C.T compound (Tissue-Tek).
- EasyDip™ Slide Staining System.
- 1X PBS.
- Milli-Q water.
- 100% Ethanol.

2. Method

Below is a modified protocol for RNAscope ISH that works consistently across different tissue samples. Please also visit the ACDBio website for the specific manufacturer's instructions.

2.1 Tissue Preparation:

The manufacturer's protocol provides three different methods of tissue preparation. Here, we focus on mice perfused with a fixative.

1. Perfuse the animal with nuclease-free 1X phosphate-buffered saline (1X PBS, pH 7.4), followed by freshly prepared cold 4% paraformaldehyde (4% PFA, pH 7.4) in 1X PBS. Working with fixed tissue is advantageous as the RNAscope® ISH can then be combined with immunohistochemistry (IHC) using the Multiplex v2 kit. Tissue expressing a viral reporter or tissue harvested from transgenic reporter mice can also be probed with this protocol.
2. Dissect out the tissue of interest and transfer it to 4% PFA. Post-fix for 2 hours at 4°C.
3. Then transfer the tissue to a tube of freshly prepared 10% sucrose in 1X PBS (*See* Note 1).
4. After the tissue sinks to the bottom of the tube, transfer it to 20% sucrose in 1X PBS. Repeat this step with 30% sucrose in 1X PBS.
5. Let the tissue remain in this solution for 48 hours before embedding it in OCT. Freeze the tissue in the OCT mold using dry ice and then store in an airtight container at -80°C until you are ready section it.
6. Prior to sectioning, remove the tissue from the -80°C and place it in the cryostat at -20°C for 30-45 minutes.
7. Cut the tissues onto Superfrost Plus slides leaving room on the slide to draw a hydrophobic barrier with the Pap Pen. As per the manufacturer's protocol, it is not ideal to cut tissues at a thickness greater than 20 µm.
8. After sectioning, let the slides sit in -20°C for 30 minutes before storing them at -80°C or proceed directly to step 2 under Pretreatment.

2.2 Before Starting the Assay:

- Reconstitute the fluorophore and store the stock solutions as per the manufacturer's instructions (Akoya Biosciences). Make note of which fluorophore you would like to assign to each of the probes. Do not assign the same fluorophore to probes of two different channels.
- Prepare fresh 1X Wash Buffer as per the manufacturer's instructions.

2.3 Pretreatment:

Prior to hybridization, there are a few pretreatment steps to help unmask the target nucleic acid and allow probe penetration. We use the EasyDip™ Slide Staining System for easy transfer of slides from one solution to another.

1. Before starting, turn on the HybEZ™ oven and make sure the temperature is at 40ºC. Ensure that the humidity control tray with the wet filter paper is placed inside the oven (*See* Note 2).
2. When you are ready to begin the RNAscope® *in-situ* hybridization, take the slides out of the -80°C and keep it outside for 10-15 minutes.
3. Wash the slides with 1X PBS for 2 minutes with gentle agitation in order to remove the excess OCT. Repeat this wash with fresh 1X PBS for 2 minutes.
4. Immerse the slides in freshly prepared 50% EtOH using the EasyDip™ Slide Staining System for 5 minutes at room temperature (RT).
5. Immerse the slides in 70% EtOH for 5 minutes at RT.
6. Immerse the slides in 100% EtOH for 5 minutes at RT. Repeat this step with fresh 100% EtOH.
7. Allow the slides to dry at RT for 5 minutes. Using the special PAP pen, draw a barrier around the sections.
8. To block endogenous peroxidase activity, add hydrogen peroxide from the kit to the tissue sections and incubate for 10 minutes at RT. Keep the slides in a hydrated chamber to prevent the tissues from drying up.
9. Wash the slides with 1X PBS for 2 minutes with gentle agitation. Repeat this wash with fresh 1X PBS for 2 minutes.
10. Add Protease IV from the kit to the tissue sections and incubate for 30 min at RT in a hydrated chamber. This step causes permeabilization of the tissue to allow for optimal hybridization (*See* Note 3).
11. Wash the slides with 1X PBS for 2 minutes with gentle agitation. Repeat again with fresh 1X PBS. During this time, take out your probes from the 4ºC and incubate them at 40ºC in a water bath or incubator for at least 10 minutes.
12. Let the probes cool down to RT. C2 and C3 probes must be spun down. As per the manufacturer's protocol, mix 1 volume of C2 and 1 volume of C3 to 50 volumes of C1 probe or the probe diluent in an Eppendorf tube. This is ~ 4 µL of C2/C3 probes to ~ 7 drops of C1 probe or ~7 drops of the probe diluent (*See* Note 4). Invert to mix.
13. Ensure that the slides don't have any excess liquid before adding the mixed probe solution to completely cover the sections.
14. Place the slides in the EZ-Batch™ Slide rack and insert the rack into the oven.

15. Let the probes hybridize for 2 hours at 40ºC.
16. After the hybridization, remove the slide rack from the oven (*See* Note 5).
17. Wash the slides with 1X Wash Buffer for 2 min at RT with gentle agitation. Repeat this step with fresh 1X Wash Buffer.

At this point, you have the option to stop and store the slides in freshly prepared 5X SSC buffer overnight (O/N) at RT or else proceed directly to step 4 under Amplification.

2.4 Amplification

For the subsequent amplification steps, remember to equilibrate the reagents (Amp1, Amp2, Amp3, HRPs and HRP blocker) at RT prior to starting. Do not let the slides dry out at any point during the assay.

1. Turn on the HybEZ™ oven if continuing with the protocol the next day and make sure that the temperature is at 40°C. Place the humidity control tray with the wet filter paper inside the HybEZ™ oven.
2. After the temperature of the oven is stabilized at 40°C for at least 30 minutes, proceed to the next steps.
3. Remove the slides from the 5X SSC Buffer and wash with 1X Wash Buffer in the EasyDip™ Slide Staining System. Repeat this step with fresh 1X Wash Buffer.
4. Pour off any excess liquid from the slides and place the slides in the EZ-Batch™ slide rack. Add enough drops of Amp1 to properly cover the tissue sections on the slide.
5. Carefully insert the EZ-Batch™ slide rack into the oven. Incubate for 30 minutes at 40°C in the oven.
6. Remove the slide rack and pour off any excess liquid from the slides.
7. Wash the slides with 1X Wash Buffer for 2 min at RT with gentle agitation. Repeat the wash with fresh 1X Wash Buffer.
8. Pour off any excess liquid from the slides and place the slides in the EZ-Batch™ slide rack. Add enough drops of Amp2 to properly cover the tissue sections on the slide.
9. Carefully insert the EZ-Batch™ slide rack into the oven. Incubate for 30 minutes at 40ºC in the oven.
10. Remove the slide rack and pour off any excess liquid from the slides. Wash the slides with 1X Wash Buffer for 2 min at RT with gentle agitation. Repeat the wash with fresh 1X Wash Buffer.
11. Pour off any excess liquid from the slides and place the slides in the EZ-Batch™ slide rack. Add enough drops of Amp3 to properly cover the tissue sections on the slide.
12. Carefully insert the EZ-Batch™ slide rack into the oven. Incubate for 15 minutes at 40ºC in the oven.
13. Remove the slide rack and pour off any excess liquid from the slides. Wash the slides with 1X Wash Buffer for 2 min at RT with gentle agitation. Repeat the wash with fresh 1X Wash Buffer.

The following HRP signal development steps will depend on the channels assigned to the probes. Develop the HRP signal one by one for each probe used in the experimental run. For example: develop the HRP-C1 signal for the C1-assigned probe followed by the HRP-C2 for the C2-assigned probe.

2.5 Preparation of the TSA® Fluorophores:

Use the TSA buffer provided by the RNAscope® kit to dilute the fluorophores. About 150-200 µL of the TSA buffer is sufficient to cover the slide. Follow the recommended dilution range (1:750-1:3,000) of the TSA® dyes fluorophore as mentioned in the manufacturer's protocol.

1. Pour off any excess liquid from the slides and place the slides in the EZ-Batch™ slide rack. Add enough drops of the HRP-C1 to properly cover the tissue sections on the slide and incubate in the oven for 15 min at 40ºC.
2. After incubation, remove the EZ-Batch™ slide rack from the oven and wash the slides in 1X Wash Buffer for 2 min at RT. Repeat the wash with fresh 1x Wash Buffer for 2 min at RT.
3. Pour off any excess liquid from the slide and add the prepared TSA® Plus fluorophore to the slides placed in the EZ-Batch™ slide rack. Incubate in the oven for 30 minutes at 40ºC. This fluorophore is assigned to the C1 probe.
4. After incubation, remove the EZ-Batch™ slide rack from the oven and wash the slides in 1X Wash Buffer for 2 minutes at RT. Repeat the wash with fresh 1X Wash Buffer.
5. Add enough drops of HRP blocker (provided in the kit) to properly cover the tissue sections on the slide. Incubate in the oven for 15 minutes at 40ºC.
6. After incubation, remove the EZ-Batch™ slide rack from the oven and wash the slides with 1X Wash Buffer for 2 minutes at RT. Repeat the wash with fresh 1X Wash Buffer.

Similarly, develop the signal for HRP-C2 and HRP-C3 if you have probes assigned to those channels. If you plan to do IHC following ISH, proceed to the next step, otherwise go to DAPI Counterstain and Slide Mounting.

3. Immunohistochemistry

It is important to test your antibody by staining with the buffers that the manufacturer recommends prior to running the immunohistochemistry in combination with ISH.

3.1 Materials:

- 1X TBS (pH 7.4).
- TBS-T Wash Buffer: 500 µL of 10% Tween®20 is added to 1 liter of 1X TBS Buffer.
- TBS-1% BSA: Add 0.5 g to 50 mL of 1X TBS. Aliquot and store in -20°C.

- Normal Donkey Serum (If secondary antibody is raised in donkey).

3.2 Method:

1. If needed, redraw the hydrophobic barrier with the PAP pen. Don't let the slides dry out.
2. Wash the slides in TBS-T Wash Buffer for 5 min at RT with gentle agitation. Repeat with fresh TBS-T Wash Buffer.
3. Prepare blocking solution by adding 10% Normal Donkey Serum (NDS) to TBS-1% BSA. About 150-200 µL of solution covers the slide so prepare it accordingly. If a particular primary antibody requires further permeabilization, Triton™ X-100 can be added to the blocking solution at a recommended maximum concentration of 0.1%.
4. Add the blocking solution to the slides for 1 hour at RT. Make sure the slides are kept in a humidified chamber.
5. Prepare the primary antibody solution by adding the primary antibody to TBS-1% BSA at a concentration that has already been optimized.
6. Incubate the slides O/N at 4°C (*See* Note 6).
7. Wash the slides in TBS-T Wash Buffer for 5 min at RT with gentle agitation. Repeat with fresh TBS-T Wash Buffer.
8. Add the respective Alexa Fluor-conjugated secondary antibody in TBS-1% BSA. If using HRP-conjugated secondary antibodies, please refer to the manufacturer's protocol for dilution and incubation time.
9. Incubate the slides in the secondary antibody solution for 2 hours at RT. Remember to keep the slides in a humidified chamber.
10. Wash the slides with TBS-T Wash Buffer for 2 min at RT with gentle agitation. Repeat with fresh TBS-T Wash Buffer.
11. Remove the excess liquid from the slides. Add 2 or 3 drops of Prolong Gold antifade mounting medium with DAPI on the slides and coverslip.
12. Dry the slides in the dark for 30 min.
13. Store the slides at 4°C or continue to image after the slides have dried.

4. Quantification

RNAscope® does not provide an actual quantitative measure of how many transcripts of a gene are present in the tissue. It can be used in a semi-quantitative manner by providing scores depending on the number of puncta present per cell and the number of dots lying within clusters. Refer to the ACD Scoring system for this metric. If the goal is to determine the approximate number of positive cells, a threshold of at least 3-5 puncta or more within a cell is considered to be positive. For human or non-human primate tissue, we usually recommend that the green channel remain blank due to the presence of lipofuscin (fatty deposits), which may lead to false positive signal. The background in the green channel can thus be subtracted

from the other channels. Alternatively, if all channels are needed for probe and/or staining visualization, lipofuscin is imaged in an additional channel by exciting at a lower wavelength and capturing at a much higher wavelength for example, by using the DAPI filter to excite at 405 nm and capture at 647 nm. A lipofuscin mask can then be created and subtracted from other channels that overlap with this lipofuscin mask. Newer software platforms like dotdotdot offer features to mask the lipofuscin autofluorescence as well as quantify and analyze the mRNA (Maynard et al., 2020). Software such as ImageJ, Halo™, and FISH Finder (Shirley et al., 2011) can be used to delimit areas of interest and count the cells in a more automated fashion. ImageJ also has a plugin called Cell Counter for the manual counting of cells.

5. Notes

1. After tissue fixation, the use of nuclease-free 1X PBS solution is optional.
2. Make sure the oven is at 40ºC for at least 30 min prior to the probe hybridization (Step 15).
3. If you see over-digestion of the tissue, use Protease III from the kit instead of Protease IV.
4. 1 drop of the C1 probe or probe diluent is ~ 30 µL.
5. We save the probes in an Eppendorf tube at 4°C. The probes can be reused a second time in a future experiment. Remember to place them at 40°C for at least 10 min after removing it from the 4°C. However, reusing the probes is not recommended by the manufacturer so do a trial run before attempting this for an actual experiment.
6. Incubation times may vary according to the manufacturer's recommendation time for the primary antibody.

Appendix E The use of intraspinally injected chemogenetic receptor, PSAM-GlyR, to probe the functional role of spinal dorsal horn neurons.

The following section is reprinted from a book chapter I co-authored for the book titled "Contemporary Approaches to the Study of Pain: From Molecules to Neural Networks," which is part of the Neuromethods series. Here, I provide a description for how chemogenetics can be used to investigate the functional roles of dorsal horn neurons, particularly in the context of pain, and a protocol for intraspinal injection of viruses. Commonly used somatosensory behavioral assays are also described here.

Introduction:

Our understanding of how the nervous system encodes behavior has accelerated with the advent of genetically-encoded optogenetic and chemogenetic receptors that allow for the acute and reversible in vivo manipulation of the excitability of select cell populations while measuring behavior (Rajasethupathy et al., 2016; Sternson & Roth, 2014). The optogenetic receptors are light-gated excitatory and inhibitory ion channels that act on a millisecond timescale and can be applied acutely or chronically to circuits in vivo or in vitro in a spatially restricted manner, as is described in detail in other chapters within this volume. Chemogenetic receptors on the other hand are engineered to be selectively activated by otherwise inert chemical ligands while unresponsive to physiological concentrations of endogenous ligands (Pei et al., 2010). With the use of chemogenetic receptors, cell excitability can be controlled on the order of minutes to hours depending on the pharmacokinetics of the ligand. The first chemogenetic receptors to be commonly used are based on the human muscarinic receptor subtypes, hM3Dq and hM4Di (Armbruster et al., 2007). Both are G-protein coupled receptors

that regulate ion channel activity through second messengers with hM3Dq producing membrane depolarization (excitatory) and hM4Di producing membrane hyperpolarization (inhibitory). The ligand, clozapine-n-oxide (CNO), is designed to have high selectivity for these receptors, but is also metabolized to clozapine (Jann et al.; Manvich et al., 2018). The latter compound, a known psychotropic medication, acts on a range of endogenous receptors, but importantly shows significantly greater potency for the hM3Dq and hM4Di designer receptors. Selective activation of these DREADDs thus requires using CNO at <10 mg/kg or a subthreshold dose of clozapine at 0.1 mg/kg (Gomez et al., 2017). A second Gi coupled DREADD (inhibitory) is based on the kappa opioid receptor. This designer receptor is engineered to have a high affinity for the otherwise inert ligand, salvinorin B, and thus when combined with the muscarinic based DREADD allows for the differential control of multiple cell populations within the same experiment (Vardy et al., 2015). Other synthetic agonists for these DREADDs like the JHU3712, JHU37160 and Deschloroclozapine (DCZ) appear to be promising alternatives due to their high brain penetrability and potency with minimal off-target effects (Bonaventura et al., 2019; Nagai et al., 2020). Lastly, the proper control to interpret the outcome of such studies requires testing in parallel mice that lack the receptor (e.g., injected with a reporter only).

Ionotropic chemogenetic receptors, such as the PSAM series, comprise another designer receptor system (Magnus et al., 2011). The PSAM receptors incorporate a mutated version of the ligand binding domain of the human alpha-7 nicotinic receptor fused to either the ion channel domain of the human serotonin (5-HT) subtype 3 receptor to generate an excitatory receptor, PSAM-5HT3, or to the human glycine receptor to generate an inhibitory receptor, PSAM-GlyR. Further refinements have been made to the ligand binding domain of these receptors to increase their potency for highly selective FDA approved ligands, such as

varenicline as well as other newly designed ligands called μPSEMs, such as PSEM 792, PSEM 793 and PSEM 819 (Magnus et al., 2019).

Chemogenetic studies of the neural circuitry underlying somatosensation in mice have been applied to populations throughout the nervous system including peripheral sensory neurons, spinal cord and brain (Francois et al., 2017; Peirs et al., 2021; Peirs et al., 2015; Petitjean et al., 2015; Saloman et al., 2016). Studies have also utilized these receptors to study the contribution of glial cells to the transmission of pain (Grace et al., 2018; Jayaraj et al., 2018; Kohro et al., 2020). To gain access to select cell populations, many laboratories have taken advantage of the Cre-lox system in mice, though efforts to identify regulatory elements that can drive cell-type specific expression is allowing researchers to perform these types of experiments independent of the Cre-lox system as well as in other species (Grace et al., 2018; Tashima et al., 2021). Expression of the chemogenetic receptor is typically accomplished through injection of an AAV encoding the Cre-dependent receptor either intrathecally or intraperitoneally in the case of primary sensory ganglia, intraspinally for spinal cord cells or intracranially to target brain cells, in mice expressing Cre recombinase in the target cell population. Alternatively, mouse lines that have incorporated the second messenger coupled receptors in the genome are also available. Because the ligands are typically delivered systemically, precise cellular targeting of the receptor is key. Focal delivery of the ligand is however another strategy that can be used to further refine which cells are manipulated.

Here we describe the use of the chemogenetic receptor, PSAM^{L141F}-GlyR targeted to specific excitatory neurons in the spinal cord to determine their role in acute somatosensory behavior and in persistent pain after injury (Peirs et al., 2021). The paradigm involves intraspinal injection of Cre-dependent PSAM^{L141F}-GlyR packaged into AAV8 and behavioral testing three weeks later. Use of the AAV8 serotype injected intraspinally confers selective expression in the spinal cord with little to none in primary afferents or brain (Peirs et al., 2021;

Peirs et al., 2015). Mice are typically injected at P21, but also can be injected at younger or older ages as needed. Behaviors are typically assessed when the mice reach 6 weeks of age.

In initial experiments, we have demonstrated that activation of PSAM^{L141F}-GlyR inhibits dorsal horn excitatory neurons in spinal cord slices using patch clamp electrophysiology (Peirs et al., 2021). For this purpose, we injected AAV8 hSyn-Flex-PSAM^{L141F}-GlyR-IRES-GFP in mice expressing Cre in a large population of excitatory neurons (Tlx3^{Cre}). After 2 weeks, we recorded from the neurons. Bath application of the PSAM^{L141F}-GlyR agonist, PSEM^{89S} (30μM) hyperpolarized the membrane and blocked action potentials in response to current injection in GFP^{+} neurons. The ligand had no effect on GFP^{-} neurons. A recent report using the newer PSAM4-GlyR inhibitory DREADD suggests that it may alter the chloride gradient of striatal dopamine receptor 1 containing medium spiny neurons, resulting in excitation rather than inhibition with receptor activation (Gantz et al., 2021). This may extend to chloride channel DREADDs in general. It is therefore recommended that all cell types are tested in slices prior to performing behavioral experiments. Interestingly, although the behavioral outcome was as expected for activation of hM4Di in primary afferents that express TRPV1, it was reported that the neuron showed altered sodium and calcium currents and that the activity of morphine receptors in the cells was altered presumably due to changes in the availability in second messengers, thus providing a note of caution for those using the designer receptor (Saloman et al., 2016).

To assess the role of PSAM-GlyR expressing neurons in somatosensory behaviors, we measure punctate mechanical thresholds with von Frey filaments, dynamic mechanical responses with a cotton swab, the sensitivity to a piece of sticky tape, the noxious mechanical pain response with a pinprick as well as thermal response with the Hargreaves assay or acetone test. All are measured on the plantar surface of the hind paw. We also test the mice with the

rotarod to check for any deficits in fore- and hind limb motor coordination. Measurements are taken 30-90 minutes following injection of saline or ligand (30 mg/kg).

Next, we determine whether the targeted excitatory neuronal population has a role in the transmission of persistent pain using both neuropathic and inflammatory pain models since our findings indicate that the dorsal horn network for mechanical allodynia differs depending on the type of injury (Peirs et al., 2021). We also typically assay for both dynamic and punctate allodynia and we also assay for heat or cold hypersensitivity depending on the pain model used. There are a number of validated chronic pain models. The spared nerve injury (SNI) is a commonly used neuropathic pain model because it is highly reproducible and produces robust mechanical and cold allodynia (Decosterd & Woolf, 2000). In the sural version of this model, which produces both punctate and dynamic allodynia, the tibial and common peroneal nerves are cut and ligated and the sural nerve remains intact. The region of the hind paw innervated by the sural nerve becomes hypersensitive (the lateral edge of the paw at the border between the plantar surface and the hairy skin). In the spared tibial version of the model, the common peroneal and sural nerves are cut and ligated and the tibial nerve is spared (Shields et al., 2003). This model only shows punctate mechanical allodynia and cold allodynia and the hypersensitivity is located in the middle of the plantar surface of the hind paw which corresponds to where the tibial nerve innervates. We typically perform the surgery two weeks after the virus injection and measure mechanical thresholds at 1, 2 and 6 weeks after the surgery. Cold hypersensitivity using the acetone assay can also be measured at these time points. A statistically significant decrease in the mechanical threshold to von Frey filaments or a statistically significant increase in the response to the cotton swab indicates the expression of punctate and dynamic mechanical allodynia, respectively. A significant increase in the time spent responding to the acetone indicates cold allodynia. A significant reversal in the sensitivity to punctate or dynamic mechanical stimuli or to acetone in mice expressing PSAM-GlyR after

receiving the ligand, compared to saline injection, indicates a role for the neurons in the transmission of allodynia caused by neuropathic injury.

To test the role of the neurons in an inflammatory pain model, we use carrageenan (acute) or complete Freund's adjuvant (CFA), which model acute and more chronic inflammatory injuries, respectively. For the carrageenan model, 10 µl of lambda-carrageenan is injected in the plantar hind paw and then punctate and dynamic allodynia as well as heat hypersensitivity are measured 1-3 days later. For the CFA model, the plantar hind paw is injected with 10 µl of a solution that is equal parts CFA and sterile 0.9% saline. The time courses for the expression of punctate allodynia, dynamic allodynia and heat hypersensitivity differ in this model, with heat hypersensitivity peaking typically 3 days following injection, dynamic allodynia peaking 4 to 5 days following injection and punctate allodynia lasting at least 1 week. Measurements after saline or PSEM^{89S} ligand injection are therefore taken at these time points.

Following behavioral testing, we confirm expression of the PSAM^{L141F}-GlyR receptor in the dorsal horn of the mice by staining fixed sections with alpha-bungarotoxin conjugated to a fluorophore (e.g., Alexa-647). The α-bungarotoxin binds to the ligand binding domain of the α7-nicotinic receptor of PSAM^{L141F}-GlyR. Fortuitously, we do not observe α-bungarotoxin staining in the dorsal horn of mice lacking the PSAM^{L141F}-GlyR, thus simplifying the interpretation (Peirs et al., 2021). If α-bungarotoxin staining is absent at the expected site of injection, behavioral data from the mouse is excluded from the study.

I. "Minimally Invasive" Intraspinal Injection

Herein, a modified intraspinal injection method based on Kohro et al. (2015) is described (Kohro et al., 2015). This "minimally invasive" microinjection method allows delivery of AAV vectors into the spinal dorsal horn without laminectomy or drilling.

1. Materials

Reagents:

- Ethanol, 70%
- Iodine solution
- Saline, sterile, 0.9%
- Lactated Ringers Solution with 5% dextrose
- Ketoprofen, sterile (5mg/kg)
- Isoflurane
- Ocular lubricant, sterile
- Mineral Oil

Surgical Tools:

- 2 Dumont #5 fine forceps
- Spring scissors 8mm Cutting Edge
- 2 Schwartz Micro Serrefines
- Fine Scissors
- Noyes Spring Scissors
- Needle holder
- Dumont #7 Forceps

Equipment:

- Sterilization pack
- 6-0 Silk sutures
- 6-0 Nylon sutures
- Sterile Cotton swabs
- Sterile Eye spears
- Rechargeable clipper
- Sterile gauze
- Parafilm
- Kimwipes
- Heating pad
- Absorbent pad
- Isoflurane vaporizer
- Anaesthesia induction chamber
- Isoflurane scavenger
- Micropipette puller (P-97, Sutter)
- Fire polished glass capillaries (World Precision Instruments, #504949)
- CV-5-1GU headstage and compatible glass capillary holder (Axon Instruments)
- 5 µL glass microliter syringe (Hamilton, Model 7105 KH)
- Dental cement
- Polyethylene tubing
- Stereotaxic injector (Stoelting)
- Small animal stereotaxic frame with small animal spinal unit (Kopf)
    - Spinal base plate (Kopf, model 912)
    - 2 Adjustable base mounts with post and clamp (Kopf, model 982)
    - “V” notch spikes (Kopf, model 987)
- Surgical microscope
- Mini microcentrifuge

- 30-gauge needle
- 10 mL syringe
- 3 way luer lock
- 1 mL syringes

2. Methods

2.1 Custom Stereotaxic Injection Setup (optional)

In our laboratory, we created a custom stereotaxic injection setup which uses patch clamp amplifier headstage as a glass capillary holder (Figure 20). We attached a CV-5-1GU headstage from Axon Instruments to the stereotaxic frame. Then, we connected a 5 µL Hamilton model 7105 syringe to the glass pipette holder attached to the CV-5-1GU headstage by polyethylene tubing. Finally, to ensure a tight seal, we applied dental cement to each end of the polyethylene tube. While this custom setup works consistently in our hands, any stereotaxic injection setup will be fully compatible with the methods described in this chapter.

2.2 Preparation for the Surgery

1. Autoclave surgical tools in sterilization pack prior to surgery.
2. Pull glass microinjection needle using micropipette puller and store it in a container.
    a. P-97 protocol: Heat=580, Pull=200, Vel.=20 Time=250 (You may decrease or increase the heat setting to control the length of tapered tip).
3. Obtain necessary AAV aliquots containing vector of your choice and store it in an ice bucket.
    a. Titres between 10^{12}-10^{13} has worked consistently in our hands.
    b. Multiple AAV vectors can be injected at the same time.
4. Load 1 mL syringe with sterile saline
    a. This will be used to keep the surgical area moist throughout the procedure.
5. Load 1 mL syringes with 50% Lactated Ringers Solution (LRS) with 5% dextrose and 50% sterile saline.
    a. This will be injected subcutaneously after the procedure to prevent severe dehydration.
6. Load 1 mL syringe with necessary amount of ketoprofen solution (5 mg/kg final dose).
7. All solutions prepared in steps 4, 5, and 6 should be kept warm on heating pad before injection.

2.3 Preparation for the Stereotaxic Injector

Prior to surgery, glass microinjection needle should be mounted, trimmed, and loaded with mineral oil. Methods described below is specific to our setup and this may vary depending on type of stereotaxic injector unit.

1. Mount the headstage to the stereotaxic frame.
2. Mount the 5 µL Hamilton syringe to stereotaxic injector.
3. Prepare a 10 mL syringe with mineral oil and 3-way luer lock connected to a 30-guage needle. This is used to flush the injection loop and remove any air bubbles.
    a. Ensure there is no air bubbles in the 10 mL syringes.
4. Carefully pull out the needle from Hamilton syringe and insert 10 mL syringe needle into the opening of Hamilton syringe needle.
5. Slowly flush out any bubbles in the injection loop. It is critical to completely fill the loop with mineral oil to ensure a smooth injection procedure without clog.
    a. Excess mineral oil on the electrode holder should be cleaned with Kimwipe.
6. Once the stereotaxic injector loop is filled with mineral oil, close the 3-way luer lock, and glass microinjection needle may be inserted into the electrode holder.
    a. Tightly close the electrode holder by rotating the fitting counter-clockwise.
7. Using the surgical microscope trim the tip of the glass microinjection needle.
    a. Having a coloured paper underneath the needle helps with contrast.
    b. Tip diameter should be small enough to minimize the trauma to the spinal cord, and large enough to allow sufficient flowrate of AAV solution.
    c. Gently touch the tip of the needle with spring scissors and trim where the tip no longer sharply bends with little pressure from the spring scissors. The tip must be rigid and sharp enough to break through the pia membrane.
8. Opening the 3-way luer lock on the 10 mL syringe will push mineral oil through glass needle.
    a. Pull the 10 mL syringe out when mineral oil fills approximately 30% of the glass microinjection needle. This is done to account for Hamilton syringe's plunger volume.
9. Reassemble the Hamilton syringe by inserting the needle through the plunger.
    a. Mineral oil will have been pushed out of the needle. Using the stereotaxic injector, draw back the Hamilton syringe to equilibrate the pressure. No mineral oil should be coming out of the needle.
10. Set the injection volume to 1 µL and rate of injection to 200 to 300 nL/min. Ensure the stereotaxic injector is set to dispense.

2.4 Surgical Procedures to Expose the Spinal Cord Segment

1. Weigh the animal before inducing anesthesia.

2. Deeply anesthetize the mice in the anesthesia induction chamber with 5% isoflurane and oxygen.
3. Transfer the mice from induction chamber to heating pad into a nose cone with 1.5-2% isoflurane and oxygen flow.
    a. We prefer to orient the mice horizontally during the surgical procedure; however, any orientation may be used.
    b. It is critical to maintain and monitor the respiration rate of the mice throughout the procedure and adjust the concentration of isoflurane accordingly.
4. Apply ocular lubricant with sterile cotton swab.
5. Subcutaneously inject 5mg/kg Ketoprofen.
6. Shave the thoracolumbar area with electric clipper.
7. Apply 70% ethanol to exposed skin area with sterile gauze to remove excess hair and let it dry.
8. Subsequently, apply iodine solution to the shaved area with sterile cotton swab and let it dry.
9. Lift the skin up with Dumont #7 forceps and make a small cut with Noyes spring scissors. Then, cut along the midline to expose the thoracolumbar area underneath the skin. Carefully tease away the facia by opening the spring scissors from closed position. No damage to the muscle tissue should be done during this step. Finally, clip the skin away from the exposed muscle tissue with Schwartz Micro Serrefines.
10. Make sure to keep the surgical area moist by applying small volume of sterile saline throughout the procedure.
11. Intervertebral space between T12 and T13 vertebral spine allows injection to L3-L4 region of the spinal cord. Alternatively, you may choose to inject into intervertebral space between T13 and L1 vertebral spine to target L4-L5 region of the spinal cord. There are landmarks that may help with identification of these regions (See Harrison et al., 2013 for detailed MRI images of mice spinal cord segments) (Harrison et al., 2013). The T13 vertebra is connected to the last rib of the mice, and this can be identified by gently pushing along the ribs of the animal with forceps (below T13 there will be no resistance when you push with forceps). Alternatively, one may choose to count the vertebral column from the iliac crest which is attached to the L6 vertebra (See Haenraets et al., 2018 for an excellent video guide to identifying vertebral landmarks) (Haenraets et al.). Once the correct vertebral spines have been identified, you may gently push between the vertebral spines with forceps to identify the intervertebral space (intervertebral space will have no resistance when pushed with forceps). This step is critical for this procedure as correct identification of the intervertebral space minimizes the damage to the muscle tissue.
12. Gently tease away the muscle tissue by blunt dissection using 2 Dumont #5 fine forceps under the surgical microscope.
    a. If bleeding occurs during this step, use the sterile eye spears to apply gentle pressure to the area until the bleeding stops.
    b. Slightly lifting the muscle tissue with one forceps, and teasing away the muscle tissue with the other forceps may minimize the potential damage to the spinal cord. It is absolutely critical that you do not damage the spinal cord during this step.

c. Spinal cord underneath the muscle tissue will be clearly visible when blunt dissection is done properly.

13. Once spinal cord is exposed, dura must be removed before the injection procedure. Gently scrape the dura with sterile 30 gauge needle to create an opening. Once dura is opened you will notice cerebrospinal fluid (CSF) leaks out and spinal cord bulges out slightly. Alternatively, you may use the Dumont #5 fine forceps to scrape the dura repeatedly. Great care must be taken not to damage the spinal cord.
14. Transfer the animal to the isofluorane adapter on the stereotaxic frame. Depending on the frame, you will need to lift the mice up to proper height (we use a Styrofoam block layered with absorbent pad to lift up the mice).
15. Clamp the vertebral column with "V" notch spikes. Other spinal adaptor kits and vertebrae clamp compatible with stereotaxic frame may be used. Vertebrae clamp (Kopf) may provide the best stability during the injection; however, this cannot be used for younger mice.
16. Using the surgical microscope, ensure exposed spinal cord and dorsal blood vessel is clearly visible. If bleeding occurs, it is critical to stop the bleeding with eye spear before proceeding with intraspinal injection. Bleeding during the injection will cause clog.

2.5 Intraspinal Injection

1. Spin down the virus solution with mini microcentrifuge.
2. Dispense viral solution to parafilm. For single AAV solution, dispense 1.2 μL (for 1 μL injection), and for two AAV solutions dispense 0.6 μL of each virus solution and mix thoroughly by pipetting the droplet up and down.
3. Under the surgical microscope, lower the microinjection needle to the droplet and draw up the virus solution gradually with stereotaxic injector. Once enough virus solution is drawn up, apply small positive pressure with the stereotaxic injector to ensure virus solution flows out.
4. Align the microinjection needle to the dorsal blood vessel of the exposed spinal cord segment. Reset the x-axis of stereotaxic coordinates.
5. From the dorsal blood vessel adjust the x coordinate 300 to 350 μm away from the dorsal blood vessel.
    a. For targeting L4 segment, target the most caudal spinal cord segment between T12 and T13 intervertebral space or most rostral segment between T13 and L1 intervertebral space.
    b. Align the needle to an area where the dura is open (Critical).
6. Slowly lower the microinjection needle to touch the spinal cord. Small dimple will form when you have touched the spinal cord (*See* Note 1).
7. Reset the z-axis of the stereotaxic coordinates. Then, slowly lower the z-axis to penetrate the spinal cord. Depending on the age and location of the injection, you may need to lower the needle as deep as 500 μm to break through (If severe deformation of spinal cord occurs, get a new microinjection needle and trim. Then repeat steps 2 to 7). Once needle is inside the spinal cord, slowly retract the needle back up to 250 μm to target the spinal dorsal horn and wait at least 2-3 minutes at this position before starting the injection to reach equilibrium (*See* Note 2).
8. Start the injector to dispense virus solution. Use the surgical microscope's grid to monitor the meniscus of the virus solution to monitor the flow.

    a. We are injecting relatively high volume (1 µL) of virus solution to ensure good mediolateral and rostrocaudal spread. However, this may cause overflow of the virus solution.
    b. Occasionally, a pool of CSF may form immediately after needle breaks through the spinal cord. Use the eye spears to carefully absorb any CSF overflow.
9. Once the injection is complete, wait at least 2-3 minutes before retracting the microinjection needle.
    a. You must ensure no mineral oil leaks out of the microinjection needle.
10. Slowly retract the microinjection needle out of the spinal cord. Clean the area with eye spear (*See* Note 3).
11. Remove the "V" notch clamps and suture the *latissimus dorsi* muscle with 6-0 nylon sutures.
12. Suture the skin with 6-0 silk sutures.
13. Subcutaneously inject appropriate volume of 50/50 LRS with 5% dextrose and saline solution. Maximum volume will depend on weight and age of the animal (we have been giving 300-400 µL to p14-p30 mice).
14. Stop the isoflurane and allow the animal to fully recover on heating pad before returning the animal to its cage.

2.6 Post-operative Care of Animals

Once animals have been returned to the cage, health of the animal must be monitored closely over the next 48 hours. We always provide mushed pellets during this period, and we monitor the weight, sutures, activity levels, gait, and signs of dehydration. Furthermore, post-operative analgesic (5 mg/kg ketoprofen) is given by subcutaneous injection with 50/50 LRS and saline mixture once a day over 48 hours.

3. Notes

1. This may be difficult to confirm if the spinal cord opening is filled with CSF or blood. It is a good idea to remove as much CSF as possible with an eye spear before this step.
2. It is critical to monitor the tip of the needle for any blood. Occasionally you may hit small blood vessels inside the spinal cord. This will clog the microinjection needle and ruin the injection. If you see any blood in the microinjection needle, immediately apply small positive pressure to push it out.
3. Wait period and slow retraction minimizes backflow of injected virus solution.

II. Chemogenetics to assess the behavioral role of dorsal horn neurons.

1. Materials:

- PSEM^{89s} (Tocris Cat. No. 6426)
- 0.9% sterile NaCl
- Von Frey/Semmes-Weinstein Monofilaments
- IITC Mesh Stand and Animal Enclosures for mice (Part #410 and #435)
- Cotton buds
- Plantar Analgesia Meter (IITC)
- CaviCide® disinfectant
- Paper towels
- Acetone
- Stopwatch
- 1 mL syringes

2. Methods

2.1 Acclimation Prior to Behavior

It is important to habituate the mice in their animal enclosures prior to beginning behavioral testing. The measurements obtained will be more reliable when the mice are not stressed from being away from their home cages and in a new environment. It is best to acclimate the mice a day before von Frey or cotton swab tests. The Hargreaves assay requires more time for acclimation, so it is recommended to acclimate the mice at least 2-3 times to the Hargreaves apparatus before the day of experimentation.

Acclimation Period for Cotton Swab and von Frey

1. Choose a quiet room for your behavioral testing so that the mice do not get agitated by other people or noise.
2. Spray the animal enclosures and mesh stand with disinfectant.
3. Place the animal enclosures on the mesh stand and keep paper towels below the wire mesh to prevent mice droppings from making a mess.
4. Remove the mice from their home cages and place each of them in their own compartment in the Plexiglass chambers (animal enclosures).
5. Let them remain in their animal enclosures for an hour. It is ideal to remain in the room for half or more of that time so that the mice get acclimated to your scent as well.

6. After an hour, remove the mice from the Plexiglass chamber and return them to their home cages.
7. Spray down the animal enclosures and mesh stand with disinfectant.

Acclimation Period for Hargreaves

1. Choose a quiet room for your behavioral testing so that the mice do not get agitated by other people or noise.
2. Spray the temperature-regulated glass panel and Plexiglass chambers with disinfectant. Wipe it down.
3. Place the animal enclosures on the glass panel.
4. Make sure the glass panel is set at 30ºC.
5. Remove mice from their home cage and set them each in a compartment in the Plexiglass chamber.
6. Allow them to explore their compartments for an hour.
7. Return the mice to their home cages.
8. Spray the glass panel and Plexiglass chambers with disinfectant and wipe down.

2.2 Control Experiments for Off-target Behavioral Effects of the Ligand

Prior to testing the mice intraspinally injected with the PSAM-GlyR virus, it is critical to rule out any effects the ligand PSEM^{89s} has on somatosensation. To determine this, we intraperitoneally inject mice that have no virus with PSEM^{89s} and test behavior. We measure cotton swab before von Frey because the former assay requires the mice not be at all agitated. After von Frey, mice are sometimes agitated (*See* Note [1]) is also important to avoid taking behavioral measurements when the mice are grooming as this results in false negative responses.

2.2.1 Cotton Swab and von Frey Assay:

1. Weigh the mice to be tested and note down their measurements.
2. Before behavioral testing, habituate the mice in their Plexiglass chambers for thirty minutes. Make sure the surfaces of the wire mesh and Plexiglass chambers are clean.
3. Prepare PSEM^{89s} (30-50 mg/kg) in 0.9% sterile saline 15 minutes before testing. Keep on ice. Control animals will receive 0.9% saline alone.
4. Measure the dynamic response using the cotton swab test. Puff out the cotton bud until it is three times its original size. The cotton swab is gently brushed against the plantar hind paw in the heel-to-toe direction. This is done six times for each paw, leaving three minutes between each stimulation. A response is when the mice withdraw their paw,

flick their paw or start licking the paw. The percentage of times the mice respond to the cotton swab can then be calculated for both the left and right hind paws separately.

5. Next, the mechanical threshold of the mice is determined using the von Frey assay by the Up-Down (Chaplan) or simplified Up-Down (SUDO) method, starting with the 0.4 filament (Bonin et al., 2014; Chaplan et al., 1994). Each filament is applied to the plantar hind paw until the filament starts to bend and held in place for 3 s or until a sharp response is observed. A response includes paw withdrawal, shaking or licking. An interval of 5 minutes is given between each stimulation.
6. Mice are then injected (30-50 mg/kg, i.p) with PSEM^{89s} or saline. **The tester should be blind to the treatments.**
7. The mice are placed back in the Plexiglass chambers in the same compartment as they were in before.
8. Twenty minutes after drug/saline treatment, the dynamic response is measured again with the cotton swab.
9. After the cotton swab test, we measure the von Frey threshold in the mice.
10. After testing, return the mice back to their home cages.
11. Clean the Plexiglass chambers, wire mesh and surrounding area.

2.2.2. Hargreaves Thermal Assay (Hargreaves et al., 1988):

It is recommended that the thermal assay be conducted on a different day (*See* Note 2).

1. Acclimate the mice in their Plexiglass chambers for 30 minutes. Make sure the surfaces of the glass panel and Plexiglass chambers are clean. The temperature-regulated glass panel should be set at 30ºC.
2. During the acclimation time, you can prepare the PSEM^{89s} (30-50 mg/kg) in 0.9% sterile saline. Control animals will receive 0.9% saline alone.
3. The Plantar Analgesia Meter is set at 20% intensity with a cut off time of 20 s.
4. Keep paper towels nearby and wipe off any droppings on the glass panel. Liquid on the glass panel can reduce the temperature of the glass panel, hindering accurate measurement.
5. Focus the heat source on the plantar hind paw. As soon as the paw is withdrawn, shut off the heat source. The latency to thermal response is noted. If the mice don't withdraw their paw even after 20 s, the heat source will automatically turn off.
6. Take three measurements per paw with an interval of 5 minutes between each stimulation. The measurements can then be averaged for each paw.
7. Mice are then injected (30-50 mg/kg, i.p) with PSEM^{89s} or saline. **The tester should be blind to the treatments.**
8. Twenty minutes after drug/saline treatment, the paw withdrawal latency is measured as before. Three measurements are taken for each paw with an interval of 5 minutes between each stimulation. Make sure to wipe any droppings on the glass panel before testing.
9. Return the mice to their home cage after testing.
10. Spray the Plexiglass chambers and glass panel with disinfectant.

2.3. Baseline Measurements:

To test the functional role of spinal cord dorsal horn neurons in pain transmission, transgenic Cre-driver lines are utilized. This allows for acute inhibition of specific excitatory neuron populations expressing the PSAM-GlyR virus by delivering the PSEM^{89S} ligand (i.p.). In mice injected with the PSAM-GlyR virus, the baseline somatosensory responses are measured two weeks after the intraspinal injection. After ligand administration, we measure their mechanical threshold with von Frey, dynamic response using the cotton swab test, heat sensitivity with the Hargreaves assay and acetone evaporation test to measure sensitivity to cold. You may choose to include other behavioral pain assays such as the pinprick test for noxious pain detection.

2.3.1. Cotton Swab and von Frey Assay:

1. Two weeks after intraspinal injection of the PSAM-GlyR virus, acclimate the mice in the Plexiglass chambers a day before testing as instructed above.
2. On the day of testing, acclimate the mice in the Plexiglass chambers for 30 minutes.
3. Prepare PSEM^{89s} (30-50 mg/kg) in 0.9% sterile saline 15 minutes before testing. Keep on ice. Control animals will receive 0.9% saline alone.
4. Measure the dynamic response and paw withdrawal threshold with the cotton swab and von Frey assays respectively.
5. Inject (i.p.) mice with PSEM^{89s} or sterile saline. **The tester should be blind to the treatments.**
6. Twenty minutes after injection, perform the cotton swab and von Frey assay.
7. Return the mice to their home cages and clean up the surfaces with disinfectant.

2.3.2. Hargreaves Thermal Assay:

Interweave the days on which you measure the static and dynamic thresholds with latency to thermal response.

1. Two weeks after intraspinal injection of the PSAM-GlyR virus, acclimate the mice as instructed above.
2. On the day of testing, acclimate the mice in the Plexiglass chambers for at least 30 minutes. Make sure the glass panel is at 30ºC.
3. Prepare PSEM^{89s} (30-50 mg/kg) in 0.9% sterile saline 15 minutes before testing. Keep on ice. Control animals will receive 0.9% saline alone.

4. Measure the paw withdrawal latency to heat. Wipe any droppings from the mice found on the glass floor with paper towels.
5. Inject (i.p.) mice with PSEM^{89s} or sterile saline. **The tester should be blind to the treatments.**
6. Twenty minutes after injection, perform the Hargreaves assay again.
7. Return the mice to their home cages and clean up the surfaces with disinfectant.

2.3.3. Acetone Evaporation Test:

Here, we measure the time taken by the mouse in responding (which includes quick paw withdrawal, flicking or licking of the paw) to acetone application(Golden et al., 2010).

1. The von Frey threshold setup with the plexiglass chambers on the wire mesh can be used for the acetone evaporation test.
2. On the day of testing, acclimate the mice injected with PSAM-GlyR in the Plexiglass chambers for at least 30 minutes.
3. Prepare PSEM^{89s} (30-50 mg/kg) in 0.9% sterile saline 15 minutes before testing. Keep on ice. Control animals will receive 0.9% saline alone.
4. Once the mice are acclimated, draw up acetone into a 1 mL syringe. Form uniform drops of acetone and apply one drop of acetone to the plantar surface of the mouse hind paw (*See* Note 3).
5. The amount of time spent in flicking or licking the paw after the acetone application is measured using a stopwatch up to 30 seconds.
6. Perform three trials on each hind paw, with an interval of five minutes between each trial.
7. Inject (i.p.) mice with PSEM^{89s} or sterile saline. **The tester should be blind to the treatments.**
8. Twenty minutes after injection, perform the acetone test again.
9. Return the mice to their home cages and clean up the surfaces with disinfectant.

3. Notes

1. The cotton swab assay requires the mice to not be at all agitated. After von Frey, mice are sometimes agitated and become sensitized to the mechanical stimulation. It is recommended therefore to start with the least stressful assay before proceeding with the more stressful assay.
2. Conducting too many behavioral pain assays on the same day can stress out the mice, resulting in variable results.
3. One limitation of the acetone evaporation assay is the difficulty in creating consistent droplets of acetone. We insert a sharply cut piece of a P20 pipette tip on to the 1 mL syringe in order to draw up approximately 10 µl of acetone for each application.

III. Persistent Pain Models

1. Materials:

Spared Nerve Injury Neuropathic Pain Model:

- 2% Isofluorane
- Electric shaver
- Silk, non-absorbable suture, 6-0
- Nylon suture, 8-0
- Forceps
- Fine scissors
- Dissection scissors
- Spring scissors
- Blue drapes
- Eye ointment
- Betadine

Complete Freund's Adjuvant Inflammatory Pain Model:

- 2% Isofluorane
- Complete Freund's adjuvant (1 mg/ml heat killed and dried mycobacterium tuberculosis)
- 0.9% sterile NaCl
- 70% Ethanol
- 3cc glass syringe
- 23-G, ¾ inch needle
- Blue drapes

2. Methods:

Spared Nerve Injury Neuropathic Pain Model:

1. After carrying out baseline measurements in the mice injected with PSAM-GlyR virus, perform SNI surgery ipsilateral to the side of injection. Here, we spare the sural nerve and cut and ligate the tibial and common peroneal nerves.
2. One week after the SNI surgery, acclimate the mice for 30 minutes in the Plexiglass chambers.
3. Measure the dynamic and static mechanical thresholds using the cotton swab and von Frey assays respectively by applying the stimulations to lateral region of the injured hind paw.
4. Return the mice to their home cages and clean up the surrounding area and equipment.
5. The next day, acclimate the mice in the Plexiglass chambers for 30 minutes.
6. Prepare PSEM^{89s} (30-50 mg/kg) in 0.9% sterile saline 15 minutes before testing. Control animals will receive 0.9% saline alone.
7. Inject (i.p.) mice with PSEM^{89s} or sterile saline. **The tester should be blind to the treatments.**

8. Twenty minutes after injection, measure the dynamic and static mechanical thresholds as before.
9. To measure cold allodynia, perform the acetone evaporation assay on the injured mice, preferably on a separate day from the cotton swab and von Frey assays. Acclimate the mice for 30 minutes in the Plexiglass chambers.
10. Prepare PSEM^{89s} (30-50 mg/kg) in 0.9% sterile saline 15 minutes before testing. Control animals will receive 0.9% saline alone.
11. Measure the time spent in responding to the acetone application with a stopwatch. Again, disregard the initial 10 s where the mice show reaction to the acetone.
12. Inject (i.p.) mice with PSEM^{89s} or sterile saline. **The tester should be blind to the treatments.**
13. Twenty minutes after injection, perform the acetone assay again and measure the time response.

Complete Freund's Adjuvant Inflammatory Pain Model:

1. After baseline measurements carried out as stated above, prepare an equal parts emulsion of Complete Freund's adjuvant and 0.9% sterile saline. This should be prepared fresh prior to injection into the footpad. Draw the solution into the glass syringe with a 23-G, ¾ in needle attached and mix by drawing the solution up and down.
2. Inject 20 µl of CFA in the glabrous skin of the hind paw ipsilateral to the side of injection.
3. 24 hours later, check the ipsilateral paws for signs of inflammation. If there is no inflammation, inject an extra 5 µl.
4. Five days after CFA injection, acclimate the mice in the Plexiglass chambers for 30 min.
5. Prepare PSEM^{89s} (30-50 mg/kg) in 0.9% sterile saline 15 minutes before testing. Control animals will receive 0.9% saline alone.
6. After the acclimation period, measure the dynamic and static mechanical thresholds or heat latency as instructed before.
7. Inject (i.p.) mice with PSEM^{89s} or sterile saline. **The tester should be blind to the treatments.**
8. Twenty minutes after injection, measure the dynamic and static mechanical thresholds or heat latency as before.

IV Validation of Viral Injection with Immunohistochemistry

1. Materials:

- 4% paraformaldehyde (Prepare fresh)
- 30% sucrose in 1X PBS
- α-bungarotoxin, Alexa Fluor™ 647 conjuagate (Catalog number B35450, Thermofisher)
- O.C.T Compound (Tissue-Tek)
- 1 x PBS
- 1% Triton in 1X PBS
- 1.5 ml microcentrifuge tubes
- Tube Revolver/Rotator (Thermo Scientific)

- Fluoromount-G® (SouthernBiotech)
- Coverslips
- Superfrost Plus Microscope Slides (Fisherbrand)

2. Methods:

1. Perfuse the mice with 1X PBS, followed by cold 4% paraformaldehyde.
2. Dissect out the spinal cords, taking care not to damage the lumbar region.
3. Place the spinal cords in 4% PFA for 2 hours at 4ºC.
4. Transfer the cords to 30% sucrose in 1X PBS and leave at 4ºC for 1-2 days.
5. Embed the lumbar spinal cord in OCT and freeze down in the -80ºC.
6. When you are ready to section the tissue, transfer the embedded tissue to the cryostat. Let it sit at -20ºC for 30-45 minutes.
7. Section the tissue using the cryostat at 30 µm into wells containing 1X PBS. You can later transfer the tissues into 1.5 ml microcentrifuge tubes for staining.
8. Wash the sections with 1X PBS again.
9. Prepare a staining solution of 1% Triton, 2% NDS (optional) and α-bungarotoxin, Alexa Fluor™ 647 (1:1000).
10. Remove the 1X PBS and add the staining solution to the tissues.
11. Rotate using the Tube Rotator in the dark for 2 hours at room temperature.
12. Remove the staining solution and wash with 1X PBS.
13. Rotate for 2 minutes and then repeat the wash with fresh 1X PBS.
14. Mount the sections on to Superfrost Slides and cover with one or two drops of mounting medium (e.g., Fluoromount-G®).
15. Coverslip and view under the microscope to confirm viral expression in the dorsal horn. Mice with no α-bungarotoxin staining should be excluded from the behavioral analysis.

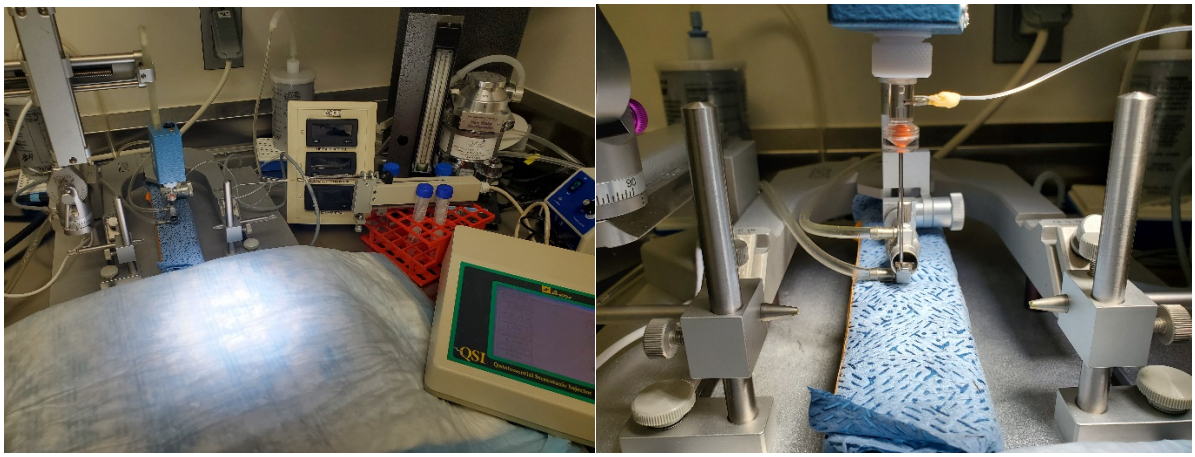

Figure 20. Intraspinal Setup Example

In this image, (Left) the small animal stereotaxic instrument with digital display console, heat pad, isofluorane anesthesia unit and stereotaxic injector can be seen. In the image on the right, glass capillary for injection as well as the spinal clamp area can be seen.

Bibliography

Abraira, V. E., & Ginty, D. D. (2013, Aug 21). The sensory neurons of touch. *Neuron, 79*(4), 618-639. https://doi.org/10.1016/j.neuron.2013.07.051

Abraira, V. E., Kuehn, E. D., Chirila, A. M., Springel, M. W., Toliver, A. A., Zimmerman, A. L., Orefice, L. L., Boyle, K. A., Bai, L., Song, B. J., Bashista, K. A., O'Neill, T. G., Zhuo, J., Tsan, C., Hoynoski, J., Rutlin, M., Kus, L., Niederkofler, V., Watanabe, M., Dymecki, S. M., Nelson, S. B., Heintz, N., Hughes, D. I., & Ginty, D. D. (2017, Jan 12). The Cellular and Synaptic Architecture of the Mechanosensory Dorsal Horn. *Cell, 168*(1-2), 295-310 e219. https://doi.org/10.1016/j.cell.2016.12.010

Akiyama, T., Carstens, M. I., Ikoma, A., Cevikbas, F., Steinhoff, M., & Carstens, E. (2012, Jul). Mouse model of touch-evoked itch (alloknesis). *J Invest Dermatol, 132*(7), 1886-1891. https://doi.org/10.1038/jid.2012.52

Akopian, A. N., Sivilotti, L., & Wood, J. N. (1996, Jan 18). A tetrodotoxin-resistant voltage-gated sodium channel expressed by sensory neurons. *Nature, 379*(6562), 257-262. https://doi.org/10.1038/379257a0

Al-Chaer, E. D., Feng, Y., & Willis, W. D. (1999, Oct). Comparative study of viscerosomatic input onto postsynaptic dorsal column and spinothalamic tract neurons in the primate. *J Neurophysiol, 82*(4), 1876-1882. https://doi.org/10.1152/jn.1999.82.4.1876

Al-Khater, K. M., Kerr, R., & Todd, A. J. (2008, Nov 1). A quantitative study of spinothalamic neurons in laminae I, III, and IV in lumbar and cervical segments of the rat spinal cord. *J Comp Neurol, 511*(1), 1-18. https://doi.org/10.1002/cne.21811

Alaynick, W. A., Jessell, T. M., & Pfaff, S. L. (2011, Jul 8). SnapShot: spinal cord development. *Cell, 146*(1), 178-178 e171. https://doi.org/10.1016/j.cell.2011.06.038

Alba-Delgado, C., Mountadem, S., Mermet-Joret, N., Monconduit, L., Dallel, R., Artola, A., & Antri, M. (2018, Dec 5). 5-HT2A Receptor-Induced Morphological Reorganization of PKCgamma-Expressing Interneurons Gates Inflammatory Mechanical Allodynia in Rat. *J Neurosci, 38*(49), 10489-10504. https://doi.org/10.1523/JNEUROSCI.1294-18.2018

Albisetti, G. W., Pagani, M., Platonova, E., Hosli, L., Johannssen, H. C., Fritschy, J. M., Wildner, H., & Zeilhofer, H. U. (2019, Mar 20). Dorsal Horn Gastrin-Releasing Peptide Expressing Neurons Transmit Spinal Itch But Not Pain Signals. *J Neurosci, 39*(12), 2238-2250. https://doi.org/10.1523/JNEUROSCI.2559-18.2019

Allard, J. (2019, Apr). Physiological properties of the lamina I spinoparabrachial neurons in the mouse. *J Physiol, 597*(7), 2097-2113. https://doi.org/10.1113/JP277447

Alsulaiman, W. A. A., Quillet, R., Bell, A. M., Dickie, A. C., Polgar, E., Boyle, K. A., Watanabe, M., Roome, R. B., Kania, A., Todd, A. J., & Gutierrez-Mecinas, M. (2021, Sep 9). Characterisation of lamina I anterolateral system neurons that express Cre in a

Phox2a-Cre mouse line. *Sci Rep, 11*(1), 17912. https://doi.org/10.1038/s41598-021-97105-w

Andrew, D. (2009, May 1). Sensitization of lamina I spinoparabrachial neurons parallels heat hyperalgesia in the chronic constriction injury model of neuropathic pain. *J Physiol, 587*(Pt 9), 2005-2017. https://doi.org/10.1113/jphysiol.2009.170290

Arcourt, A., Gorham, L., Dhandapani, R., Prato, V., Taberner, F. J., Wende, H., Gangadharan, V., Birchmeier, C., Heppenstall, P. A., & Lechner, S. G. (2017, Jan 4). Touch Receptor-Derived Sensory Information Alleviates Acute Pain Signaling and Fine-Tunes Nociceptive Reflex Coordination. *Neuron, 93*(1), 179-193. https://doi.org/10.1016/j.neuron.2016.11.027

Armbruster, B. N., Li, X., Pausch, M. H., Herlitze, S., & Roth, B. L. (2007, Mar 20). Evolving the lock to fit the key to create a family of G protein-coupled receptors potently activated by an inert ligand. *Proc Natl Acad Sci U S A, 104*(12), 5163-5168. https://doi.org/10.1073/pnas.0700293104

Arokiaraj, C. M., Noh, M. C., & Seal, R. P. (2022). The Use of Intraspinally Injected Chemogenetic Receptor, PSAM-GlyR, to Probe the Functional Role of Spinal Dorsal Horn Neurons. In R. P. Seal (Ed.), *Contemporary Approaches to the Study of Pain: from molecules to neural networks* (Vol. 178). Springer US.

Bai, L., Lehnert, B. P., Liu, J., Neubarth, N. L., Dickendesher, T. L., Nwe, P. H., Cassidy, C., Woodbury, C. J., & Ginty, D. D. (2015, Dec 17). Genetic Identification of an Expansive Mechanoreceptor Sensitive to Skin Stroking. *Cell, 163*(7), 1783-1795. https://doi.org/10.1016/j.cell.2015.11.060

Bais, A. S., & Kostka, D. (2020, Feb 15). scds: computational annotation of doublets in single-cell RNA sequencing data. *Bioinformatics, 36*(4), 1150-1158. https://doi.org/10.1093/bioinformatics/btz698

Baker, M. D., & Nassar, M. A. (2020, Jul). Painful and painless mutations of SCN9A and SCN11A voltage-gated sodium channels. *Pflugers Arch, 472*(7), 865-880. https://doi.org/10.1007/s00424-020-02419-9

Baker, M. L., & Giesler, G. J., Jr. (1984). Anatomical studies of the spinocervical tract of the rat. *Somatosens Res, 2*(1), 1-18. https://www.ncbi.nlm.nih.gov/pubmed/6505460

Bardoni, R., Shen, K. F., Li, H., Jeffry, J., Barry, D. M., Comitato, A., Li, Y. Q., & Chen, Z. F. (2019, Nov 1). Pain Inhibits GRPR Neurons via GABAergic Signaling in the Spinal Cord. *Sci Rep, 9*(1), 15804. https://doi.org/10.1038/s41598-019-52316-0

Beal, J. A., & Cooper, M. H. (1978, May 1). The neurons in the gelatinosal complex (Laminae II and III) of the monkey (Macaca mulatta): a Golgi study. *J Comp Neurol, 179*(1), 89-121. https://doi.org/10.1002/cne.901790107

Beissner, F., Brandau, A., Henke, C., Felden, L., Baumgartner, U., Treede, R. D., Oertel, B. G., & Lotsch, J. (2010, Sep 23). Quick discrimination of A(delta) and C fiber mediated

pain based on three verbal descriptors. *PLoS One, 5*(9), e12944. https://doi.org/10.1371/journal.pone.0012944

Beliveau, B. J., Boettiger, A. N., Avendaño, M. S., Jungmann, R., McCole, R. B., Joyce, E. F., Kim-Kiselak, C., Bantignies, F., Fonseka, C. Y., Erceg, J., Hannan, M. A., Hoang, H. G., Colognori, D., Lee, J. T., Shih, W. M., Yin, P., Zhuang, X., & Wu, C. T. (2015, May 12). Single-molecule super-resolution imaging of chromosomes and in situ haplotype visualization using Oligopaint FISH probes. *Nat Commun, 6*, 7147. https://doi.org/10.1038/ncomms8147

Bell, A. M., Gutierrez-Mecinas, M., Stevenson, A., Casas-Benito, A., Wildner, H., West, S. J., Watanabe, M., & Todd, A. J. (2020, Aug 6). Expression of green fluorescent protein defines a specific population of lamina II excitatory interneurons in the GRP::eGFP mouse. *Sci Rep, 10*(1), 13176. https://doi.org/10.1038/s41598-020-69711-7

Bennett, G. J., Abdelmoumene, M., Hayashi, H., & Dubner, R. (1980, Dec 15). Physiology and morphology of substantia gelatinosa neurons intracellularly stained with horseradish peroxidase. *J Comp Neurol, 194*(4), 809-827. https://doi.org/10.1002/cne.901940407

Bester, H., Chapman, V., Besson, J. M., & Bernard, J. F. (2000, Apr). Physiological properties of the lamina I spinoparabrachial neurons in the rat. *J Neurophysiol, 83*(4), 2239-2259. https://doi.org/10.1152/jn.2000.83.4.2239

Bice, T. N., & Beal, J. A. (1997, Dec 1). Quantitative and neurogenic analysis of the total population and subpopulations of neurons defined by axon projection in the superficial dorsal horn of the rat lumbar spinal cord. *J Comp Neurol, 388*(4), 550-564. https://doi.org/10.1002/(sici)1096-9861(19971201)388:4<550::aid-cne4>3.0.co;2-1

Bonaventura, J., Eldridge, M. A. G., Hu, F., Gomez, J. L., Sanchez-Soto, M., Abramyan, A. M., Lam, S., Boehm, M. A., Ruiz, C., Farrell, M. R., Moreno, A., Galal Faress, I. M., Andersen, N., Lin, J. Y., Moaddel, R., Morris, P. J., Shi, L., Sibley, D. R., Mahler, S. V., Nabavi, S., Pomper, M. G., Bonci, A., Horti, A. G., Richmond, B. J., & Michaelides, M. (2019, Oct 11). High-potency ligands for DREADD imaging and activation in rodents and monkeys. *Nat Commun, 10*(1), 4627. https://doi.org/10.1038/s41467-019-12236-z

Bonin, R. P., Bories, C., & De Koninck, Y. (2014, Apr 16). A simplified up-down method (SUDO) for measuring mechanical nociception in rodents using von Frey filaments. *Mol Pain, 10*, 26. https://doi.org/10.1186/1744-8069-10-26

Bourane, S., Duan, B., Koch, S. C., Dalet, A., Britz, O., Garcia-Campmany, L., Kim, E., Cheng, L., Ghosh, A., Ma, Q., & Goulding, M. (2015, Oct 30). Gate control of mechanical itch by a subpopulation of spinal cord interneurons. *Science, 350*(6260), 550-554. https://doi.org/10.1126/science.aac8653

Boyle, K. A., Gradwell, M. A., Yasaka, T., Dickie, A. C., Polgar, E., Ganley, R. P., Orr, D. P. H., Watanabe, M., Abraira, V. E., Kuehn, E. D., Zimmerman, A. L., Ginty, D. D., Callister, R. J., Graham, B. A., & Hughes, D. I. (2019, Jul 9). Defining a Spinal Microcircuit that Gates Myelinated Afferent Input: Implications for Tactile Allodynia. *Cell Rep, 28*(2), 526-540 e526. https://doi.org/10.1016/j.celrep.2019.06.040

Boyle, K. A., Gutierrez-Mecinas, M., Polgar, E., Mooney, N., O'Connor, E., Furuta, T., Watanabe, M., & Todd, A. J. (2017, Nov 5). A quantitative study of neurochemically defined populations of inhibitory interneurons in the superficial dorsal horn of the mouse spinal cord. *Neuroscience, 363*, 120-133. https://doi.org/10.1016/j.neuroscience.2017.08.044

Broman, J. (1994, Mar). Neurotransmitters in subcortical somatosensory pathways. *Anat Embryol (Berl), 189*(3), 181-214. https://doi.org/10.1007/BF00239008

Broman, J., Anderson, S., & Ottersen, O. P. (1993, Aug 1). Enrichment of glutamate-like immunoreactivity in primary afferent terminals throughout the spinal cord dorsal horn. *Eur J Neurosci, 5*(8), 1050-1061. https://doi.org/10.1111/j.1460-9568.1993.tb00958.x

Brown, A. G. (1982, Apr). The dorsal horn of the spinal cord. *Q J Exp Physiol, 67*(2), 193-212. https://doi.org/10.1113/expphysiol.1982.sp002630

Brown, A. G., & Iggo, A. (1967, Dec). A quantitative study of cutaneous receptors and afferent fibres in the cat and rabbit. *J Physiol, 193*(3), 707-733. https://doi.org/10.1113/jphysiol.1967.sp008390

Brown, A. G., Rose, P. K., & Snow, P. J. (1977, Nov). The morphology of hair follicle afferent fibre collaterals in the spinal cord of the cat. *J Physiol, 272*(3), 779-797. https://doi.org/10.1113/jphysiol.1977.sp012073

Buckley, D. M., Burroughs-Garcia, J., Kriks, S., Lewandoski, M., & Waters, S. T. (2020, Apr 1). Gbx1 and Gbx2 Are Essential for Normal Patterning and Development of Interneurons and Motor Neurons in the Embryonic Spinal Cord. *J Dev Biol, 8*(2). https://doi.org/10.3390/jdb8020009

Buenrostro, J. D., Wu, B., Chang, H. Y., & Greenleaf, W. J. (2015, Jan 5). ATAC-seq: A Method for Assaying Chromatin Accessibility Genome-Wide. *Curr Protoc Mol Biol, 109*, 21 29 21-21 29 29. https://doi.org/10.1002/0471142727.mb2129s109

Burgess, P. R., Petit, D., & Warren, R. M. (1968, Nov). Receptor types in cat hairy skin supplied by myelinated fibers. *J Neurophysiol, 31*(6), 833-848. https://doi.org/10.1152/jn.1968.31.6.833

Cameron, D., Polgar, E., Gutierrez-Mecinas, M., Gomez-Lima, M., Watanabe, M., & Todd, A. J. (2015, Oct). The organisation of spinoparabrachial neurons in the mouse. *Pain, 156*(10), 2061-2071. https://doi.org/10.1097/j.pain.0000000000000270

Cano-Gamez, E., & Trynka, G. (2020). From GWAS to Function: Using Functional Genomics to Identify the Mechanisms Underlying Complex Diseases. *Front Genet, 11*, 424. https://doi.org/10.3389/fgene.2020.00424

Cao, Y. Q., Mantyh, P. W., Carlson, E. J., Gillespie, A. M., Epstein, C. J., & Basbaum, A. I. (1998, Mar 26). Primary afferent tachykinins are required to experience moderate to intense pain. *Nature, 392*(6674), 390-394. https://doi.org/10.1038/32897

Carstens, E., & Trevino, D. L. (1978, Nov 1). Laminar origins of spinothalamic projections in the cat as determined by the retrograde transport of horseradish peroxidase. *J Comp Neurol, 182*(1), 161-165. https://www.ncbi.nlm.nih.gov/pubmed/701487

Carstens, E. E., Carstens, M. I., Simons, C. T., & Jinks, S. L. (2010, Mar 10). Dorsal horn neurons expressing NK-1 receptors mediate scratching in rats. *Neuroreport, 21*(4), 303-308. https://doi.org/10.1097/WNR.0b013e328337310a

Caterina, M. J., Schumacher, M. A., Tominaga, M., Rosen, T. A., Levine, J. D., & Julius, D. (1997, Oct 23). The capsaicin receptor: a heat-activated ion channel in the pain pathway. *Nature, 389*(6653), 816-824. https://doi.org/10.1038/39807

Chamessian, A., Young, M., Qadri, Y., Berta, T., Ji, R. R., & Van de Ven, T. (2018, May 1). Transcriptional Profiling of Somatostatin Interneurons in the Spinal Dorsal Horn. *Sci Rep, 8*(1), 6809. https://doi.org/10.1038/s41598-018-25110-7

Chaplan, S. R., Bach, F. W., Pogrel, J. W., Chung, J. M., & Yaksh, T. L. (1994, Jul). Quantitative assessment of tactile allodynia in the rat paw. *J Neurosci Methods, 53*(1), 55-63. https://doi.org/10.1016/0165-0270(94)90144-9

Chen, S., Gao, X. F., Zhou, Y., Liu, B. L., Liu, X. Y., Zhang, Y., Barry, D. M., Liu, K., Jiao, Y., Bardoni, R., Yu, W., & Chen, Z. F. (2020, Oct 8). A spinal neural circuitry for converting touch to itch sensation. *Nat Commun, 11*(1), 5074. https://doi.org/10.1038/s41467-020-18895-7

Cheng, L., Duan, B., Huang, T., Zhang, Y., Chen, Y., Britz, O., Garcia-Campmany, L., Ren, X., Vong, L., Lowell, B. B., Goulding, M., Wang, Y., & Ma, Q. (2017, Jun). Identification of spinal circuits involved in touch-evoked dynamic mechanical pain. *Nat Neurosci, 20*(6), 804-814. https://doi.org/10.1038/nn.4549

Chesler, A. T., Szczot, M., Bharucha-Goebel, D., Ceko, M., Donkervoort, S., Laubacher, C., Hayes, L. H., Alter, K., Zampieri, C., Stanley, C., Innes, A. M., Mah, J. K., Grosmann, C. M., Bradley, N., Nguyen, D., Foley, A. R., Le Pichon, C. E., & Bonnemann, C. G. (2016, Oct 6). The Role of PIEZO2 in Human Mechanosensation. *N Engl J Med, 375*(14), 1355-1364. https://doi.org/10.1056/NEJMoa1602812

Chisholm, K. I., Lo Re, L., Polgar, E., Gutierrez-Mecinas, M., Todd, A. J., & McMahon, S. B. (2021, Sep 1). Encoding of cutaneous stimuli by lamina I projection neurons. *Pain, 162*(9), 2405-2417. https://doi.org/10.1097/j.pain.0000000000002226

Chiu, I. M., Barrett, L. B., Williams, E. K., Strochlic, D. E., Lee, S., Weyer, A. D., Lou, S., Bryman, G. S., Roberson, D. P., Ghasemlou, N., Piccoli, C., Ahat, E., Wang, V., Cobos, E. J., Stucky, C. L., Ma, Q., Liberles, S. D., & Woolf, C. J. (2014, Dec 19). Transcriptional profiling at whole population and single cell levels reveals somatosensory neuron molecular diversity. *Elife, 3*. https://doi.org/10.7554/eLife.04660

Choi, S., Hachisuka, J., Brett, M. A., Magee, A. R., Omori, Y., Iqbal, N. U., Zhang, D., DeLisle, M. M., Wolfson, R. L., Bai, L., Santiago, C., Gong, S., Goulding, M., Heintz, N., Koerber, H. R., Ross, S. E., & Ginty, D. D. (2020, Nov). Parallel ascending spinal

pathways for affective touch and pain. *Nature, 587*(7833), 258-263. https://doi.org/10.1038/s41586-020-2860-1

Christensen, B. N., & Perl, E. R. (1970, Mar). Spinal neurons specifically excited by noxious or thermal stimuli: marginal zone of the dorsal horn. *J Neurophysiol, 33*(2), 293-307. https://doi.org/10.1152/jn.1970.33.2.293

Coste, B., Mathur, J., Schmidt, M., Earley, T. J., Ranade, S., Petrus, M. J., Dubin, A. E., & Patapoutian, A. (2010, Oct 1). Piezo1 and Piezo2 are essential components of distinct mechanically activated cation channels. *Science, 330*(6000), 55-60. https://doi.org/10.1126/science.1193270

Cox, J. J., Sheynin, J., Shorer, Z., Reimann, F., Nicholas, A. K., Zubovic, L., Baralle, M., Wraige, E., Manor, E., Levy, J., Woods, C. G., & Parvari, R. (2010, Sep). Congenital insensitivity to pain: novel SCN9A missense and in-frame deletion mutations. *Hum Mutat, 31*(9), E1670-1686. https://doi.org/10.1002/humu.21325

Craig, A. D. (2003). Pain mechanisms: labeled lines versus convergence in central processing. *Annu Rev Neurosci, 26*, 1-30. https://doi.org/10.1146/annurev.neuro.26.041002.131022

Craig, A. D. (2008, May 10). Retrograde analyses of spinothalamic projections in the macaque monkey: input to the ventral lateral nucleus. *J Comp Neurol, 508*(2), 315-328. https://doi.org/10.1002/cne.21672

Craig, A. D., Broman, J., & Blomqvist, A. (1992, Aug 1). Lamina I spinocervical tract terminations in the medial part of the lateral cervical nucleus in the cat. *J Comp Neurol, 322*(1), 99-110. https://doi.org/10.1002/cne.903220108

Craig, A. D., Krout, K., & Andrew, D. (2001, Sep). Quantitative response characteristics of thermoreceptive and nociceptive lamina I spinothalamic neurons in the cat. *J Neurophysiol, 86*(3), 1459-1480. https://doi.org/10.1152/jn.2001.86.3.1459

Cui, L., Miao, X., Liang, L., Abdus-Saboor, I., Olson, W., Fleming, M. S., Ma, M., Tao, Y. X., & Luo, W. (2016, Sep 7). Identification of Early RET+ Deep Dorsal Spinal Cord Interneurons in Gating Pain. *Neuron, 91*(5), 1137-1153. https://doi.org/10.1016/j.neuron.2016.07.038

Cusanovich, D. A., Daza, R., Adey, A., Pliner, H. A., Christiansen, L., Gunderson, K. L., Steemers, F. J., Trapnell, C., & Shendure, J. (2015, May 22). Multiplex single cell profiling of chromatin accessibility by combinatorial cellular indexing. *Science, 348*(6237), 910-914. https://doi.org/10.1126/science.aab1601

Das Gupta, R. R., Scheurer, L., Pelczar, P., Wildner, H., & Zeilhofer, H. U. (2021, Mar 4). Neuron-specific spinal cord translatomes reveal a neuropeptide code for mouse dorsal horn excitatory neurons. *Sci Rep, 11*(1), 5232. https://doi.org/10.1038/s41598-021-84667-y

Davidson, S., Zhang, X., Khasabov, S. G., Moser, H. R., Honda, C. N., Simone, D. A., & Giesler, G. J., Jr. (2012, Sep). Pruriceptive spinothalamic tract neurons: physiological

properties and projection targets in the primate. *J Neurophysiol, 108*(6), 1711-1723. https://doi.org/10.1152/jn.00206.2012

De Biasi, S., & Rustioni, A. (1988, Oct). Glutamate and substance P coexist in primary afferent terminals in the superficial laminae of spinal cord. *Proc Natl Acad Sci U S A, 85*(20), 7820-7824. https://doi.org/10.1073/pnas.85.20.7820

Decosterd, I., & Woolf, C. J. (2000, Aug). Spared nerve injury: an animal model of persistent peripheral neuropathic pain. *Pain, 87*(2), 149-158. https://doi.org/10.1016/S0304-3959(00)00276-1

Del Barrio, M. G., Bourane, S., Grossmann, K., Schule, R., Britsch, S., O'Leary, D. D., & Goulding, M. (2013). A transcription factor code defines nine sensory interneuron subtypes in the mechanosensory area of the spinal cord. *PLoS One, 8*(11), e77928. https://doi.org/10.1371/journal.pone.0077928

Delile, J., Rayon, T., Melchionda, M., Edwards, A., Briscoe, J., & Sagner, A. (2019, Mar 27). Single cell transcriptomics reveals spatial and temporal dynamics of gene expression in the developing mouse spinal cord. *Development, 146*(12). https://doi.org/10.1242/dev.173807

Dhandapani, R., Arokiaraj, C. M., Taberner, F. J., Pacifico, P., Raja, S., Nocchi, L., Portulano, C., Franciosa, F., Maffei, M., Hussain, A. F., de Castro Reis, F., Reymond, L., Perlas, E., Garcovich, S., Barth, S., Johnsson, K., Lechner, S. G., & Heppenstall, P. A. (2018, Apr 24). Control of mechanical pain hypersensitivity in mice through ligand-targeted photoablation of TrkB-positive sensory neurons. *Nat Commun, 9*(1), 1640. https://doi.org/10.1038/s41467-018-04049-3

Dickie, A. C., Bell, A. M., Iwagaki, N., Polgar, E., Gutierrez-Mecinas, M., Kelly, R., Lyon, H., Turnbull, K., West, S. J., Etlin, A., Braz, J., Watanabe, M., Bennett, D. L. H., Basbaum, A. I., Riddell, J. S., & Todd, A. J. (2019, Feb). Morphological and functional properties distinguish the substance P and gastrin-releasing peptide subsets of excitatory interneuron in the spinal cord dorsal horn. *Pain, 160*(2), 442-462. https://doi.org/10.1097/j.pain.0000000000001406

Dimidschstein, J., Chen, Q., Tremblay, R., Rogers, S. L., Saldi, G. A., Guo, L., Xu, Q., Liu, R., Lu, C., Chu, J., Grimley, J. S., Krostag, A. R., Kaykas, A., Avery, M. C., Rashid, M. S., Baek, M., Jacob, A. L., Smith, G. B., Wilson, D. E., Kosche, G., Kruglikov, I., Rusielewicz, T., Kotak, V. C., Mowery, T. M., Anderson, S. A., Callaway, E. M., Dasen, J. S., Fitzpatrick, D., Fossati, V., Long, M. A., Noggle, S., Reynolds, J. H., Sanes, D. H., Rudy, B., Feng, G., & Fishell, G. (2016, Dec). A viral strategy for targeting and manipulating interneurons across vertebrate species. *Nat Neurosci, 19*(12), 1743-1749. https://doi.org/10.1038/nn.4430

Ding, Y. Q., Yin, J., Kania, A., Zhao, Z. Q., Johnson, R. L., & Chen, Z. F. (2004, Aug). Lmx1b controls the differentiation and migration of the superficial dorsal horn neurons of the spinal cord. *Development, 131*(15), 3693-3703. https://doi.org/10.1242/dev.01250

Disotell, T. R., & Tosi, A. J. (2007). The monkey's perspective. *Genome Biol, 8*(9), 226. https://doi.org/10.1186/gb-2007-8-9-226

Djouhri, L., & Lawson, S. N. (2004, Oct). Abeta-fiber nociceptive primary afferent neurons: a review of incidence and properties in relation to other afferent A-fiber neurons in mammals. *Brain Res Brain Res Rev, 46*(2), 131-145. https://doi.org/10.1016/j.brainresrev.2004.07.015

Dobin, A., Davis, C. A., Schlesinger, F., Drenkow, J., Zaleski, C., Jha, S., Batut, P., Chaisson, M., & Gingeras, T. R. (2013, Jan 1). STAR: ultrafast universal RNA-seq aligner. *Bioinformatics, 29*(1), 15-21. https://doi.org/10.1093/bioinformatics/bts635

Duan, B., Cheng, L., Bourane, S., Britz, O., Padilla, C., Garcia-Campmany, L., Krashes, M., Knowlton, W., Velasquez, T., Ren, X., Ross, S., Lowell, B. B., Wang, Y., Goulding, M., & Ma, Q. (2014, Dec 4). Identification of spinal circuits transmitting and gating mechanical pain. *Cell, 159*(6), 1417-1432. https://doi.org/10.1016/j.cell.2014.11.003

Emery, E. C., Luiz, A. P., & Wood, J. N. (2016, Aug). Nav1.7 and other voltage-gated sodium channels as drug targets for pain relief. *Expert Opin Ther Targets, 20*(8), 975-983. https://doi.org/10.1517/14728222.2016.1162295

Fatima, M., Ren, X., Pan, H., Slade, H. F. E., Asmar, A. J., Xiong, C. M., Shi, A., Xiong, A. E., Wang, L., & Duan, B. (2019, May). Spinal somatostatin-positive interneurons transmit chemical itch. *Pain, 160*(5), 1166-1174. https://doi.org/10.1097/j.pain.0000000000001499

Ferreira, D. W., Arokiaraj, C. M., & Seal, R. P. (2022). *Multiplex in situ hybridization of the pirmate and rodent drg and spinal cord* (R. P. Seal, Ed. 1st ed.). Springer US.

Foster, E., Wildner, H., Tudeau, L., Haueter, S., Ralvenius, W. T., Jegen, M., Johannssen, H., Hosli, L., Haenraets, K., Ghanem, A., Conzelmann, K. K., Bosl, M., & Zeilhofer, H. U. (2015, Mar 18). Targeted ablation, silencing, and activation establish glycinergic dorsal horn neurons as key components of a spinal gate for pain and itch. *Neuron, 85*(6), 1289-1304. https://doi.org/10.1016/j.neuron.2015.02.028

Francois, A., Low, S. A., Sypek, E. I., Christensen, A. J., Sotoudeh, C., Beier, K. T., Ramakrishnan, C., Ritola, K. D., Sharif-Naeini, R., Deisseroth, K., Delp, S. L., Malenka, R. C., Luo, L., Hantman, A. W., & Scherrer, G. (2017, Feb 22). A Brainstem-Spinal Cord Inhibitory Circuit for Mechanical Pain Modulation by GABA and Enkephalins. *Neuron, 93*(4), 822-839 e826. https://doi.org/10.1016/j.neuron.2017.01.008

Fukuoka, M., Miyachi, Y., & Ikoma, A. (2013, Jun). Mechanically evoked itch in humans. *Pain, 154*(6), 897-904. https://doi.org/10.1016/j.pain.2013.02.021

Gantz, S. C., Ortiz, M. M., Belilos, A. J., & Moussawi, K. (2021, Apr 6). Excitation of medium spiny neurons by 'inhibitory' ultrapotent chemogenetics via shifts in chloride reversal potential. *Elife, 10*. https://doi.org/10.7554/eLife.64241

Gatto, G., Bourane, S., Ren, X., Di Costanzo, S., Fenton, P. K., Halder, P., Seal, R. P., & Goulding, M. D. (2021, Jan 6). A Functional Topographic Map for Spinal Sensorimotor Reflexes. *Neuron, 109*(1), 91-104 e105. https://doi.org/10.1016/j.neuron.2020.10.003

Gobel, S. (1978, Jul 15). Golgi studies of the neurons in layer II of the dorsal horn of the medulla (trigeminal nucleus caudalis). *J Comp Neurol, 180*(2), 395-413. https://doi.org/10.1002/cne.901800213

Golden, J. P., Hoshi, M., Nassar, M. A., Enomoto, H., Wood, J. N., Milbrandt, J., Gereau, R. W. t., Johnson, E. M., Jr., & Jain, S. (2010, Mar 17). RET signaling is required for survival and normal function of nonpeptidergic nociceptors. *J Neurosci, 30*(11), 3983-3994. https://doi.org/10.1523/JNEUROSCI.5930-09.2010

Gomez, J. L., Bonaventura, J., Lesniak, W., Mathews, W. B., Sysa-Shah, P., Rodriguez, L. A., Ellis, R. J., Richie, C. T., Harvey, B. K., Dannals, R. F., Pomper, M. G., Bonci, A., & Michaelides, M. (2017). Chemogenetics revealed: DREADD occupancy and activation via converted clozapine. *Science (New York, N.Y.), 357*(6350), 503-507. https://doi.org/10.1126/science.aan2475

Gorkin, D. U., Barozzi, I., Zhao, Y., Zhang, Y., Huang, H., Lee, A. Y., Li, B., Chiou, J., Wildberg, A., Ding, B., Zhang, B., Wang, M., Strattan, J. S., Davidson, J. M., Qiu, Y., Afzal, V., Akiyama, J. A., Plajzer-Frick, I., Novak, C. S., Kato, M., Garvin, T. H., Pham, Q. T., Harrington, A. N., Mannion, B. J., Lee, E. A., Fukuda-Yuzawa, Y., He, Y., Preissl, S., Chee, S., Han, J. Y., Williams, B. A., Trout, D., Amrhein, H., Yang, H., Cherry, J. M., Wang, W., Gaulton, K., Ecker, J. R., Shen, Y., Dickel, D. E., Visel, A., Pennacchio, L. A., & Ren, B. (2020, Jul). An atlas of dynamic chromatin landscapes in mouse fetal development. *Nature, 583*(7818), 744-751. https://doi.org/10.1038/s41586-020-2093-3

Grace, P. M., Wang, X., Strand, K. A., Baratta, M. V., Zhang, Y., Galer, E. L., Yin, H., Maier, S. F., & Watkins, L. R. (2018, Jun). DREADDed microglia in pain: Implications for spinal inflammatory signaling in male rats. *Exp Neurol, 304*, 125-131. https://doi.org/10.1016/j.expneurol.2018.03.005

Gradwell, M. A., Boyle, K. A., Browne, T. J., Bell, A. M., Leonardo, J., Peralta Reyes, F. S., Dickie, A. C., Smith, K. M., Callister, R. J., Dayas, C. V., Hughes, D. I., & Graham, B. A. (2021, Jul 28). Diversity of inhibitory and excitatory parvalbumin interneuron circuits in the dorsal horn. *Pain*. https://doi.org/10.1097/j.pain.0000000000002422

Graham, B. A., & Hughes, D. I. (2020, Nov). Defining populations of dorsal horn interneurons. *Pain, 161*(11), 2434-2436. https://doi.org/10.1097/j.pain.0000000000002067

Granja, J. M., Corces, M. R., Pierce, S. E., Bagdatli, S. T., Choudhry, H., Chang, H. Y., & Greenleaf, W. J. (2021, Mar). ArchR is a scalable software package for integrative single-cell chromatin accessibility analysis. *Nat Genet, 53*(3), 403-411. https://doi.org/10.1038/s41588-021-00790-6

Gross, M. K., Dottori, M., & Goulding, M. (2002, May 16). Lbx1 specifies somatosensory association interneurons in the dorsal spinal cord. *Neuron, 34*(4), 535-549. https://doi.org/10.1016/s0896-6273(02)00690-6

Grudt, T. J., & Perl, E. R. (2002, Apr 1). Correlations between neuronal morphology and electrophysiological features in the rodent superficial dorsal horn [Research Support,

U.S. Gov't, P.H.S.]. *J Physiol, 540*(Pt 1), 189-207. http://www.ncbi.nlm.nih.gov/pubmed/11927679

Gutierrez-Mecinas, M., Bell, A., Polgar, E., Watanabe, M., & Todd, A. J. (2019, Sep 15). Expression of Neuropeptide FF Defines a Population of Excitatory Interneurons in the Superficial Dorsal Horn of the Mouse Spinal Cord that Respond to Noxious and Pruritic Stimuli. *Neuroscience, 416*, 281-293. https://doi.org/10.1016/j.neuroscience.2019.08.013

Gutierrez-Mecinas, M., Bell, A. M., Shepherd, F., Polgar, E., Watanabe, M., Furuta, T., & Todd, A. J. (2019, Aug 1). Expression of cholecystokinin by neurons in mouse spinal dorsal horn. *J Comp Neurol, 527*(11), 1857-1871. https://doi.org/10.1002/cne.24657

Gutierrez-Mecinas, M., Davis, O., Polgar, E., Shahzad, M., Navarro-Batista, K., Furuta, T., Watanabe, M., Hughes, D. I., & Todd, A. J. (2019, Feb 1). Expression of Calretinin Among Different Neurochemical Classes of Interneuron in the Superficial Dorsal Horn of the Mouse Spinal Cord. *Neuroscience, 398*, 171-181. https://doi.org/10.1016/j.neuroscience.2018.12.009

Gutierrez-Mecinas, M., Furuta, T., Watanabe, M., & Todd, A. J. (2016). A quantitative study of neurochemically defined excitatory interneuron populations in laminae I-III of the mouse spinal cord. *Mol Pain, 12*. https://doi.org/10.1177/1744806916629065

Gutierrez-Mecinas, M., Polgar, E., Bell, A. M., Herau, M., & Todd, A. J. (2018, Jun). Substance P-expressing excitatory interneurons in the mouse superficial dorsal horn provide a propriospinal input to the lateral spinal nucleus. *Brain Struct Funct, 223*(5), 2377-2392. https://doi.org/10.1007/s00429-018-1629-x

Hachisuka, J., Koerber, H. R., & Ross, S. E. (2020, Jan). Selective-cold output through a distinct subset of lamina I spinoparabrachial neurons. *Pain, 161*(1), 185-194. https://doi.org/10.1097/j.pain.0000000000001710

Hachisuka, J., Omori, Y., Chiang, M. C., Gold, M. S., Koerber, H. R., & Ross, S. E. (2018, Aug). Wind-up in lamina I spinoparabrachial neurons: a role for reverberatory circuits. *Pain, 159*(8), 1484-1493. https://doi.org/10.1097/j.pain.0000000000001229

Haenraets, K., Albisetti, G. W., Foster, E., & Wildner, H. Adeno-associated Virus-mediated Transgene Expression in Genetically Defined Neurons of the Spinal Cord. LID - 10.3791/57382 [doi] LID - 57382. (1940-087X (Electronic)).

Han, L., Ma, C., Liu, Q., Weng, H. J., Cui, Y., Tang, Z., Kim, Y., Nie, H., Qu, L., Patel, K. N., Li, Z., McNeil, B., He, S., Guan, Y., Xiao, B., Lamotte, R. H., & Dong, X. (2013, Feb). A subpopulation of nociceptors specifically linked to itch. *Nat Neurosci, 16*(2), 174-182. https://doi.org/10.1038/nn.3289

Han, Z. S., Zhang, E. T., & Craig, A. D. (1998, Jul). Nociceptive and thermoreceptive lamina I neurons are anatomically distinct. *Nat Neurosci, 1*(3), 218-225. https://doi.org/10.1038/665

Hargreaves, K., Dubner, R., Brown, F., Flores, C., & Joris, J. (1988, Jan). A new and sensitive method for measuring thermal nociception in cutaneous hyperalgesia. *Pain, 32*(1), 77-88. https://doi.org/10.1016/0304-3959(88)90026-7

Haring, M., Zeisel, A., Hochgerner, H., Rinwa, P., Jakobsson, J. E. T., Lonnerberg, P., La Manno, G., Sharma, N., Borgius, L., Kiehn, O., Lagerstrom, M. C., Linnarsson, S., & Ernfors, P. (2018, Jun). Neuronal atlas of the dorsal horn defines its architecture and links sensory input to transcriptional cell types. *Nat Neurosci, 21*(6), 869-880. https://doi.org/10.1038/s41593-018-0141-1

Harrison, M., O'Brien, A., Adams, L., Cowin, G., Ruitenberg, M. J., Sengul, G., & Watson, C. (2013, Mar). Vertebral landmarks for the identification of spinal cord segments in the mouse. *Neuroimage, 68*, 22-29. https://doi.org/10.1016/j.neuroimage.2012.11.048

He, J., Kleyman, M., Chen, J., Alikaya, A., Rothenhoefer, K. M., Ozturk, B. E., Wirthlin, M., Fish, K., Byrne, L. C., Pfenning, A. R., & Stauffer, W. R. (2021). Transcriptional Diversity of Medium Spiny Neurons in the Primate Striatum. *bioRxiv*, 2020.2010.2025.354159. https://doi.org/10.1101/2020.10.25.354159

Heinricher, M. M., Tavares, I., Leith, J. L., & Lumb, B. M. (2009, Apr). Descending control of nociception: Specificity, recruitment and plasticity. *Brain Res Rev, 60*(1), 214-225. https://doi.org/10.1016/j.brainresrev.2008.12.009

Heise, C., & Kayalioglu, G. (2009). Chapter 6 - Cytoarchitecture of the Spinal Cord. In C. Watson, G. Paxinos, & G. Kayalioglu (Eds.), *The Spinal Cord* (pp. 64-93). Academic Press. https://doi.org/10.1016/B978-0-12-374247-6.50010-9

Herrero, J. F., Laird, J. M., & Lopez-Garcia, J. A. (2000, Jun). Wind-up of spinal cord neurones and pain sensation: much ado about something? *Prog Neurobiol, 61*(2), 169-203. https://doi.org/10.1016/s0301-0082(99)00051-9

Hie, B., Bryson, B., & Berger, B. (2019, Jun). Efficient integration of heterogeneous single-cell transcriptomes using Scanorama. *Nat Biotechnol, 37*(6), 685-691. https://doi.org/10.1038/s41587-019-0113-3

Hill, R. (2000, Jul). NK1 (substance P) receptor antagonists--why are they not analgesic in humans? *Trends Pharmacol Sci, 21*(7), 244-246. https://doi.org/10.1016/s0165-6147(00)01502-9

Hirshberg, R. M., Al-Chaer, E. D., Lawand, N. B., Westlund, K. N., & Willis, W. D. (1996, Oct). Is there a pathway in the posterior funiculus that signals visceral pain? *Pain, 67*(2-3), 291-305. https://doi.org/10.1016/0304-3959(96)03127-2

Honda, C. N. (1985, Apr). Visceral and somatic afferent convergence onto neurons near the central canal in the sacral spinal cord of the cat. *J Neurophysiol, 53*(4), 1059-1078. https://doi.org/10.1152/jn.1985.53.4.1059

Huang, J., Polgar, E., Solinski, H. J., Mishra, S. K., Tseng, P. Y., Iwagaki, N., Boyle, K. A., Dickie, A. C., Kriegbaum, M. C., Wildner, H., Zeilhofer, H. U., Watanabe, M., Riddell, J. S., Todd, A. J., & Hoon, M. A. (2018, May). Circuit dissection of the role of

somatostatin in itch and pain. *Nat Neurosci, 21*(5), 707-716. https://doi.org/10.1038/s41593-018-0119-z

Huang, T., Lin, S. H., Malewicz, N. M., Zhang, Y., Zhang, Y., Goulding, M., LaMotte, R. H., & Ma, Q. (2019, Jan). Identifying the pathways required for coping behaviours associated with sustained pain. *Nature, 565*(7737), 86-90. https://doi.org/10.1038/s41586-018-0793-8

Huber, D., Voith von Voithenberg, L., & Kaigala, G. V. (2018, 2018/11/01/). Fluorescence in situ hybridization (FISH): History, limitations and what to expect from micro-scale FISH? *Micro and Nano Engineering, 1*, 15-24. https://doi.org/10.1016/j.mne.2018.10.006

Hughes, D. I., Sikander, S., Kinnon, C. M., Boyle, K. A., Watanabe, M., Callister, R. J., & Graham, B. A. (2012, Aug 15). Morphological, neurochemical and electrophysiological features of parvalbumin-expressing cells: a likely source of axo-axonic inputs in the mouse spinal dorsal horn. *J Physiol, 590*(16), 3927-3951. https://doi.org/10.1113/jphysiol.2012.235655

Hughes, D. I., & Todd, A. J. (2020, Jul). Central Nervous System Targets: Inhibitory Interneurons in the Spinal Cord. *Neurotherapeutics, 17*(3), 874-885. https://doi.org/10.1007/s13311-020-00936-0

Iwagaki, N., Ganley, R. P., Dickie, A. C., Polgar, E., Hughes, D. I., Del Rio, P., Revina, Y., Watanabe, M., Todd, A. J., & Riddell, J. S. (2016, Mar). A combined electrophysiological and morphological study of neuropeptide Y-expressing inhibitory interneurons in the spinal dorsal horn of the mouse. *Pain, 157*(3), 598-612. https://doi.org/10.1097/j.pain.0000000000000407

Jann, M. W., Lam Yw Fau - Chang, W. H., & Chang, W. H. Rapid formation of clozapine in guinea-pigs and man following clozapine-N-oxide administration. (0003-9780 (Print)).

Jayaraj, N. D., Bhattacharyya, B. J., Belmadani, A. A., Ren, D., Rathwell, C. A., Hackelberg, S., Hopkins, B. E., Gupta, H. R., Miller, R. J., & Menichella, D. M. (2018, Jun 1). Reducing CXCR4-mediated nociceptor hyperexcitability reverses painful diabetic neuropathy. *J Clin Invest, 128*(6), 2205-2225. https://doi.org/10.1172/JCI92117

Jensen, E. (2014, Aug). Technical review: In situ hybridization. *Anat Rec (Hoboken), 297*(8), 1349-1353. https://doi.org/10.1002/ar.22944

Ju, G., Hokfelt, T., Brodin, E., Fahrenkrug, J., Fischer, J. A., Frey, P., Elde, R. P., & Brown, J. C. (1987, Feb). Primary sensory neurons of the rat showing calcitonin gene-related peptide immunoreactivity and their relation to substance P-, somatostatin-, galanin-, vasoactive intestinal polypeptide- and cholecystokinin-immunoreactive ganglion cells. *Cell Tissue Res, 247*(2), 417-431. https://doi.org/10.1007/BF00218323

Kardon, A. P., Polgar, E., Hachisuka, J., Snyder, L. M., Cameron, D., Savage, S., Cai, X., Karnup, S., Fan, C. R., Hemenway, G. M., Bernard, C. S., Schwartz, E. S., Nagase, H., Schwarzer, C., Watanabe, M., Furuta, T., Kaneko, T., Koerber, H. R., Todd, A. J., & Ross, S. E. (2014, May 7). Dynorphin acts as a neuromodulator to inhibit itch in the

dorsal horn of the spinal cord. *Neuron, 82*(3), 573-586. https://doi.org/10.1016/j.neuron.2014.02.046

Kelley, D. R., Snoek, J., & Rinn, J. L. (2016, Jul). Basset: learning the regulatory code of the accessible genome with deep convolutional neural networks. *Genome Res, 26*(7), 990-999. https://doi.org/10.1101/gr.200535.115

Knowlton, W. M., Palkar, R., Lippoldt, E. K., McCoy, D. D., Baluch, F., Chen, J., & McKemy, D. D. (2013, Feb 13). A sensory-labeled line for cold: TRPM8-expressing sensory neurons define the cellular basis for cold, cold pain, and cooling-mediated analgesia. *J Neurosci, 33*(7), 2837-2848. https://doi.org/10.1523/JNEUROSCI.1943-12.2013

Koch, S. C., Acton, D., & Goulding, M. (2018, Feb 10). Spinal Circuits for Touch, Pain, and Itch. *Annu Rev Physiol, 80*, 189-217. https://doi.org/10.1146/annurev-physiol-022516-034303

Kohro, Y., Matsuda, T., Yoshihara, K., Kohno, K., Koga, K., Katsuragi, R., Oka, T., Tashima, R., Muneta, S., Yamane, T., Okada, S., Momokino, K., Furusho, A., Hamase, K., Oti, T., Sakamoto, H., Hayashida, K., Kobayashi, R., Horii, T., Hatada, I., Tozaki-Saitoh, H., Mikoshiba, K., Taylor, V., Inoue, K., & Tsuda, M. (2020, Nov). Spinal astrocytes in superficial laminae gate brainstem descending control of mechanosensory hypersensitivity. *Nat Neurosci, 23*(11), 1376-1387. https://doi.org/10.1038/s41593-020-00713-4

Kohro, Y., Sakaguchi, E., Tashima, R., Tozaki-Saitoh, H., Okano, H., Inoue, K., & Tsuda, M. (2015, 2015/09/21). A new minimally-invasive method for microinjection into the mouse spinal dorsal horn. *Scientific Reports, 5*(1), 14306. https://doi.org/10.1038/srep14306

Kupari, J., Usoskin, D., Parisien, M., Lou, D., Hu, Y., Fatt, M., Lonnerberg, P., Spangberg, M., Eriksson, B., Barkas, N., Kharchenko, P. V., Lore, K., Khoury, S., Diatchenko, L., & Ernfors, P. (2021, Mar 8). Single cell transcriptomics of primate sensory neurons identifies cell types associated with chronic pain. *Nat Commun, 12*(1), 1510. https://doi.org/10.1038/s41467-021-21725-z

Kwon, S. (2013, Feb). Single-molecule fluorescence in situ hybridization: quantitative imaging of single RNA molecules. *BMB Rep, 46*(2), 65-72. https://doi.org/10.5483/bmbrep.2013.46.2.016

Lai, H. C., Seal, R. P., & Johnson, J. E. (2016, Oct 1). Making sense out of spinal cord somatosensory development. *Development, 143*(19), 3434-3448. https://doi.org/10.1242/dev.139592

Landt, S. G., Marinov, G. K., Kundaje, A., Kheradpour, P., Pauli, F., Batzoglou, S., Bernstein, B. E., Bickel, P., Brown, J. B., Cayting, P., Chen, Y., DeSalvo, G., Epstein, C., Fisher-Aylor, K. I., Euskirchen, G., Gerstein, M., Gertz, J., Hartemink, A. J., Hoffman, M. M., Iyer, V. R., Jung, Y. L., Karmakar, S., Kellis, M., Kharchenko, P. V., Li, Q., Liu, T., Liu, X. S., Ma, L., Milosavljevic, A., Myers, R. M., Park, P. J., Pazin, M. J., Perry, M. D., Raha, D., Reddy, T. E., Rozowsky, J., Shoresh, N., Sidow, A., Slattery, M., Stamatoyannopoulos, J. A., Tolstorukov, M. Y., White, K. P., Xi, S., Farnham, P. J.,

Lieb, J. D., Wold, B. J., & Snyder, M. (2012, Sep). ChIP-seq guidelines and practices of the ENCODE and modENCODE consortia. *Genome Res, 22*(9), 1813-1831. https://doi.org/10.1101/gr.136184.111

Langer-Safer, P. R., Levine, M., & Ward, D. C. (1982, Jul). Immunological method for mapping genes on Drosophila polytene chromosomes. *Proc Natl Acad Sci U S A, 79*(14), 4381-4385. https://doi.org/10.1073/pnas.79.14.4381

Latremoliere, A., & Woolf, C. J. (2009, Sep). Central sensitization: a generator of pain hypersensitivity by central neural plasticity. *J Pain, 10*(9), 895-926. https://doi.org/10.1016/j.jpain.2009.06.012

Lawler, A. J., Brown, A. R., Bouchard, R. S., Toong, N., Kim, Y., Velraj, N., Fox, G., Kleyman, M., Kang, B., Gittis, A. H., & Pfenning, A. R. (2020, Dec 9). Cell Type-Specific Oxidative Stress Genomic Signatures in the Globus Pallidus of Dopamine-Depleted Mice. *J Neurosci, 40*(50), 9772-9783. https://doi.org/10.1523/JNEUROSCI.1634-20.2020

Levsky, J. M., & Singer, R. H. (2003, Jul 15). Fluorescence in situ hybridization: past, present and future. *J Cell Sci, 116*(Pt 14), 2833-2838. https://doi.org/10.1242/jcs.00633

Li, C. L., Li, K. C., Wu, D., Chen, Y., Luo, H., Zhao, J. R., Wang, S. S., Sun, M. M., Lu, Y. J., Zhong, Y. Q., Hu, X. Y., Hou, R., Zhou, B. B., Bao, L., Xiao, H. S., & Zhang, X. (2016, Jan). Somatosensory neuron types identified by high-coverage single-cell RNA-sequencing and functional heterogeneity. *Cell Res, 26*(1), 83-102. https://doi.org/10.1038/cr.2015.149

Li, L., Rutlin, M., Abraira, V. E., Cassidy, C., Kus, L., Gong, S., Jankowski, M. P., Luo, W., Heintz, N., Koerber, H. R., Woodbury, C. J., & Ginty, D. D. (2011, Dec 23). The functional organization of cutaneous low-threshold mechanosensory neurons. *Cell, 147*(7), 1615-1627. https://doi.org/10.1016/j.cell.2011.11.027

Light, A. R. (1993, 1993). Peripheral sensory systems. *Periperal neuropathy*, 149-163. https://ci.nii.ac.jp/naid/10012308437/en/

Light, A. R., & Perl, E. R. (1979a, Jul 15). Reexamination of the dorsal root projection to the spinal dorsal horn including observations on the differential termination of coarse and fine fibers. *J Comp Neurol, 186*(2), 117-131. https://doi.org/10.1002/cne.901860202

Light, A. R., & Perl, E. R. (1979b, Jul 15). Spinal termination of functionally identified primary afferent neurons with slowly conducting myelinated fibers. *J Comp Neurol, 186*(2), 133-150. https://doi.org/10.1002/cne.901860203

Light, A. R., Trevino, D. L., & Perl, E. R. (1979, Jul 15). Morphological features of functionally defined neurons in the marginal zone and substantia gelatinosa of the spinal dorsal horn. *J Comp Neurol, 186*(2), 151-171. https://doi.org/10.1002/cne.901860204

Lima, D., Avelino, A., & Coimbra, A. (1993, Jan-Feb). Morphological characterization of marginal (lamina I) neurons immunoreactive for substance P, enkephalin, dynorphin

and gamma-aminobutyric acid in the rat spinal cord. *J Chem Neuroanat, 6*(1), 43-52. https://doi.org/10.1016/0891-0618(93)90006-p

Lima, D., & Coimbra, A. (1986, Feb 1). A Golgi study of the neuronal population of the marginal zone (lamina I) of the rat spinal cord. *J Comp Neurol, 244*(1), 53-71. https://doi.org/10.1002/cne.902440105

Littlewood, N. K., Todd, A. J., Spike, R. C., Watt, C., & Shehab, S. A. (1995, Jun). The types of neuron in spinal dorsal horn which possess neurokinin-1 receptors. *Neuroscience, 66*(3), 597-608. https://doi.org/10.1016/0306-4522(95)00039-l

Liu, C., Wang, M., Wei, X., Wu, L., Xu, J., Dai, X., Xia, J., Cheng, M., Yuan, Y., Zhang, P., Li, J., Feng, T., Chen, A., Zhang, W., Chen, F., Shang, Z., Zhang, X., Peters, B. A., & Liu, L. (2019, May 20). An ATAC-seq atlas of chromatin accessibility in mouse tissues. *Sci Data, 6*(1), 65. https://doi.org/10.1038/s41597-019-0071-0

Liu, Q., Tang, Z., Surdenikova, L., Kim, S., Patel, K. N., Kim, A., Ru, F., Guan, Y., Weng, H. J., Geng, Y., Undem, B. J., Kollarik, M., Chen, Z. F., Anderson, D. J., & Dong, X. (2009, Dec 24). Sensory neuron-specific GPCR Mrgprs are itch receptors mediating chloroquine-induced pruritus. *Cell, 139*(7), 1353-1365. https://doi.org/10.1016/j.cell.2009.11.034

Liu, T. T., Bannatyne, B. A., & Maxwell, D. J. (2010, Dec 1). Organization and neurochemical properties of intersegmental interneurons in the lumbar enlargement of the adult rat. *Neuroscience, 171*(2), 461-484. https://doi.org/10.1016/j.neuroscience.2010.09.012

Liu, Y., Latremoliere, A., Li, X., Zhang, Z., Chen, M., Wang, X., Fang, C., Zhu, J., Alexandre, C., Gao, Z., Chen, B., Ding, X., Zhou, J. Y., Zhang, Y., Chen, C., Wang, K. H., Woolf, C. J., & He, Z. (2018, Sep). Touch and tactile neuropathic pain sensitivity are set by corticospinal projections. *Nature, 561*(7724), 547-550. https://doi.org/10.1038/s41586-018-0515-2

Loken, L. S., Wessberg, J., Morrison, I., McGlone, F., & Olausson, H. (2009, May). Coding of pleasant touch by unmyelinated afferents in humans. *Nat Neurosci, 12*(5), 547-548. https://doi.org/10.1038/nn.2312

Long, H. K., Prescott, S. L., & Wysocka, J. (2016, Nov 17). Ever-Changing Landscapes: Transcriptional Enhancers in Development and Evolution. *Cell, 167*(5), 1170-1187. https://doi.org/10.1016/j.cell.2016.09.018

Lu, Y., Dong, H., Gao, Y., Gong, Y., Ren, Y., Gu, N., Zhou, S., Xia, N., Sun, Y. Y., Ji, R. R., & Xiong, L. (2013, Sep). A feed-forward spinal cord glycinergic neural circuit gates mechanical allodynia. *J Clin Invest, 123*(9), 4050-4062. https://doi.org/10.1172/JCI70026

Lu, Y., & Perl, E. R. (2005, Apr 13). Modular organization of excitatory circuits between neurons of the spinal superficial dorsal horn (laminae I and II). *J Neurosci, 25*(15), 3900-3907. https://doi.org/10.1523/JNEUROSCI.0102-05.2005

Lubeck, E., Coskun, A. F., Zhiyentayev, T., Ahmad, M., & Cai, L. (2014, Apr). Single-cell in situ RNA profiling by sequential hybridization. *Nat Methods, 11*(4), 360-361. https://doi.org/10.1038/nmeth.2892

Lun, A. T., Bach, K., & Marioni, J. C. (2016, Apr 27). Pooling across cells to normalize single-cell RNA sequencing data with many zero counts. *Genome Biol, 17*, 75. https://doi.org/10.1186/s13059-016-0947-7

Lun, A. T., McCarthy, D. J., & Marioni, J. C. (2016). A step-by-step workflow for low-level analysis of single-cell RNA-seq data with Bioconductor. *F1000Res, 5*, 2122. https://doi.org/10.12688/f1000research.9501.2

Lun, A. T. L., Riesenfeld, S., Andrews, T., Dao, T. P., Gomes, T., participants in the 1st Human Cell Atlas, J., & Marioni, J. C. (2019, Mar 22). EmptyDrops: distinguishing cells from empty droplets in droplet-based single-cell RNA sequencing data. *Genome Biol, 20*(1), 63. https://doi.org/10.1186/s13059-019-1662-y

Ma, Q. (2010, Nov). Labeled lines meet and talk: population coding of somatic sensations. *J Clin Invest, 120*(11), 3773-3778. https://doi.org/10.1172/JCI43426

Ma, W., & Ribeiro-da-Silva, A. (1995, Sep 18). Substance P- and GABA-like immunoreactivities are co-localized in axonal varicosities in the superficial laminae of cat but not rat spinal cord. *Brain Res, 692*(1-2), 99-110. https://doi.org/10.1016/0006-8993(95)00666-e

Mackenzie, R. A., Burke, D., Skuse, N. F., & Lethlean, A. K. (1975). Fibre function and perception during cutaneous nerve block. *Proc Aust Assoc Neurol, 12*, 65-73. https://www.ncbi.nlm.nih.gov/pubmed/1215398

Magnus, C. J., Lee, P. H., Atasoy, D., Su, H. H., Looger, L. L., & Sternson, S. M. (2011, Sep 2). Chemical and genetic engineering of selective ion channel-ligand interactions. *Science, 333*(6047), 1292-1296. https://doi.org/10.1126/science.1206606

Magnus, C. J., Lee, P. H., Bonaventura, J., Zemla, R., Gomez, J. L., Ramirez, M. H., Hu, X., Galvan, A., Basu, J., Michaelides, M., & Sternson, S. M. (2019). Ultrapotent chemogenetics for research and potential clinical applications. *Science (New York, N.Y.), 364*(6436), eaav5282. https://doi.org/10.1126/science.aav5282

Malmberg, A. B., Chen, C., Tonegawa, S., & Basbaum, A. I. (1997, Oct 10). Preserved acute pain and reduced neuropathic pain in mice lacking PKCgamma. *Science, 278*(5336), 279-283. https://doi.org/10.1126/science.278.5336.279

Manning, J. E., Hershey, N. D., Broker, T. R., Pellegrini, M., Mitchell, H. K., & Davidson, N. (1975, Nov 24). A new method of in situ hybridization. *Chromosoma, 53*(2), 107-117. https://doi.org/10.1007/bf00333039

Mantyh, P. W., DeMaster, E., Malhotra, A., Ghilardi, J. R., Rogers, S. D., Mantyh, C. R., Liu, H., Basbaum, A. I., Vigna, S. R., Maggio, J. E., & et al. (1995, Jun 16). Receptor endocytosis and dendrite reshaping in spinal neurons after somatosensory stimulation. *Science, 268*(5217), 1629-1632. https://doi.org/10.1126/science.7539937

Manvich, D. F., Webster, K. A., Foster, S. L., Farrell, M. S., Ritchie, J. C., Porter, J. H., & Weinshenker, D. (2018, 2018/03/01). The DREADD agonist clozapine N-oxide (CNO) is reverse-metabolized to clozapine and produces clozapine-like interoceptive stimulus effects in rats and mice. *Scientific Reports, 8*(1), 3840. https://doi.org/10.1038/s41598-018-22116-z

Martelotto, L. G. (2020). *'Frankenstein' protocol for nuclei isolation from fresh and frozen tissue for snRNAseq.*

.

Maxwell, D. J., & Bannatyne, B. A. (1983, Dec 12). Ultrastructure of muscle spindle afferent terminations in lamina VI of the cat spinal cord. *Brain Res, 288*(1-2), 297-301. https://doi.org/10.1016/0006-8993(83)90106-3

Maxwell, D. J., Bannatyne, B. A., Fyffe, R. E., & Brown, A. G. (1984, Apr). Fine structure of primary afferent axon terminals projecting from rapidly adapting mechanoreceptors of the toe and foot pads of the cat. *Q J Exp Physiol, 69*(2), 381-392. https://doi.org/10.1113/expphysiol.1984.sp002813

Maxwell, D. J., Belle, M. D., Cheunsuang, O., Stewart, A., & Morris, R. (2007, Oct 15). Morphology of inhibitory and excitatory interneurons in superficial laminae of the rat dorsal horn. *J Physiol, 584*(Pt 2), 521-533. https://doi.org/10.1113/jphysiol.2007.140996

Maxwell, D. J., & Riddell, J. S. (1999, Jun). Axoaxonic synapses on terminals of group II muscle spindle afferent axons in the spinal cord of the cat. *Eur J Neurosci, 11*(6), 2151-2159. https://doi.org/10.1046/j.1460-9568.1999.00632.x

Maynard, K. R., Tippani, M., Takahashi, Y., Phan, B. N., Hyde, T. M., Jaffe, A. E., & Martinowich, K. (2020, Jun 19). dotdotdot: an automated approach to quantify multiplex single molecule fluorescent in situ hybridization (smFISH) images in complex tissues. *Nucleic Acids Res, 48*(11), e66. https://doi.org/10.1093/nar/gkaa312

McCarthy, D. J., Campbell, K. R., Lun, A. T., & Wills, Q. F. (2017, Apr 15). Scater: pre-processing, quality control, normalization and visualization of single-cell RNA-seq data in R. *Bioinformatics, 33*(8), 1179-1186. https://doi.org/10.1093/bioinformatics/btw777

McMahon, S. B., & Wall, P. D. (1983, Feb 20). A system of rat spinal cord lamina 1 cells projecting through the contralateral dorsolateral funiculus. *J Comp Neurol, 214*(2), 217-223. https://doi.org/10.1002/cne.902140209

Mears, S. C., & Frank, E. (1997, May 1). Formation of specific monosynaptic connections between muscle spindle afferents and motoneurons in the mouse. *J Neurosci, 17*(9), 3128-3135. https://www.ncbi.nlm.nih.gov/pubmed/9096147

Mich, J. K., Graybuck, L. T., Hess, E. E., Mahoney, J. T., Kojima, Y., Ding, Y., Somasundaram, S., Miller, J. A., Kalmbach, B. E., Radaelli, C., Gore, B. B., Weed, N., Omstead, V., Bishaw, Y., Shapovalova, N. V., Martinez, R. A., Fong, O., Yao, S.,

Mortrud, M., Chong, P., Loftus, L., Bertagnolli, D., Goldy, J., Casper, T., Dee, N., Opitz-Araya, X., Cetin, A., Smith, K. A., Gwinn, R. P., Cobbs, C., Ko, A. L., Ojemann, J. G., Keene, C. D., Silbergeld, D. L., Sunkin, S. M., Gradinaru, V., Horwitz, G. D., Zeng, H., Tasic, B., Lein, E. S., Ting, J. T., & Levi, B. P. (2021, Mar 30). Functional enhancer elements drive subclass-selective expression from mouse to primate neocortex. *Cell Rep, 34*(13), 108754. https://doi.org/10.1016/j.celrep.2021.108754

Middleton, S. J., Barry, A. M., Comini, M., Li, Y., Ray, P. R., Shiers, S., Themistocleous, A. C., Uhelski, M. L., Yang, X., Dougherty, P. M., Price, T. J., & Bennett, D. L. (2021, Jun 22). Studying human nociceptors: from fundamentals to clinic. *Brain, 144*(5), 1312-1335. https://doi.org/10.1093/brain/awab048

Miraucourt, L. S., Dallel, R., & Voisin, D. L. (2007, Nov 7). Glycine inhibitory dysfunction turns touch into pain through PKCgamma interneurons. *PLoS One, 2*(11), e1116. https://doi.org/10.1371/journal.pone.0001116

Molander, C., Xu, Q., & Grant, G. (1984, Nov 20). The cytoarchitectonic organization of the spinal cord in the rat. I. The lower thoracic and lumbosacral cord. *J Comp Neurol, 230*(1), 133-141. https://doi.org/10.1002/cne.902300112

Molander, C., Xu, Q., Rivero-Melian, C., & Grant, G. (1989, Nov 15). Cytoarchitectonic organization of the spinal cord in the rat: II. The cervical and upper thoracic cord. *J Comp Neurol, 289*(3), 375-385. https://doi.org/10.1002/cne.902890303

Mori, M., Kose, A., Tsujino, T., & Tanaka, C. (1990, Sep 8). Immunocytochemical localization of protein kinase C subspecies in the rat spinal cord: light and electron microscopic study. *J Comp Neurol, 299*(2), 167-177. https://doi.org/10.1002/cne.902990204

Muller, T., Brohmann, H., Pierani, A., Heppenstall, P. A., Lewin, G. R., Jessell, T. M., & Birchmeier, C. (2002, May 16). The homeodomain factor lbx1 distinguishes two major programs of neuronal differentiation in the dorsal spinal cord. *Neuron, 34*(4), 551-562. https://doi.org/10.1016/s0896-6273(02)00689-x

Nagai, Y., Miyakawa, N., Takuwa, H., Hori, Y., Oyama, K., Ji, B., Takahashi, M., Huang, X. P., Slocum, S. T., DiBerto, J. F., Xiong, Y., Urushihata, T., Hirabayashi, T., Fujimoto, A., Mimura, K., English, J. G., Liu, J., Inoue, K. I., Kumata, K., Seki, C., Ono, M., Shimojo, M., Zhang, M. R., Tomita, Y., Nakahara, J., Suhara, T., Takada, M., Higuchi, M., Jin, J., Roth, B. L., & Minamimoto, T. (2020, Sep). Deschloroclozapine, a potent and selective chemogenetic actuator enables rapid neuronal and behavioral modulations in mice and monkeys. *Nat Neurosci, 23*(9), 1157-1167. https://doi.org/10.1038/s41593-020-0661-3

Nagi, S. S., Marshall, A. G., Makdani, A., Jarocka, E., Liljencrantz, J., Ridderstrom, M., Shaikh, S., O'Neill, F., Saade, D., Donkervoort, S., Foley, A. R., Minde, J., Trulsson, M., Cole, J., Bonnemann, C. G., Chesler, A. T., Bushnell, M. C., McGlone, F., & Olausson, H. (2019, Jul). An ultrafast system for signaling mechanical pain in human skin. *Sci Adv, 5*(7), eaaw1297. https://doi.org/10.1126/sciadv.aaw1297

Nagy, I., & Rang, H. (1999). Noxious heat activates all capsaicin-sensitive and also a sub-population of capsaicin-insensitive dorsal root ganglion neurons. *Neuroscience, 88*(4), 995-997. https://doi.org/10.1016/s0306-4522(98)00535-1

Naim, M., Spike, R. C., Watt, C., Shehab, S. A., & Todd, A. J. (1997, Jul 15). Cells in laminae III and IV of the rat spinal cord that possess the neurokinin-1 receptor and have dorsally directed dendrites receive a major synaptic input from tachykinin-containing primary afferents. *J Neurosci, 17*(14), 5536-5548. https://www.ncbi.nlm.nih.gov/pubmed/9204935

Nakagawa, T., Yasaka, T., Nakashima, N., Takeya, M., Oshita, K., Tsuda, M., Yamaura, K., & Takano, M. (2020, Sep 18). Expression of the pacemaker channel HCN4 in excitatory interneurons in the dorsal horn of the murine spinal cord. *Mol Brain, 13*(1), 127. https://doi.org/10.1186/s13041-020-00666-6

Nguyen, E., Lim, G., Ding, H., Hachisuka, J., Ko, M. C., & Ross, S. E. (2021, Feb 3). Morphine acts on spinal dynorphin neurons to cause itch through disinhibition. *Sci Transl Med, 13*(579). https://doi.org/10.1126/scitranslmed.abc3774

Nicholl, B. I., Holliday, K. L., Macfarlane, G. J., Thomson, W., Davies, K. A., O'Neill, T. W., Bartfai, G., Boonen, S., Casanueva, F. F., Finn, J. D., Forti, G., Giwercman, A., Huhtaniemi, I. T., Kula, K., Punab, M., Silman, A. J., Vanderschueren, D., Wu, F. C., McBeth, J., & European Male Ageing Study, G. (2011, Mar). Association of HTR2A polymorphisms with chronic widespread pain and the extent of musculoskeletal pain: results from two population-based cohorts. *Arthritis Rheum, 63*(3), 810-818. https://doi.org/10.1002/art.30185

Nichols, M. L., Allen, B. J., Rogers, S. D., Ghilardi, J. R., Honore, P., Luger, N. M., Finke, M. P., Li, J., Lappi, D. A., Simone, D. A., & Mantyh, P. W. (1999, Nov 19). Transmission of chronic nociception by spinal neurons expressing the substance P receptor. *Science, 286*(5444), 1558-1561. https://doi.org/10.1126/science.286.5444.1558

Olausson, H., Lamarre, Y., Backlund, H., Morin, C., Wallin, B. G., Starck, G., Ekholm, S., Strigo, I., Worsley, K., Vallbo, A. B., & Bushnell, M. C. (2002, Sep). Unmyelinated tactile afferents signal touch and project to insular cortex. *Nat Neurosci, 5*(9), 900-904. https://doi.org/10.1038/nn896

Oliveira, A. L., Hydling, F., Olsson, E., Shi, T., Edwards, R. H., Fujiyama, F., Kaneko, T., Hokfelt, T., Cullheim, S., & Meister, B. (2003, Nov). Cellular localization of three vesicular glutamate transporter mRNAs and proteins in rat spinal cord and dorsal root ganglia. *Synapse, 50*(2), 117-129. https://doi.org/10.1002/syn.10249

Osseward, P. J., 2nd, Amin, N. D., Moore, J. D., Temple, B. A., Barriga, B. K., Bachmann, L. C., Beltran, F., Jr., Gullo, M., Clark, R. C., Driscoll, S. P., Pfaff, S. L., & Hayashi, M. (2021, Apr 23). Conserved genetic signatures parcellate cardinal spinal neuron classes into local and projection subsets. *Science, 372*(6540), 385-393. https://doi.org/10.1126/science.abe0690

Ouyang, J. F., Kamaraj, U. S., Cao, E. Y., & Rackham, O. J. L. (2021, Mar 28). ShinyCell: Simple and sharable visualisation of single-cell gene expression data. *Bioinformatics*. https://doi.org/10.1093/bioinformatics/btab209

Pagani, M., Albisetti, G. W., Sivakumar, N., Wildner, H., Santello, M., Johannssen, H. C., & Zeilhofer, H. U. (2019, Jul 3). How Gastrin-Releasing Peptide Opens the Spinal Gate for Itch. *Neuron, 103*(1), 102-117 e105. https://doi.org/10.1016/j.neuron.2019.04.022

Paixao, S., Loschek, L., Gaitanos, L., Alcala Morales, P., Goulding, M., & Klein, R. (2019, Nov 20). Identification of Spinal Neurons Contributing to the Dorsal Column Projection Mediating Fine Touch and Corrective Motor Movements. *Neuron, 104*(4), 749-764 e746. https://doi.org/10.1016/j.neuron.2019.08.029

Pan, H., Fatima, M., Li, A., Lee, H., Cai, W., Horwitz, L., Hor, C. C., Zaher, N., Cin, M., Slade, H., Huang, T., Xu, X. Z. S., & Duan, B. (2019, Sep 25). Identification of a Spinal Circuit for Mechanical and Persistent Spontaneous Itch. *Neuron, 103*(6), 1135-1149 e1136. https://doi.org/10.1016/j.neuron.2019.06.016

Pardue, M. L., & Gall, J. G. (1969, Oct). Molecular hybridization of radioactive DNA to the DNA of cytological preparations. *Proc Natl Acad Sci U S A, 64*(2), 600-604. https://doi.org/10.1073/pnas.64.2.600

Pei, Y., Dong, S., & Roth, B. L. (2010, Jan). Generation of designer receptors exclusively activated by designer drugs (DREADDs) using directed molecular evolution. *Curr Protoc Neurosci, Chapter 4*, Unit 4 33. https://doi.org/10.1002/0471142301.ns0433s50

Peier, A. M., Moqrich, A., Hergarden, A. C., Reeve, A. J., Andersson, D. A., Story, G. M., Earley, T. J., Dragoni, I., McIntyre, P., Bevan, S., & Patapoutian, A. (2002, Mar 8). A TRP channel that senses cold stimuli and menthol. *Cell, 108*(5), 705-715. https://doi.org/10.1016/s0092-8674(02)00652-9

Peirs, C., Dallel, R., & Todd, A. J. (2020, Apr). Recent advances in our understanding of the organization of dorsal horn neuron populations and their contribution to cutaneous mechanical allodynia. *J Neural Transm (Vienna), 127*(4), 505-525. https://doi.org/10.1007/s00702-020-02159-1

Peirs, C., & Seal, R. P. (2016, Nov 4). Neural circuits for pain: Recent advances and current views. *Science, 354*(6312), 578-584. https://doi.org/10.1126/science.aaf8933

Peirs, C., Williams, S. G., Zhao, X., Arokiaraj, C. M., Ferreira, D. W., Noh, M. C., Smith, K. M., Halder, P., Corrigan, K. A., Gedeon, J. Y., Lee, S. J., Gatto, G., Chi, D., Ross, S. E., Goulding, M., & Seal, R. P. (2021, Jan 6). Mechanical Allodynia Circuitry in the Dorsal Horn Is Defined by the Nature of the Injury. *Neuron, 109*(1), 73-90 e77. https://doi.org/10.1016/j.neuron.2020.10.027

Peirs, C., Williams, S. P., Zhao, X., Walsh, C. E., Gedeon, J. Y., Cagle, N. E., Goldring, A. C., Hioki, H., Liu, Z., Marell, P. S., & Seal, R. P. (2015, Aug 19). Dorsal Horn Circuits for Persistent Mechanical Pain. *Neuron, 87*(4), 797-812. https://doi.org/10.1016/j.neuron.2015.07.029

Perl, E. R. (1992). Function of dorsal root ganglion neurons: an overview. *Sensory neurons: diversity, development, and plasticity*, 3-23.

Perry, M. J., & Lawson, S. N. (1998, Jul). Differences in expression of oligosaccharides, neuropeptides, carbonic anhydrase and neurofilament in rat primary afferent neurons retrogradely labelled via skin, muscle or visceral nerves. *Neuroscience, 85*(1), 293-310. https://doi.org/10.1016/s0306-4522(97)00629-5

Petitjean, H., Pawlowski, S. A., Fraine, S. L., Sharif, B., Hamad, D., Fatima, T., Berg, J., Brown, C. M., Jan, L. Y., Ribeiro-da-Silva, A., Braz, J. M., Basbaum, A. I., & Sharif-Naeini, R. (2015, Nov 10). Dorsal Horn Parvalbumin Neurons Are Gate-Keepers of Touch-Evoked Pain after Nerve Injury. *Cell Rep, 13*(6), 1246-1257. https://doi.org/10.1016/j.celrep.2015.09.080

Polgar, E., Bell, A. M., Gutierrez-Mecinas, M., Dickie, A. C., Akar, O., Costreie, M., Watanabe, M., & Todd, A. J. (2020, Dec 1). Substance P-expressing Neurons in the Superficial Dorsal Horn of the Mouse Spinal Cord: Insights into Their Functions and their Roles in Synaptic Circuits. *Neuroscience, 450*, 113-125. https://doi.org/10.1016/j.neuroscience.2020.06.038

Polgar, E., Durrieux, C., Hughes, D. I., & Todd, A. J. (2013). A quantitative study of inhibitory interneurons in laminae I-III of the mouse spinal dorsal horn. *PLoS One, 8*(10), e78309. https://doi.org/10.1371/journal.pone.0078309

Polgar, E., Fowler, J. H., McGill, M. M., & Todd, A. J. (1999, Jun 26). The types of neuron which contain protein kinase C gamma in rat spinal cord. *Brain Res, 833*(1), 71-80. https://doi.org/10.1016/s0006-8993(99)01500-0

Porreca, F., Ossipov, M. H., & Gebhart, G. F. (2002, Jun). Chronic pain and medullary descending facilitation. *Trends Neurosci, 25*(6), 319-325. https://doi.org/10.1016/s0166-2236(02)02157-4

Powell, J. J., & Todd, A. J. (1992, Jan 8). Light and electron microscope study of GABA-immunoreactive neurones in lamina III of rat spinal cord. *J Comp Neurol, 315*(2), 125-136. https://doi.org/10.1002/cne.903150202

Prasoon, P., Kumar, R., Gautam, M., Sebastian, E. K., Reeta, K. H., & Ray, S. B. (2015, Feb). Role of somatostatin and somatostatin receptor type 2 in postincisional nociception in rats. *Neuropeptides, 49*, 47-54. https://doi.org/10.1016/j.npep.2014.12.002

Prescott, S. A., & De Koninck, Y. (2002, Mar 15). Four cell types with distinctive membrane properties and morphologies in lamina I of the spinal dorsal horn of the adult rat. *J Physiol, 539*(Pt 3), 817-836. https://doi.org/10.1113/jphysiol.2001.013437

Price, D. D., Hayashi, H., Dubner, R., & Ruda, M. A. (1979, Nov). Functional relationships between neurons of marginal and substantia gelatinosa layers of primate dorsal horn. *J Neurophysiol, 42*(6), 1590-1608. https://doi.org/10.1152/jn.1979.42.6.1590

Raj, A., van den Bogaard, P., Rifkin, S. A., van Oudenaarden, A., & Tyagi, S. (2008, Oct). Imaging individual mRNA molecules using multiple singly labeled probes. *Nat Methods, 5*(10), 877-879. https://doi.org/10.1038/nmeth.1253

Rajasethupathy, P., Ferenczi, E., & Deisseroth, K. (2016, Apr 21). Targeting Neural Circuits. *Cell, 165*(3), 524-534. https://doi.org/10.1016/j.cell.2016.03.047

Ranade, S. S., Woo, S. H., Dubin, A. E., Moshourab, R. A., Wetzel, C., Petrus, M., Mathur, J., Begay, V., Coste, B., Mainquist, J., Wilson, A. J., Francisco, A. G., Reddy, K., Qiu, Z., Wood, J. N., Lewin, G. R., & Patapoutian, A. (2014, Dec 4). Piezo2 is the major transducer of mechanical forces for touch sensation in mice. *Nature, 516*(7529), 121-125. https://doi.org/10.1038/nature13980

Ray, P., Torck, A., Quigley, L., Wangzhou, A., Neiman, M., Rao, C., Lam, T., Kim, J. Y., Kim, T. H., Zhang, M. Q., Dussor, G., & Price, T. J. (2018, Jul). Comparative transcriptome profiling of the human and mouse dorsal root ganglia: an RNA-seq-based resource for pain and sensory neuroscience research. *Pain, 159*(7), 1325-1345. https://doi.org/10.1097/j.pain.0000000000001217

Rexed, B. (1952, Jun). The cytoarchitectonic organization of the spinal cord in the cat. *J Comp Neurol, 96*(3), 414-495. https://doi.org/10.1002/cne.900960303

Rexed, B. (1954, Apr). A cytoarchitectonic atlas of the spinal cord in the cat. *J Comp Neurol, 100*(2), 297-379. https://doi.org/10.1002/cne.901000205

Reynolds, D. V. (1969, Apr 25). Surgery in the rat during electrical analgesia induced by focal brain stimulation. *Science, 164*(3878), 444-445. https://doi.org/10.1126/science.164.3878.444

Ribeiro-da-Silva, A. (1995, Jul). Ultrastructural features of the colocalization of calcitonin gene related peptide with substance P or somatostatin in the dorsal horn of the spinal cord. *Can J Physiol Pharmacol, 73*(7), 940-944. https://doi.org/10.1139/y95-130

Roome, R. B., Bourojeni, F. B., Mona, B., Rastegar-Pouyani, S., Blain, R., Dumouchel, A., Salesse, C., Thompson, W. S., Brookbank, M., Gitton, Y., Tessarollo, L., Goulding, M., Johnson, J. E., Kmita, M., Chedotal, A., & Kania, A. (2020, Nov 24). Phox2a Defines a Developmental Origin of the Anterolateral System in Mice and Humans. *Cell Rep, 33*(8), 108425. https://doi.org/10.1016/j.celrep.2020.108425

Rosenberg, A. B., Roco, C. M., Muscat, R. A., Kuchina, A., Sample, P., Yao, Z., Graybuck, L. T., Peeler, D. J., Mukherjee, S., Chen, W., Pun, S. H., Sellers, D. L., Tasic, B., & Seelig, G. (2018, Apr 13). Single-cell profiling of the developing mouse brain and spinal cord with split-pool barcoding. *Science, 360*(6385), 176-182. https://doi.org/10.1126/science.aam8999

Ross, S. E., Mardinly, A. R., McCord, A. E., Zurawski, J., Cohen, S., Jung, C., Hu, L., Mok, S. I., Shah, A., Savner, E. M., Tolias, C., Corfas, R., Chen, S., Inquimbert, P., Xu, Y., McInnes, R. R., Rice, F. L., Corfas, G., Ma, Q., Woolf, C. J., & Greenberg, M. E. (2010, Mar 25). Loss of inhibitory interneurons in the dorsal spinal cord and elevated itch in

Bhlhb5 mutant mice. *Neuron, 65*(6), 886-898. https://doi.org/10.1016/j.neuron.2010.02.025

Rudkin, G. T., & Stollar, B. D. (1977, Feb 3). High resolution detection of DNA-RNA hybrids in situ by indirect immunofluorescence. *Nature, 265*(5593), 472-473. https://doi.org/10.1038/265472a0

Rusin, K. I., Ryu, P. D., & Randic, M. (1992, Jul). Modulation of excitatory amino acid responses in rat dorsal horn neurons by tachykinins. *J Neurophysiol, 68*(1), 265-286. https://doi.org/10.1152/jn.1992.68.1.265

Russ, D. E., Cross, R. B. P., Li, L., Koch, S. C., Matson, K. J. E., Yadav, A., Alkaslasi, M. R., Lee, D. I., Le Pichon, C. E., Menon, V., & Levine, A. J. (2021, 2021/09/29). A harmonized atlas of mouse spinal cord cell types and their spatial organization. *Nature Communications, 12*(1), 5722. https://doi.org/10.1038/s41467-021-25125-1

Rustioni, A., & Kaufman, A. B. (1977, Jan 18). Identification of cells or origin of non-primary afferents to the dorsal column nuclei of the cat. *Exp Brain Res, 27*(1), 1-14. https://doi.org/10.1007/BF00234821

Rutlin, M., Ho, C. Y., Abraira, V. E., Cassidy, C., Bai, L., Woodbury, C. J., & Ginty, D. D. (2014, Dec 18). The cellular and molecular basis of direction selectivity of Adelta-LTMRs. *Cell, 159*(7), 1640-1651. https://doi.org/10.1016/j.cell.2014.11.038

Saloman, J. L., Scheff, N. N., Snyder, L. M., Ross, S. E., Davis, B. M., & Gold, M. S. (2016, Oct 19). Gi-DREADD Expression in Peripheral Nerves Produces Ligand-Dependent Analgesia, as well as Ligand-Independent Functional Changes in Sensory Neurons. *J Neurosci, 36*(42), 10769-10781. https://doi.org/10.1523/JNEUROSCI.3480-15.2016

Sapio, M. R., Kim, J. J., Loydpierson, A. J., Maric, D., Goto, T., Vazquez, F. A., Dougherty, M. K., Narasimhan, R., Muhly, W. T., Iadarola, M. J., & Mannes, A. J. (2021, Apr 20). The Persistent Pain Transcriptome: Identification of Cells and Molecules Activated by Hyperalgesia. *J Pain*. https://doi.org/10.1016/j.jpain.2021.03.155

Sardella, T. C., Polgar, E., Garzillo, F., Furuta, T., Kaneko, T., Watanabe, M., & Todd, A. J. (2011, Sep 29). Dynorphin is expressed primarily by GABAergic neurons that contain galanin in the rat dorsal horn. *Mol Pain, 7*, 76. https://doi.org/10.1186/1744-8069-7-76

Sathyamurthy, A., Johnson, K. R., Matson, K. J. E., Dobrott, C. I., Li, L., Ryba, A. R., Bergman, T. B., Kelly, M. C., Kelley, M. W., & Levine, A. J. (2018, Feb 20). Massively Parallel Single Nucleus Transcriptional Profiling Defines Spinal Cord Neurons and Their Activity during Behavior. *Cell Rep, 22*(8), 2216-2225. https://doi.org/10.1016/j.celrep.2018.02.003

Schneider, S. P., & Perl, E. R. (1988, Jun). Comparison of primary afferent and glutamate excitation of neurons in the mammalian spinal dorsal horn. *J Neurosci, 8*(6), 2062-2073. https://www.ncbi.nlm.nih.gov/pubmed/2898513

Schneider, V. A., Graves-Lindsay, T., Howe, K., Bouk, N., Chen, H. C., Kitts, P. A., Murphy, T. D., Pruitt, K. D., Thibaud-Nissen, F., Albracht, D., Fulton, R. S., Kremitzki, M.,

Magrini, V., Markovic, C., McGrath, S., Steinberg, K. M., Auger, K., Chow, W., Collins, J., Harden, G., Hubbard, T., Pelan, S., Simpson, J. T., Threadgold, G., Torrance, J., Wood, J. M., Clarke, L., Koren, S., Boitano, M., Peluso, P., Li, H., Chin, C. S., Phillippy, A. M., Durbin, R., Wilson, R. K., Flicek, P., Eichler, E. E., & Church, D. M. (2017, May). Evaluation of GRCh38 and de novo haploid genome assemblies demonstrates the enduring quality of the reference assembly. *Genome Res, 27*(5), 849-864. https://doi.org/10.1101/gr.213611.116

Schoenen, J. (1982). The dendritic organization of the human spinal cord: the dorsal horn. *Neuroscience, 7*(9), 2057-2087. https://doi.org/10.1016/0306-4522(82)90120-8

Schoenen, J., & Faul, R. L. M. (1990). *Cytoarchitectural, dendroarchitectural and myeloarchitectural organization* (G. Paxinos, Ed.). Academic Press Inc.

Schoenen, J., & Faul, R. L. M. (2004). *Spinal Cord: Cyto- and Chemoarchitecture* (G. Paxinos & J. K. Mai, Eds. Second ed.). Elsevier Academic Press.

Seal, R. P., Wang, X., Guan, Y., Raja, S. N., Woodbury, C. J., Basbaum, A. I., & Edwards, R. H. (2009, Dec 3). Injury-induced mechanical hypersensitivity requires C-low threshold mechanoreceptors. *Nature, 462*(7273), 651-655. https://doi.org/10.1038/nature08505

Sengul, G., Puchalski, R. B., & Watson, C. (2012, May). Cytoarchitecture of the spinal cord of the postnatal (P4) mouse. *Anat Rec (Hoboken), 295*(5), 837-845. https://doi.org/10.1002/ar.22450

Serafin, E. K., Paranjpe, A., Brewer, C. L., & Baccei, M. L. (2021, Jan). Single-nucleus characterization of adult mouse spinal dynorphin-lineage cells and identification of persistent transcriptional effects of neonatal hindpaw incision. *Pain, 162*(1), 203-218. https://doi.org/10.1097/j.pain.0000000000002007

Sharif, B., Ase, A. R., Ribeiro-da-Silva, A., & Seguela, P. (2020, Jun 17). Differential Coding of Itch and Pain by a Subpopulation of Primary Afferent Neurons. *Neuron, 106*(6), 940-951 e944. https://doi.org/10.1016/j.neuron.2020.03.021

Shields, S. D., Eckert, W. A., 3rd, & Basbaum, A. I. (2003, Oct). Spared nerve injury model of neuropathic pain in the mouse: a behavioral and anatomic analysis. *J Pain, 4*(8), 465-470. https://doi.org/10.1067/s1526-5900(03)00781-8

Shiers, S., Klein, R. M., & Price, T. J. (2020, Oct). Quantitative differences in neuronal subpopulations between mouse and human dorsal root ganglia demonstrated with RNAscope in situ hybridization. *Pain, 161*(10), 2410-2424. https://doi.org/10.1097/j.pain.0000000000001973

Shiers, S. I., Sankaranarayanan, I., Jeevakumar, V., Cervantes, A., Reese, J. C., & Price, T. J. (2021, Jul 1). Convergence of peptidergic and non-peptidergic protein markers in the human dorsal root ganglion and spinal dorsal horn. *J Comp Neurol, 529*(10), 2771-2788. https://doi.org/10.1002/cne.25122

Shirley, J. W., Ty, S., Takebayashi, S., Liu, X., & Gilbert, D. M. (2011, Apr 1). FISH Finder: a high-throughput tool for analyzing FISH images. *Bioinformatics, 27*(7), 933-938. https://doi.org/10.1093/bioinformatics/btr053

Shumate, A., & Salzberg, S. L. (2020, Dec 15). Liftoff: accurate mapping of gene annotations. *Bioinformatics*. https://doi.org/10.1093/bioinformatics/btaa1016

Sidman, R., Angevine, J. B., & Pierce, E. T. (1971). *Atlas of the Mouse Brain and Spinal Cord*. Harvard University Press.

Silverman, J. D., & Kruger, L. (1990, Oct). Selective neuronal glycoconjugate expression in sensory and autonomic ganglia: relation of lectin reactivity to peptide and enzyme markers. *J Neurocytol, 19*(5), 789-801. https://doi.org/10.1007/BF01188046

Sivilotti, L., & Woolf, C. J. (1994, Jul). The contribution of GABAA and glycine receptors to central sensitization: disinhibition and touch-evoked allodynia in the spinal cord. *J Neurophysiol, 72*(1), 169-179. https://doi.org/10.1152/jn.1994.72.1.169

Smith, K. M., Boyle, K. A., Madden, J. F., Dickinson, S. A., Jobling, P., Callister, R. J., Hughes, D. I., & Graham, B. A. (2015, Oct 1). Functional heterogeneity of calretinin-expressing neurons in the mouse superficial dorsal horn: implications for spinal pain processing. *J Physiol, 593*(19), 4319-4339. https://doi.org/10.1113/JP270855

Smith, K. M., Boyle, K. A., Mustapa, M., Jobling, P., Callister, R. J., Hughes, D. I., & Graham, B. A. (2016, Jun 21). Distinct forms of synaptic inhibition and neuromodulation regulate calretinin-positive neuron excitability in the spinal cord dorsal horn. *Neuroscience, 326*, 10-21. https://doi.org/10.1016/j.neuroscience.2016.03.058

Smith, K. M., Browne, T. J., Davis, O. C., Coyle, A., Boyle, K. A., Watanabe, M., Dickinson, S. A., Iredale, J. A., Gradwell, M. A., Jobling, P., Callister, R. J., Dayas, C. V., Hughes, D. I., & Graham, B. A. (2019, Nov 12). Calretinin positive neurons form an excitatory amplifier network in the spinal cord dorsal horn. *Elife, 8*. https://doi.org/10.7554/eLife.49190

Song, L., & Crawford, G. E. (2010, Feb). DNase-seq: a high-resolution technique for mapping active gene regulatory elements across the genome from mammalian cells. *Cold Spring Harb Protoc, 2010*(2), pdb prot5384. https://doi.org/10.1101/pdb.prot5384

Spike, R. C., Puskar, Z., Andrew, D., & Todd, A. J. (2003, Nov). A quantitative and morphological study of projection neurons in lamina I of the rat lumbar spinal cord. *Eur J Neurosci, 18*(9), 2433-2448. https://doi.org/10.1046/j.1460-9568.2003.02981.x

Srinivasan, C., Phan, B. N., Lawler, A. J., Ramamurthy, E., Kleyman, M., Brown, A. R., Kaplow, I. M., Wirthlin, M. E., & Pfenning, A. R. (2021, Aug 30). Addiction-associated genetic variants implicate brain cell type- and region-specific cis-regulatory elements in addiction neurobiology. *J Neurosci*. https://doi.org/10.1523/JNEUROSCI.2534-20.2021

Sternson, S. M., & Roth, B. L. (2014). Chemogenetic tools to interrogate brain functions. *Annu Rev Neurosci, 37*, 387-407. https://doi.org/10.1146/annurev-neuro-071013-014048

Sun, S., Xu, Q., Guo, C., Guan, Y., Liu, Q., & Dong, X. (2017, Feb 22). Leaky Gate Model: Intensity-Dependent Coding of Pain and Itch in the Spinal Cord. *Neuron, 93*(4), 840-853 e845. https://doi.org/10.1016/j.neuron.2017.01.012

Sun, Y. G., & Chen, Z. F. (2007, Aug 9). A gastrin-releasing peptide receptor mediates the itch sensation in the spinal cord. *Nature, 448*(7154), 700-703. https://doi.org/10.1038/nature06029

Sun, Y. G., Zhao, Z. Q., Meng, X. L., Yin, J., Liu, X. Y., & Chen, Z. F. (2009, Sep 18). Cellular basis of itch sensation. *Science, 325*(5947), 1531-1534. https://doi.org/10.1126/science.1174868

Szentagothai, J. (1964, Apr). Neuronal and Synaptic Arrangement in the Substantia Gelatinosa Rolandi. *J Comp Neurol, 122*, 219-239. https://doi.org/10.1002/cne.901220207

Tashima, R., Koga, K., Yoshikawa, Y., Sekine, M., Watanabe, M., Tozaki-Saitoh, H., Furue, H., Yasaka, T., & Tsuda, M. (2021, Jan 19). A subset of spinal dorsal horn interneurons crucial for gating touch-evoked pain-like behavior. *Proc Natl Acad Sci U S A, 118*(3). https://doi.org/10.1073/pnas.2021220118

Todd, A. J. (2010, Dec). Neuronal circuitry for pain processing in the dorsal horn. *Nat Rev Neurosci, 11*(12), 823-836. https://doi.org/10.1038/nrn2947

Todd, A. J. (2017, Jan). Identifying functional populations among the interneurons in laminae I-III of the spinal dorsal horn. *Mol Pain, 13*, 1744806917693003. https://doi.org/10.1177/1744806917693003

Todd, A. J., Hughes, D. I., Polgar, E., Nagy, G. G., Mackie, M., Ottersen, O. P., & Maxwell, D. J. (2003, Jan). The expression of vesicular glutamate transporters VGLUT1 and VGLUT2 in neurochemically defined axonal populations in the rat spinal cord with emphasis on the dorsal horn. *Eur J Neurosci, 17*(1), 13-27. https://doi.org/10.1046/j.1460-9568.2003.02406.x

Todd, A. J., McGill, M. M., & Shehab, S. A. (2000, Feb). Neurokinin 1 receptor expression by neurons in laminae I, III and IV of the rat spinal dorsal horn that project to the brainstem. *Eur J Neurosci, 12*(2), 689-700. https://doi.org/10.1046/j.1460-9568.2000.00950.x

Traag, V. A., Waltman, L., & van Eck, N. J. (2019, Mar 26). From Louvain to Leiden: guaranteeing well-connected communities. *Sci Rep, 9*(1), 5233. https://doi.org/10.1038/s41598-019-41695-z

Usoskin, D., Furlan, A., Islam, S., Abdo, H., Lonnerberg, P., Lou, D., Hjerling-Leffler, J., Haeggstrom, J., Kharchenko, O., Kharchenko, P. V., Linnarsson, S., & Ernfors, P. (2015, Jan). Unbiased classification of sensory neuron types by large-scale single-cell RNA sequencing. *Nat Neurosci, 18*(1), 145-153. https://doi.org/10.1038/nn.3881

Vardy, E., Robinson, J. E., Li, C., Olsen, R. H. J., DiBerto, J. F., Giguere, P. M., Sassano, F. M., Huang, X. P., Zhu, H., Urban, D. J., White, K. L., Rittiner, J. E., Crowley, N. A.,

Pleil, K. E., Mazzone, C. M., Mosier, P. D., Song, J., Kash, T. L., Malanga, C. J., Krashes, M. J., & Roth, B. L. (2015, May 20). A New DREADD Facilitates the Multiplexed Chemogenetic Interrogation of Behavior. *Neuron, 86*(4), 936-946. https://doi.org/10.1016/j.neuron.2015.03.065

Varga, A., Meszar, Z., Sivado, M., Bacskai, T., Vegh, B., Kokai, E., Nagy, I., & Szucs, P. (2021, Feb 25). Spinal Excitatory Dynorphinergic Interneurons Contribute to Burn Injury-Induced Nociception Mediated by Phosphorylated Histone 3 at Serine 10 in Rodents. *Int J Mol Sci, 22*(5). https://doi.org/10.3390/ijms22052297

Wang, F., Flanagan, J., Su, N., Wang, L. C., Bui, S., Nielson, A., Wu, X., Vo, H. T., Ma, X. J., & Luo, Y. (2012, Jan). RNAscope: a novel in situ RNA analysis platform for formalin-fixed, paraffin-embedded tissues. *J Mol Diagn, 14*(1), 22-29. https://doi.org/10.1016/j.jmoldx.2011.08.002

Wang, Q., Zhang, X., He, X., Du, S., Jiang, Z., Liu, P., Qi, L., Liang, C., Gu, N., & Lu, Y. (2020, May). Synaptic Dynamics of the Feed-forward Inhibitory Circuitry Gating Mechanical Allodynia in Mice. *Anesthesiology, 132*(5), 1212-1228. https://doi.org/10.1097/ALN.0000000000003194

Wang, Z., Cui, M., Shah, A. M., Tan, W., Liu, N., Bassel-Duby, R., & Olson, E. N. (2021, May 25). Cell-Type-Specific Gene Regulatory Networks Underlying Murine Neonatal Heart Regeneration at Single-Cell Resolution. *Cell Rep, 35*(8), 109211. https://doi.org/10.1016/j.celrep.2021.109211

Warren, W. C., Harris, R. A., Haukness, M., Fiddes, I. T., Murali, S. C., Fernandes, J., Dishuck, P. C., Storer, J. M., Raveendran, M., Hillier, L. W., Porubsky, D., Mao, Y., Gordon, D., Vollger, M. R., Lewis, A. P., Munson, K. M., DeVogelaere, E., Armstrong, J., Diekhans, M., Walker, J. A., Tomlinson, C., Graves-Lindsay, T. A., Kremitzki, M., Salama, S. R., Audano, P. A., Escalona, M., Maurer, N. W., Antonacci, F., Mercuri, L., Maggiolini, F. A. M., Catacchio, C. R., Underwood, J. G., O'Connor, D. H., Sanders, A. D., Korbel, J. O., Ferguson, B., Kubisch, H. M., Picker, L., Kalin, N. H., Rosene, D., Levine, J., Abbott, D. H., Gray, S. B., Sanchez, M. M., Kovacs-Balint, Z. A., Kemnitz, J. W., Thomasy, S. M., Roberts, J. A., Kinnally, E. L., Capitanio, J. P., Skene, J. H. P., Platt, M., Cole, S. A., Green, R. E., Ventura, M., Wiseman, R. W., Paten, B., Batzer, M. A., Rogers, J., & Eichler, E. E. (2020, Dec 18). Sequence diversity analyses of an improved rhesus macaque genome enhance its biomedical utility. *Science, 370*(6523). https://doi.org/10.1126/science.abc6617

Waylen, L. N., Nim, H. T., Martelotto, L. G., & Ramialison, M. (2020, Oct 23). From whole-mount to single-cell spatial assessment of gene expression in 3D. *Commun Biol, 3*(1), 602. https://doi.org/10.1038/s42003-020-01341-1

Wercberger, R., & Basbaum, A. I. (2019, Oct). Spinal cord projection neurons: a superficial, and also deep, analysis. *Curr Opin Physiol, 11*, 109-115. https://doi.org/10.1016/j.cophys.2019.10.002

Wercberger, R., Braz, J. M., Weinrich, J. A., & Basbaum, A. I. (2021, Jul 13). Pain and itch processing by subpopulations of molecularly diverse spinal and trigeminal projection neurons. *Proc Natl Acad Sci U S A, 118*(28). https://doi.org/10.1073/pnas.2105732118

Willis, W. D., Al-Chaer, E. D., Quast, M. J., & Westlund, K. N. (1999, Jul 6). A visceral pain pathway in the dorsal column of the spinal cord. *Proc Natl Acad Sci U S A, 96*(14), 7675-7679. https://doi.org/10.1073/pnas.96.14.7675

Willis, W. D., Kenshalo, D. R., Jr., & Leonard, R. B. (1979, Dec 15). The cells of origin of the primate spinothalamic tract. *J Comp Neurol, 188*(4), 543-573. https://doi.org/10.1002/cne.901880404

Willis, W. D., Trevino, D. L., Coulter, J. D., & Maunz, R. A. (1974, Mar). Responses of primate spinothalamic tract neurons to natural stimulation of hindlimb. *J Neurophysiol, 37*(2), 358-372. https://doi.org/10.1152/jn.1974.37.2.358

Wilson, P., Meyers, D. E., & Snow, P. J. (1986, Mar). The detailed somatotopic organization of the dorsal horn in the lumbosacral enlargement of the cat spinal cord. *J Neurophysiol, 55*(3), 604-617. https://doi.org/10.1152/jn.1986.55.3.604

Wolf, F. A., Angerer, P., & Theis, F. J. (2018, Feb 6). SCANPY: large-scale single-cell gene expression data analysis. *Genome Biol, 19*(1), 15. https://doi.org/10.1186/s13059-017-1382-0

Woo, S. H., Lukacs, V., de Nooij, J. C., Zaytseva, D., Criddle, C. R., Francisco, A., Jessell, T. M., Wilkinson, K. A., & Patapoutian, A. (2015, Dec). Piezo2 is the principal mechanotransduction channel for proprioception. *Nat Neurosci, 18*(12), 1756-1762. https://doi.org/10.1038/nn.4162

Yaksh, T. L. (1989, Apr). Behavioral and autonomic correlates of the tactile evoked allodynia produced by spinal glycine inhibition: effects of modulatory receptor systems and excitatory amino acid antagonists. *Pain, 37*(1), 111-123. https://doi.org/10.1016/0304-3959(89)90160-7

Yildiz, S. H., Ulasli, A. M., Ozdemir Erdogan, M., Dikici, O., Arikan Terzi, E. S., Dundar, U., & Solak, M. (2017, Mar). Assessment of Pain Sensitivity in Patients With Chronic Low Back Pain and Association With HTR2A Gene Polymorphism. *Arch Rheumatol, 32*(1), 3-9. https://doi.org/10.5606/ArchRheumatol.2017.5846

Yu, X. H., Ribeiro-da-Silva, A., & De Koninck, Y. (2005, Oct 10). Morphology and neurokinin 1 receptor expression of spinothalamic lamina I neurons in the rat spinal cord. *J Comp Neurol, 491*(1), 56-68. https://doi.org/10.1002/cne.20675

Zaret, K. (2005, Feb). Micrococcal nuclease analysis of chromatin structure. *Curr Protoc Mol Biol, Chapter 21*, Unit 21 21. https://doi.org/10.1002/0471142727.mb2101s69

Zeilhofer, H. U., Wildner, H., & Yevenes, G. E. (2012, Jan). Fast synaptic inhibition in spinal sensory processing and pain control. *Physiol Rev, 92*(1), 193-235. https://doi.org/10.1152/physrev.00043.2010

Zeisel, A., Hochgerner, H., Lonnerberg, P., Johnsson, A., Memic, F., van der Zwan, J., Haring, M., Braun, E., Borm, L. E., La Manno, G., Codeluppi, S., Furlan, A., Lee, K., Skene, N., Harris, K. D., Hjerling-Leffler, J., Arenas, E., Ernfors, P., Marklund, U., &

Linnarsson, S. (2018, Aug 9). Molecular Architecture of the Mouse Nervous System. *Cell, 174*(4), 999-1014 e1022. https://doi.org/10.1016/j.cell.2018.06.021

Zhang, E.-T., & Craig, A. (1997). Morphology and distribution of spinothalamic lamina I neurons in the monkey. *Journal of Neuroscience, 17*(9), 3274-3284.

Zhang, E. T., Han, Z. S., & Craig, A. (1996). Morphological classes of spinothalamic lamina I neurons in the cat. *Journal of Comparative Neurology, 367*(4), 537-549.

Zhang, H., Song, L., Wang, X., Cheng, H., Wang, C., Meyer, C. A., Liu, T., Tang, M., Aluru, S., Yue, F., Liu, X. S., & Li, H. (2021). Fast alignment and preprocessing of chromatin profiles with Chromap. *bioRxiv*, 2021.2006.2018.448995. https://doi.org/10.1101/2021.06.18.448995

Zhang, X., Ji, R. R., Nilsson, S., Villar, M., Ubink, R., Ju, G., Wiesenfeld-Hallin, Z., & Hokfelt, T. (1995, Mar 1). Neuropeptide Y and galanin binding sites in rat and monkey lumbar dorsal root ganglia and spinal cord and effect of peripheral axotomy. *Eur J Neurosci, 7*(3), 367-380. https://doi.org/10.1111/j.1460-9568.1995.tb00332.x

Zhang, X., Ju, G., Elde, R., & Hokfelt, T. (1993, May). Effect of peripheral nerve cut on neuropeptides in dorsal root ganglia and the spinal cord of monkey with special reference to galanin. *J Neurocytol, 22*(5), 342-381. https://doi.org/10.1007/BF01195558

Zhang, X., Kaplow, I. M., Wirthlin, M., Park, T. Y., & Pfenning, A. R. (2020, Aug 1). HALPER facilitates the identification of regulatory element orthologs across species. *Bioinformatics, 36*(15), 4339-4340. https://doi.org/10.1093/bioinformatics/btaa493

Zhou, J., & Troyanskaya, O. G. (2015, Oct). Predicting effects of noncoding variants with deep learning-based sequence model. *Nat Methods, 12*(10), 931-934. https://doi.org/10.1038/nmeth.3547

Zou, M., Li, S., Klein, W. H., & Xiang, M. (2012, Apr 15). Brn3a/Pou4f1 regulates dorsal root ganglion sensory neuron specification and axonal projection into the spinal cord. *Dev Biol, 364*(2), 114-127. https://doi.org/10.1016/j.ydbio.2012.01.021